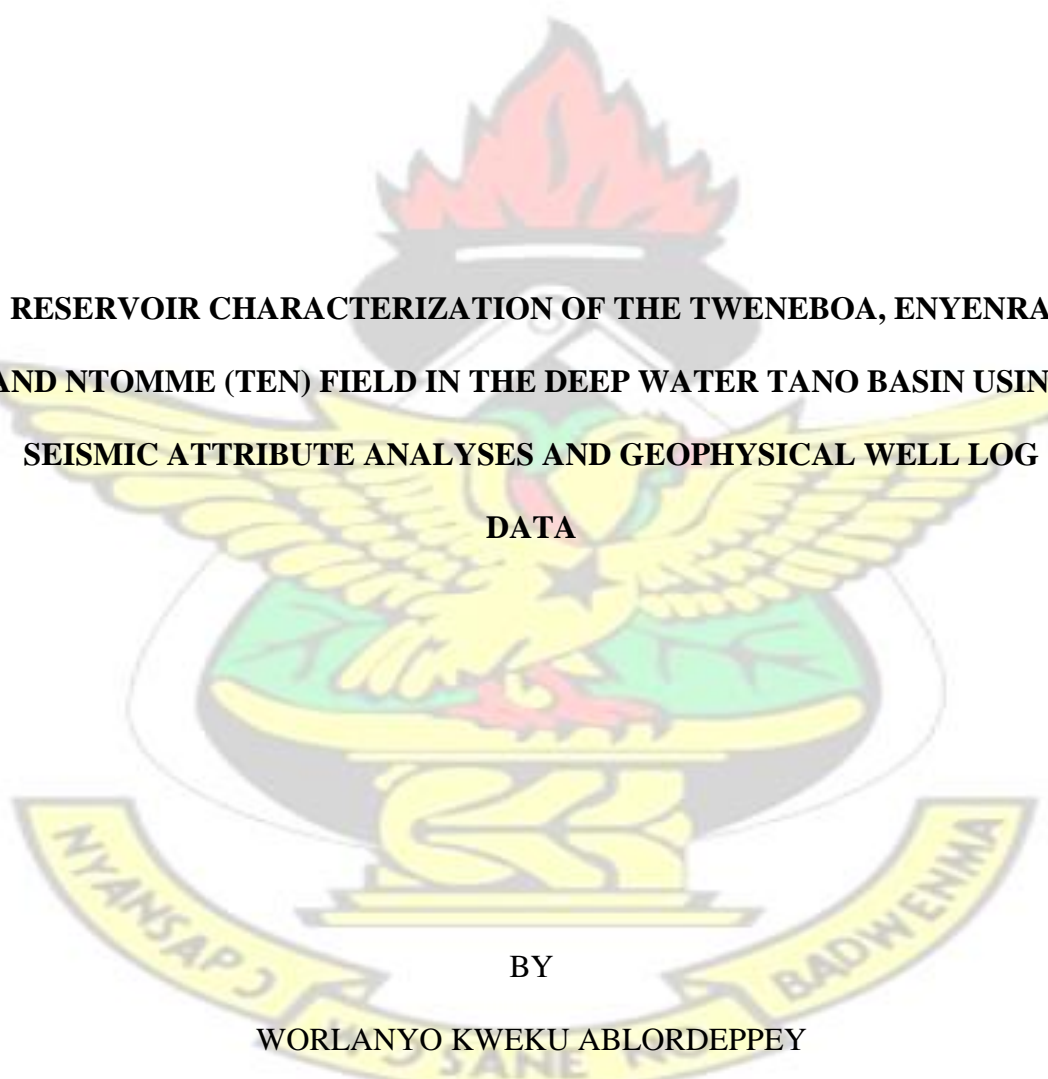


**KWAME NKRUMAH UNIVERSITY OF SCIENCE AND TECHNOLOGY**

COLLEGE OF SCIENCE

DEPARTMENT OF PHYSICS

KNUST

The logo of Kwame Nkrumah University of Science and Technology (KNUST) is centered in the background. It features a yellow eagle with its wings spread, perched on a green shield. Above the eagle is a red flame. Below the eagle is a yellow banner with the text 'NYANSAPƆ' on the left and 'BADWENMA' on the right. The entire logo is rendered in a light, semi-transparent style.

**RESERVOIR CHARACTERIZATION OF THE TWENEBOA, ENYENRA  
AND NTOMME (TEN) FIELD IN THE DEEP WATER TANO BASIN USING  
SEISMIC ATTRIBUTE ANALYSES AND GEOPHYSICAL WELL LOG  
DATA**

BY

**WORLANYO KWEKU ABLORDEPPEY**

(BSc. PHYSICS)

SEPTEMBER, 2 016

**RESERVOIR CHARACTERIZATION OF THE TWENEBOA, ENYENRA**

**AND NTOMME (TEN) FIELD IN THE DEEP WATER TANO BASIN USING  
SEISMIC ATTRIBUTE ANALYSES AND GEOPHYSICAL WELL LOG  
DATA**

BY  
WORLANYO KWEKU ABLORDEPPEY  
(BSc. PHYSICS)

A Thesis submitted to the School of Graduate Studies, Kwame Nkrumah University  
of Science And Technology, in partial fulfilment of the requirements for award of  
degree

of  
MASTER OF PHILOSOPHY  
(GEOPHYSICS)

Supervisor: Prof. S.K Danuor

College of Science  
© Department of Physics  
September, 2016

## DECLARATION

### Candidate's Declaration

I hereby declare that this thesis is the result of my own original research and that no part of it has been presented for another degree in this university or elsewhere. Any other materials used have been duly referenced.

**Candidate's Name:** Worlanyo Kweku Ablordeppey

Signature: ..... Date: .....

### Supervisor' Declaration

I hereby declare that the preparation and presentation of the thesis were supervised in accordance with the guidelines on supervision of thesis laid down by the Kwame Nkrumah University of Science and Technology

**Certified by:**

**Supervisor's Name:** Prof. Sylvester K. Danuor

Signature: ..... Date: .....

### Head of Department's Declaration

I certify that this is the Student's own research work.

**Name of Head of Department:** Prof. S.K Danuor

Signature: .....Date: .....

## DEDICATION

To God, my wonderful parents, Mr. Francis Kwesi Ablordeppey and Madam Benedicta Buade, and to myself.

# KNUST



## ACKNOWLEDGEMENTS

My most sincere thanks goes to the almighty God for His provisions and protections throughout this study. My sincere gratitude goes to my Supervisor, Prof. S. K. Danuor and Mr. Vandyke Asare, for their constructive criticisms and comments that helped to shape this work.

I would also like to express my gratitude to the Geophysics Manager of GNPC, Benjamin Kwame Asante and GNPC for granting me the opportunity and providing me with the necessary data, facilities and supervision needed to carry out this thesis in their establishment. My sincere thanks to my GNPC Supervisor, Mrs. Evelyn Brakoa Amoako Nsarful for her selfless coaching and assistance throughout this study. Sena Cyril Dzreke, Eugenia Fefoame, Kaku, and the entire Geophysics team of GNPC, I say thank you for your inputs. Also, I say thank you to Dr. Preko, Dr. Aning and Dr. Wemegah of KNUST Physics Department for their supports in diverse ways. I equally express my sincere thanks to all my friends as well as colleagues in the programme for their assistance in diverse ways.

A special thanks to Martha Adzo Nkegbe for her marvelous support, Daniel Agbezukey, Selasi Kunya, Frank Kow, Christian Galley, Dela Dzobo, Cephas Nukunu, Mr. Francis Kavi, Francis Nyanu and Araba Ackon for their moral supports throughout the entire time. I am so grateful to my parents Mr. Francis Kwesi Ablordeppey and Benedicta Ama Buade; my cousins; Anthony Ablordeppey, Apeke Young Abletor, James Ahiabor and my siblings; Enyo, Esinu, Senu, Yesutor and Kekeli Ablordeppey for their encouragement to finish this study on time. To those whose name I have not been able to mention, I say a big thank you for your supports in diverse ways.

## ABSTRACT

3-D Seismic data (Extended Elastic Impedance and reflectivity data) and well log data from five wells were used to characterize reservoirs in the Turonian and Santonian formations of the Tweneboa Enyenra and Ntomme field within the Deep Water Tano Basin. Seismic attributes such as Volume Attribute of Minimum Amplitude (VATMIN), amplitude (reflection strength) and coherency were considered and extracted from the 3-D seismic data. The extracted attributes were successful in delineating two hydrocarbon sand fairways (occurrence zones) labelled as Sovereign-1 and Sovereign-2 in the Turonian formation and one main sand fairway in the Santonian formation. Sovereign-1 sand fairway is a complex sinuous channel system with its sand depositions in a well confined to a relatively narrow channel axis. Sovereign-2 is a midslope channelized lobe with a less confined channel axis. Amalgamated straight to slightly sinuous channel system was delineated as the host of the sands in the Santonian reservoir. From the well data analysis, three main reservoir units denoted as R01, R02 and R03 were identified and correlated in Sovereign-1. R01 has average porosity of 17.33 percent, permeability of 183.75 mD, 79 percent hydrocarbon saturation and average net pay of 34 m. R02 has average porosity value of 17.13 percent, 144.45 mD permeability, 65 percent hydrocarbon saturation and 9.4 m net pay thickness. Porosity value of 15.6 percent, 75.5 percent hydrocarbon saturation, 120 mD permeability, and 8.5 m net pay thickness were recorded for R03. Similarly, two main reservoir units namely N01 and N02 were identified in Sovereign-2. N01 has porosity of 16.75 percent, 73.65 percent hydrocarbon saturation, 151.85 mD permeability and 37.3 m net pay. N02 has 17.9 percent porosity, 18.8 percent hydrocarbon saturation, 31.45 mD permeability, and net pay of 6.6 m. Reservoir quality analysis based on porosity permeability cross plot revealed that Sovereign-2 reserve was of good reservoir quality than Sovereign-1. The stock tank of oil initially in place (STOIP) was estimated to be 456 MMbbl for Sovereign-1 reserve and 388 MMbbl for Sovereign-2 reserve giving a total of 844

MMbbl in the Turonian formation. The results obtained were good indicators for commercial production of hydrocarbons in the field. The petrophysical properties were not estimated for the Santonian sand fairway due to insufficient well log data within the Santonian interval. The Santonian sand fairway was considered unprolific with no well-developed petroleum system.

# KNUST



# TABLE OF CONTENTS

DECLARATION .....	iii
DEDICATION .....	iv
ACKNOWLEDGEMENTS .....	v
ABSTRACT .....	vi
TABLE OF CONTENTS .....	viii
LIST OF TABLES .....	xiv
LIST OF FIGURES .....	xv
LIST OF ABBREVIATIONS .....	xviii
CHAPTER ONE .....	1
INTRODUCTION .....	1
1.1 Research Background .....	1
1.2 Organization of the Thesis. ....	4
1.3 Problem Statement .....	4
1.4 Objectives .....	5
1.4.1 Main Objective: .....	5
1.4.2 Specific Objectives .....	6
1.5 Scope of Thesis .....	6

1.6 Significance of Thesis .....	6
1.7 Study Area .....	7
CHAPTER TWO .....	9
LITERATURE REVIEW .....	9
CHAPTER THREE .....	12
GEOLOGY OF THE TANO BASIN OF GHANA .....	12
3.1 Introduction .....	12
3.2 The Tano-Cape Three Points Basin .....	13
3.3 Stratigraphic Setting of the Tano Basin .....	14
3.3.1 Aptian-Lower Albian (Kobnaswaso Formation) .....	14
3.3.2 The Lower-Middle Albian .....	15
3.3.3 The Uppermost Lower Albian-Middle Albian .....	15
3.3.4 Upper Albian (Domini Formation) .....	15
3.3.5 Cenomanian Formation .....	16
3.3.6 Turonian .....	17
3.3.7 Coniacian-Santonian .....	17
3.3.8 Uppermost Santonian to Intra Lower Campanian .....	18
3.3.9 Lower Campanian to Upper Campanian .....	18
3.3.10 Maastrichtian .....	18

3.3.11 Tertiary Sequences .....	19
3.4 The History of Hydrocarbon Exploration in the Tano Basin .....	21
3.5 The Petroleum System of the Tano Basin .....	22
3.5.1 Source Rocks (Aptian 120Ma – Turonian 93Ma) .....	22
3.5.2 Reservoir Rocks (Aptian 113Ma – Maastrichtian 60Ma) .....	22
3.5.3 Seals (Turonian 91 Ma – Maastrichtian 60 Ma) .....	22
3.5.4 Traps .....	23
.....	24
<b>BACKGROUND THEORY .....</b>	<b>24</b>
4.1 Introduction .....	24
4.2 Seismic Method .....	24
4.2.1 Seismic Survey .....	25
4.2.2 Seismic Waves .....	25
4.2.3 Seismic Reflection Method .....	26
4.3 History of the Extended Elastic Impedance (EEI) .....	27
4.4 Seismic Attributes .....	29
4.4.1 Amplitude .....	31
4.4.1.1 Volume Attribute of Minimum Amplitude (VATMIN) .....	32
4.4.1.2 Coherency Attribute .....	32

4.5 Seismic Data in Reservoir Characterization .....	33
4.6 Reservoir Maps .....	33
4.6.1 Depth Structure Maps .....	33
4.6.2 Isopach Maps .....	34
4.7 Depositional environment .....	34
4.7.1 Continental Deposits: .....	35
4.7.2 Transitional Deposits .....	35
4.7.3 Marine Deposits .....	36
4.8 Architecture Elements.....	37
4.9 Borehole logging.....	39
4.10 Well logs in Reservoir Characterization .....	41
4.11 Petrophysical Parameters .....	42
4.11.1 Porosity .....	42
4.11.2 Water Saturation .....	42
4.11.3 Permeability .....	43
4.11.4 Net to Gross Ratio.....	43
4.12 Volumetric Estimation .....	43
CHAPTER FIVE .....	46

METHODOLOGY .....	46
5.1 General Overview of Workflow .....	46
5.2 Data Sets .....	47
5.2.1 Seismic Data .....	47
5.2.2 Well data. ....	47
5.3 Software Package .....	48
5.4 Data Quality Check .....	49
5.5 Generation of Synthetic Seismograms. ....	50
5.5.1 Horizon Picking .....	52
5.5.2 Top Turonian and Base Turonian Picking .....	53
5.5.3 Top Santonian and Base Santonian Picking .....	53
5.6 Fault Picking .....	54
5.7 Generating Depth Structural Maps .....	54
5.8 Seismic Volume Attributes Analysis .....	55
5.8.1 Generating VATMIN Maps .....	55
5.8.2 Generating Coherency Slices .....	56
5.8.3 Generating Architecture Element Maps. ....	57
5.8.3.1 ISO-Proportional Slices .....	57

5.9 Well Logs Analysis .....	59
5.9.1 Well Correlation .....	60
5.9.2 Estimation of Petrophysical Parameters. ....	60
5.10 Reservoir Quality .....	62
CHAPTER SIX .....	64
RESULTS AND DISCUSSION .....	64
6.1 Seismic Interpretation of the Turonian .....	64
6.2 Structural Interpretation .....	65
6.2.1 Depth Structural Maps of the Turonian Formation .....	65
6.2.2 Fault Interpretation of the Turonian.....	66
6.2.3 Isopach Map of Turonian .....	67
6.3 Seismic Volume Attributes Analysis .....	69
6.3.1 Interpretation of the Amplitude Map of the Turonian. ....	69
6.3.2 Interpretation of VATMIN Extractions for the Turonian .....	70
6.4 Interpretation of the Coherence Slices .....	71
6.5 Interpretation of Architecture Element maps .....	75
6.6 Well Logs Analysis of the Turonian .....	79
6.6.1 Correlation of Wells in Sovereign-1 fairway .....	79
6.6.2 Well to Seismic (EEI Chi80 data) Tie .....	81
6.6.3 Estimation of Petrophysical Parameters of Sovereign-1 Sand Fairway. ....	85

6.6.4 Correlation of Wells in Sovereign-2 .....	86
6.6.5 Well to Seismic (EEI Chi80) ties within Sovereign-2 Sand fairway .....	88
6.6.6 Reservoir Properties of Sovereign -2 Sand Fairway .....	90
6.6.7 Reservoir quality comparison of Sovereign-1 and Sovereign-2 Fairways ..	91
6.7 Estimation of Volume of Hydrocarbon .....	92
6.7.1 Estimation of Volume of Hydrocarbons in Sovereign-1 .....	92
6.7.2 Estimation of Volume of Hydrocarbon in Sovereign-2 .....	93
6.8 Structural Interpretation of Santonian.....	94
6.8.1. Depth Structural Maps of Santonian .....	94
6.8.2 Isopach Map .....	96
6.9 Volume Attribute Maps Interpretation of the Santonian .....	97
6.10 Interpretation of Coherency Slices .....	99
6.11 Interpretation of Architecture Element Maps .....	101
<b>CHAPTER SEVEN .....</b>	<b>106</b>
<b>CONCLUSION AND RECOMMENDATIONS .....</b>	<b>106</b>
7.1 Conclusion .....	106
7.2 Recommendations .....	108
<b>REFERENCES .....</b>	<b>109</b>
<b>APPENDIX .....</b>	<b>115</b>

## LIST OF TABLES

Table 4.1. Principal Architecture elements of deep water clastic systems (Reading and Richard, 1994). .....	38
Table 6.1: Summary of Petrophysical Parameters of Wells within Sovereign-1 .....	85
Table 6.2: General Average Petrophysical Parameters of the Sovereign-1. ....	86
Table 6.3: Reservoir Properties of the Wells within Sovereign-2 .....	90
Table 6.4: Summary of Petrophysical Parameters of Sovereign-2 .....	90
Table 6.5: Volumetric Estimation of Sovereign-1 reserves .....	93
Table 6.6: Volumetric Estimation of Sovereign-2 reserve.....	94

## LIST OF FIGURES

Figure 1.1: Location Map of the Study Area (source: GNPC, 2015). ....	8
Figure 3.1: Map of Ghana showing the four sedimentary basins (GNPC, 2015) .....	13
Figure 3.2: Stratigraphic section of the formations in Tano Basin (Sutherland, 2008) .....	20
Figure 3.3: General Geology and Stratigraphy of the Tano Basin (Anadarko, 2011) .	20
Figure 4.1: Extended elastic impedance angles ranging from $-90^{\circ}$ to $+90^{\circ}$ , at which values $\sin^2\theta$ is physically impossible (adopted from Hampson-Russell, 2006). ....	28
Figure 4.2: Summary of seismic attributes (After Brown A. R., 1996) .....	31
Figure 4.3: A Schematic diagram showing depositional environments (Pyles, 2007) 36 .....	36
Figure 4.4: Slope Control Architectural Elements of Deepwater Reservoirs (Posamentier and Kolla, 2003). ....	39
Figure 5.1: Base map of the survey Area showing principal Inlines and Crosslines ...	48

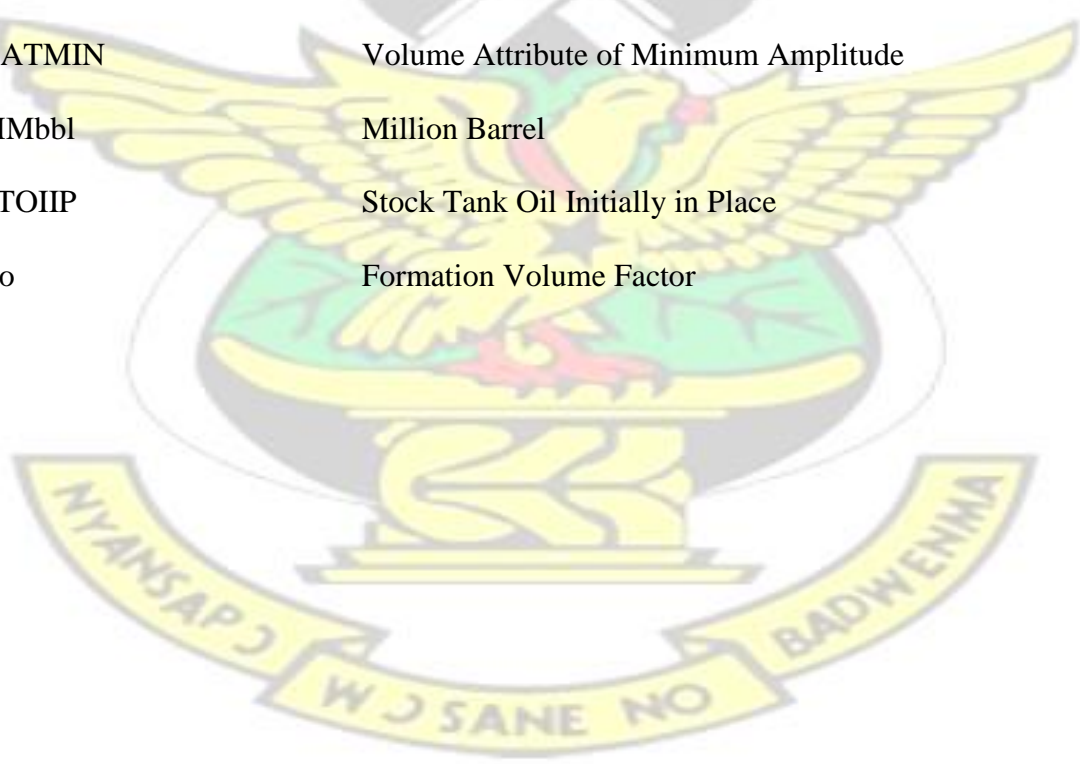
Figure 5.2: GNPC SMT Software window interface showing the Formation Tops in red Polygon for the study area.....	50
Figure 5.3: Synthetic Seismograms generated using seismic and well data of the Study Area .....	51
Figure 5.4: Seismic section showing well to seismic tying using synthetic seismogram. ....	52
Figure 5.5: Seismic Section before Interpretation (Picking of Horizons). ....	53
Figure 5.6: Seismic Section after Interpretation of Horizons .....	54
Figure 5.7: Kingdom Software window showing the interface for extracting VATMIN Amplitude .....	56
Figure 5.8a: SMT software window for calculating ISO-proportional Slices. ....	58
Figure 5.8b: Seismic Section showing the ISO proportional slices in Turonian and Santonian. ....	59
Figure 6.1: Seismic Section showing the mapped Horizons. ....	64
Figure 6.2a: Depth Structural map of the Top Turonian .....	65
Figure 6.2b: Depth Structural map of the Base Turonian .....	66
Figure 6.3: Seismic section showing faults in the Turonian formation .....	67
Figure 6.4: Turonian Isopach map .....	68
Figure 6.5: Amplitude Extraction Map (PSDM Seismic data) of the Turonian. ....	69
Figure 6.6: VATMIN Amplitude Extraction of the Turonian.....	71
Figure 6.7a: Coherency Slice (Top of Turonian). ....	72
Figure 6.7b: Coherency Slice (middle of Turonian formation) .....	73
Figure 6.7c: Coherency Slice (near base of Turonian) .....	74
Figure 6.8: Architecture Element map (Interval T1). ....	75

Figure 6.10: Architecture Element map (Interval T3). .....	76
Figure 6.11 Architecture Element map (Interval T4).....	76
Figure 6.12: Architecture element map (Interval T5). .....	77
Figure 6.13 Architecture Element Map (Interval T6). .....	77
Figure 6.14: Schematic sand depositions map within Turonian Formation.....	79
Figure 6.15: Well correlation within the Sovereign 1 channel complex.....	80
Figure 6.16: Well to Seismic (EEI Data) tie showing gamma ray log behaviour with sands and shales and ISO-Proportional Intervals. ....	82
Figure 6.17: VATMIN extraction on R03 Interval. ....	83
Figure 6.18: VATMIN extraction on R02 interval .....	84
Figure 6.19: VATMIN Extraction on Reservoir R01 Interval. ....	84
Figure 6.20: Well correlation within the Sovereign 2. ....	87
Figure 6.21 Well to Seismic (EEI data) tie showing gamma ray behaviour with sands and shales with the ISO-proportional intervals. ....	88
Figure 6.22: VATMIN Amplitude extraction on N01 Interval .....	89
Figure 6.23: VATMIN Amplitude extraction on N02 .....	89
Figure 6.24: Porosity- Permeability Cross Plot .....	91
Figure 6.25a: Depth Structural Map of Top Santonian .....	95
Figure 6.25b: Depth Structural Map of Base Santonian .....	96
Figure 6.26: Santonian Isopach map .....	97
Figure 6.27a: Reflectivity Amplitude Map for the Santonian Interval .....	98
Figure 6.27b: VATMIN Amplitude Extraction on the EEI data (EEI Chi80) .....	99
Figure 6.28a: Coherency slice near top of Santonian. ....	100
Figure 6.29: Architecture Element Map (Interval S1) .....	102
Figure 6.30: Architecture Element Map (Interval S2) .....	102
Figure 6.31: Architecture Element Map (Interval S3) .....	103

Figure 6.32: Architecture Element Map (Interval S4) .....	103
Figure 6.33: Architecture Element Map (Interval S5) .....	104
Figure 6.34: Architecture Element Map (Interval S6) .....	104
Figure 6.35: Schematic hydrocarbon sand deposition map of the Santonian. ....	105

**LIST OF ABBREVIATIONS**

DWT	Deep Water Tano
EEI	Extended Elastic Impedance
PSDM	Pre Stack Depth Migrated
EOWR	End of Well Report
GNPC	Ghana National Petroleum Corporation
OWC	Oil Water Contact
SMT	Seismic Micro Technology
TEN	Tweneboa Enyrenra Ntomme
VATMIN	Volume Attribute of Minimum Amplitude
MMbbl	Million Barrel
STOIP	Stock Tank Oil Initially in Place
Bo	Formation Volume Factor



# KNUST





## CHAPTER ONE

### INTRODUCTION

#### 1.1 Research Background

Everyday, approximately 90 million barrels or more of hydrocarbon is being used up worldwide. Due to hydrocarbon enhancing effect on our standard of living, the dependency on oil and gas has risen to the point where it had become the lifeline of modern civilization. Over the last century, oil exploration and production has fuelled world economic growth so much that several nations have become solely dependent on the exports of their oil to the international market in order to maintain economic stability (Chopra *et al.*, 2010).

According to Chopra *et al.* (2010), the proven worldwide oil reserves were reported as 238 billion barrels in 2007. Calculations based on this production rate have led to the realisation that the crude oil supply could only last for another 42 years. Although these figures are based on assumptions that may not be strictly true, the calculation does forewarn of depleting global reserves and the pressing need to explore and discover more hydrocarbon prospects before the reserves run out. This in recent times has forced the exploration and production companies to focus on exploring the deep waters due to the belief that all the easily accessible reserves have already been exploited.

With the knowledge that fine-tuning research on reservoir characterisation could lead to more efficient productive ways of extracting and managing hydrocarbon reserves, more research into reservoir characterization study has become imperative to geoscientists. Indeed, even a small increase in the recovery rate of oil or gas through detailed reservoir characterization would not only lengthen the life of the field but also reduce operational costs (Haldorsen and Damsleth, 1993).

Reservoir characterisation is the process of quantitatively assigning reservoir properties, recognizing geological and geophysical information and quantifying uncertainties in spatial variability (Fowler *et al.*, 1999). It represents an indispensable tool for optimizing costly reservoir management decisions for the development of the hydrocarbon field. It is a known fact that reservoir characterization is the first step in the reservoir development programme, taking into account structural and depositional architecture, pore systems, the mineralogy of the reservoir, post deposition diagenesis and the distribution and nature of reservoir fluids. Any reservoir characterization exercise usually begins with the available information on the geological features and the depositional and facies environment.

The structural interpretation of seismic data and the sequence stratigraphy approach are all important inputs in defining the reservoir model framework. Detailed relevant information about distributions of reservoir properties (porosity, permeability, net pay thickness, Gross Reserve Volume (GRV), net-to-gross ratio (N/G), areal extent, hydrocarbon in place etc. can be obtained from well logs data, seismic data or core data. The associated risks and uncertainties must also be estimated when building the reservoir model. The contribution of seismic data in populating 3D reservoir models in terms of petrophysical properties may be derived from seismic attributes through their calibration with log data and the relevant rock physics models (Chopra *et al.*, 2010).

Seismic attributes obtained from seismic data have been an important tool in reservoir characterization. Seismic attributes are computed quantities obtained from seismic data (Sheriff, 2002). These attributes are used to characterize the reservoir. Reservoir channels, lateral extent of a reservoir, reservoir thickness, depositional environment, fluid type, structural features and other properties of a reservoir can be obtained from

seismic data depending on which seismic attribute being extracted from the seismic data. Well data in reservoir characterization process provides direct measurement of reservoir properties. Reservoir properties such as porosity, water saturation, permeability, net pay, lithology and many others are quantitatively obtained from well data. But the limitation with using well log data alone in characterizing a reservoir is that it provides poor horizontal resolution and leave a large space between wells despite the sufficient vertical resolution (Russell, 1988). Seismic data on the other hand provide detailed reservoir characterization between wells but have poor vertical resolution when compared to the well data (Russell, 1988).

According to Chopra and Michelena (2011), characterization of reservoir is best achieved by integrating different data sets such as seismic data, well data and core data. The success of the reservoir characterisation effort depends on how well the integration of the different data sets is achieved as opposed to the application of a single type of data set. The Integrated approach in characterizing the reservoir would help to reduce the uncertainties associated with the interpretations (Kramers, 1994).

This research work therefore seek to contribute the information needed to characterize the reservoir by integrating the seismic attributes obtained from the 3d-seismic data and information from the well logs data.

Chopra and Michelena (2011) emphasized that collation of such information about a reservoir helps to estimate the volume of in-place hydrocarbon, establish the commercial viability of the reserve, improve production rates, identify future well locations, rejuvenate oil fields, predict future reservoir performance, minimise costly

expenditures and also to generate accurate financial models by management of oil companies.

## **1.2 Organization of the Thesis.**

This study is organized into seven chapters as follows:

The first chapter of the thesis includes the general research background, the problem statement, research objectives, scope of study, significance of the study and study area.

Chapter two highlights the review of relevant literatures regarding this study. Chapter

three looks at the geology of the study area. In chapter four the background theories necessary to understand the study have been discussed. The fifth chapter presents, the

data sets and the software used to carry out the study. It also outlines the various methods employed in achieving the objectives of the study. The results are presented in

the sixth chapter. In this chapter the various seismic attribute maps generated coupled with the information on reservoir properties obtained from the well logs data were

discussed. Chapter seven focuses on the conclusions based on the research objectives.

The recommendations that will be beneficial for future research work to individuals or institutions were also outlined in chapter seven.

## **1.3 Problem Statement**

While we can claim that all of the easily exploited hydrocarbon fields have already been discovered, the global energy market is still striving for more oil and gas. Higher

demands for hydrocarbon in recent years have forced oil and gas industries to focus on exploring deep water and the frigid/hot regions around the world. Aside overcoming

the geographical challenges there still remain other problematic areas that are yet to be dealt with (Shahri, 2013).

Another challenge in the world of seismic exploration involves identifying subsurface ambiguities. This can be a difficult task in most regions affecting the ability to gather and analyse data quickly and efficiently. We are always looking for the best subsurface image in order to increase work accuracy, increasing yield and decreasing the drilling risks and costs associated with poor decision making based on insufficient data. Advanced techniques provide vast amount of information that can help to address the challenges which improve our ability to interpret the subsurface structures and reveal more information about hydrocarbon prospects. Despite the efforts by exploration and production companies, it still remains a fact that oil and gas companies often run into challenges concerning poor reservoir performance as a result of the inaccurate characterisation of reservoirs (Shahri, 2013). According to a GNPC unpublished report, significant oil accumulation estimation in commercial quantity as announced in the jubilee field by the jubilee partners was attained based on vigorously enhanced techniques. These involved finding hydrocarbon potential sources and reservoirs through detailed visualization, interpretation and characterization activities.

This thesis therefore seeks to produce a detailed reservoir characterization of the TEN discovery within the Deep Water Tano Basin by integrating seismic data and well logs data sets. The results will help in making the best planning and developmental decisions of the field.

## **1.4 Objectives**

### **1.4.1 Main Objective:**

To characterize the reservoir of the TEN (Tweneboa, Ntomme and Enyenra) field within the Deep Water Tano Basin (DWT).

#### **1.4.2 Specific Objectives**

1. Delineate structural features capable of trapping the hydrocarbons in the reservoirs.
2. Delineate the occurrence of potential hydrocarbon bearing sands using seismic volume attributes of minimum amplitude (VATMIN).
3. Describe the depositional environment and architectural elements using seismic coherency attribute and VATMIN
4. Estimate the petrophysical properties of the delineated reservoir using well logs and seismic data.
5. Estimate the volume of in-place hydrocarbon.

#### **1.5 Scope of Thesis**

Ghana National Petroleum Cooperation (GNPC) is the facilitating company for this thesis by providing the needed data sets, the software and the software training, and the internal supervision for the success of this study. This study will entail the use of information from different seismic attributes (volume attribute of minimum amplitude and coherency) extracted from the 3D volume seismic data and well logs in the area of investigation, located in the Deep Tano Basin to characterize the identified reservoirs. For confidentiality reasons, the original nomenclature of wells and seismic data will be withheld. The exact location, specifically the coordinates of maps will also be withheld. However, this will not affect the authenticity of results obtained and discussed in this thesis in any way.

#### **1.6 Significance of Thesis**

This research study will give quantitative information about the identified reservoir properties in the field. The reservoir properties will establish the commercial viability of the reservoir. Insight into structural and stratigraphic traps as well as a depositional environment

setting of targeted formations will enhance oil recoverability and serve also as input for reservoir modelling. This work nevertheless will serve as precedence for other research works for students in this area.

### **1.7 Study Area**

Tweneboa, Enyenra and Ntomme fields with the acronym TEN in the Deep Water Tano block is situated in the Tano Basin and is about 60 km offshore Ghana. The TEN fields are spread across an area of more than 650 km<sup>2</sup>, about 30 km to the west of Jubilee field. The study area lies in water depth from 1000 m to 1800 m. This thesis work will be carried out specifically within the Turonian and Santonian formation within the TEN field. Figure 1.1 below is the map of the study area.



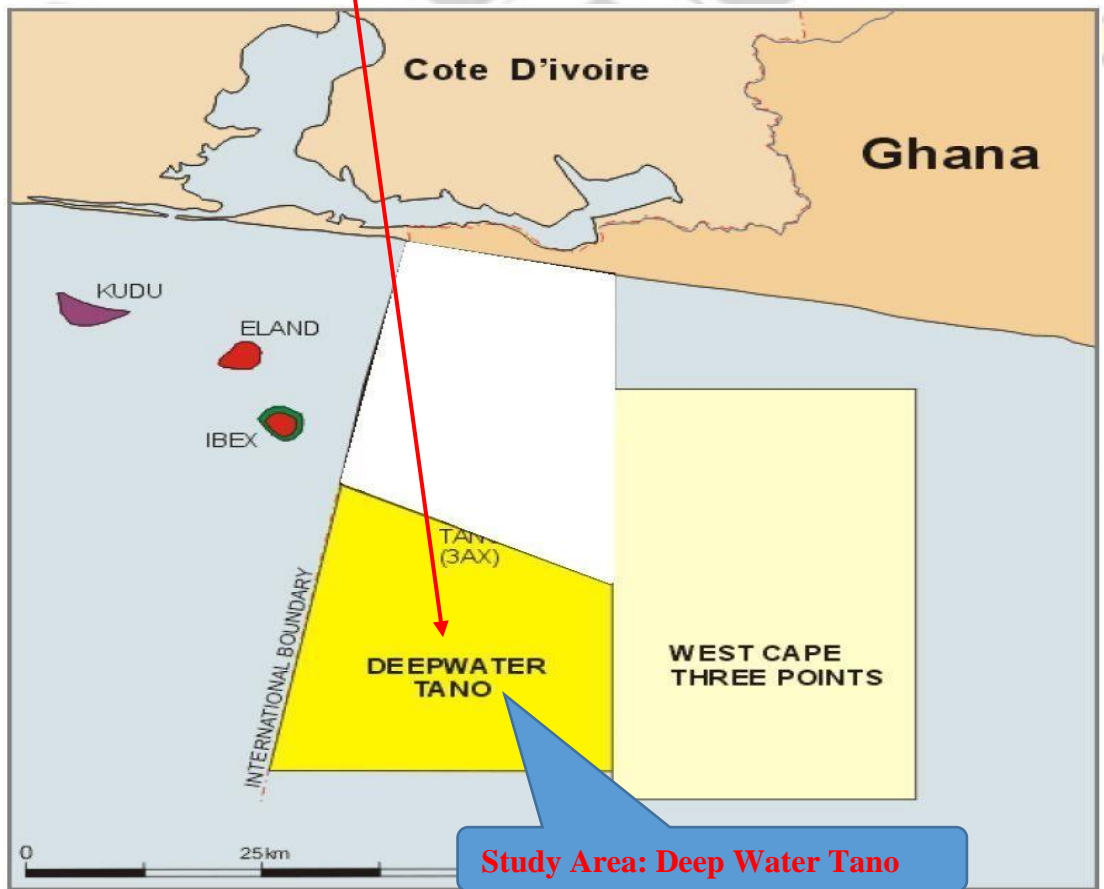
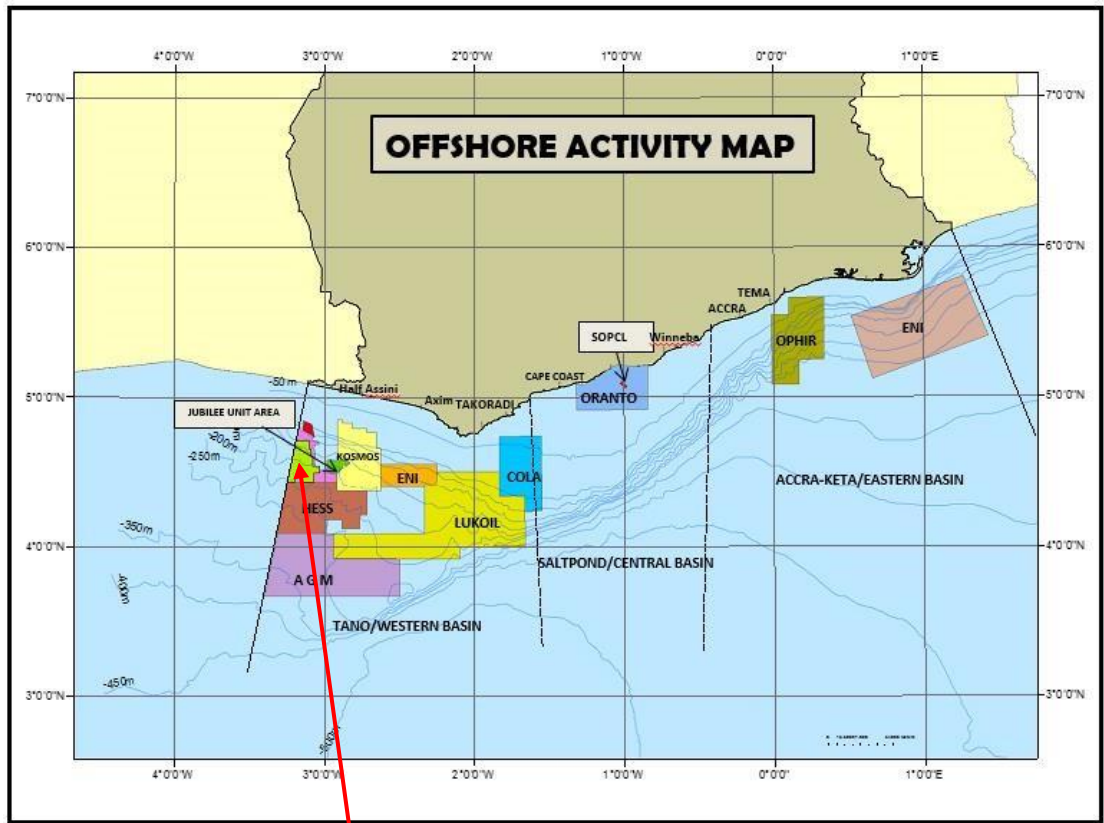


Figure 1.1: Location Map of the Study Area (source: GNPC, 2015).

## CHAPTER TWO

### LITERATURE REVIEW

Awareness about characterization of reservoir started growing slowly at first and rapid with time when geoscientists and engineers conceived the idea that more hydrocarbons could be squeezed out of existing reservoirs. Apparently, this upsurge in development of reservoir characterization may have been caused by three major reasons: First, due to upsurge in computing that led to innovative visualization packages for interactive interpretation workstations. Secondly the idea of integration of different type of data and thirdly the advancements in acquisition of data and processing techniques that have led to more accurate imaging of reservoirs and their architecture elements (Chopra and Michelena, 2011).

Reservoir characterization according to Chopra and Michelena (2011) is defined as all pertinent information that is required to describe a reservoir in terms of its capacity to store and produce hydrocarbon. This involves understanding the complete reservoir architecture including the internal and external geometry, its model with distribution of reservoir properties and understanding the fluid flow within the reservoir.

Different Researchers have highlighted varied ways that reservoir characterization was attempted, either by using a particular aspect of seismic interpretation, or using seismic attributes for prediction of some parameters of the reservoir or in terms of describing a newer approach adopted for a rock physics model and its application.

In “Integration of 3D Seismic and well log data in optimal reservoir characterization of EMI field, offshore, Niger Delta Oil Province, Nigeria”, Oyedele *et al.* (2013) employed seismic data to evaluate the structural features capable of hosting

hydrocarbon in the area. They used the presence of faults and anticlinal features (four way closures) interpretation on the seismic data as the basis for identification of good sand areas. Well log data was used to predict the petrophysical parameters such as porosity, permeability, water saturation and net-to-gross ratio. They concluded that the reservoirs were commercially viable based on petrophysical properties estimated.

Ajisafe and Ako (2013) “3D seismic attributes for reservoir characterization of “Y” Field Niger Delta, Nigeria”, used seismic attributes (maximum amplitude, root mean square amplitude) to delineate hydrocarbon sand accumulation areas. They went on to employ gamma ray logs to identify sands within wells situated in this sand prone areas vertically while the neutron and density logs were used to discriminate fluid types. Nothing has been said about the shape orientation of the reservoirs and the depositional environment in their research work.

In this paper “Hydrocarbon Volumetric Analysis Using Seismic and Bore Data over Umon Field, Niger Delta –Nigeria”, Aigbedion and Aigbedion (2011) used composite geophysical logs, seismic section and check shot data to study the hydrocarbon volume. In their work, hydrocarbon bearing reservoirs were identified using the gamma ray and resistivity logs and the petrophysical parameters computed over each reservoir zone. Using the area extent estimated from the square grid method and by matching bright spot on the seismic they estimated the volume of hydrocarbon to be 1739170.11 cubic feet.

In Lee *et al.* (2014) research work, the only published research paper on reservoir characterization in the offshore Ghana titled “Reservoir Characterization of the Paradise and Hickory Discoveries offshore Ghana: Integration of Depositional and

Diagenetic Concepts” used integration of image logs, sidewall cores, seismic data and conventional logs to understand the depositional control on reservoir quality and deliverability within the field. The amplitude extraction was used in this work to delineate the sand area and the trend and shape of the amplitude extracts used to describe depositional environment. The image logs data with the extensive sidewall cores were used for the deposition facies model and a cross plot of porosity permeability was executed to check the reservoir quality. They concluded that the depositional architecture exerts a primary control on the reservoir quality in Ghana and should be considered in reservoir characterization. In the result, they alluded that higher permeability and porosity were encountered in the course grained channel axis sands with lower permeability and porosity off the channel sand axis.

The literature however, shows that several works have been published by researchers on reservoir characterization and its application using case studies of fields in their regional basins but little has been done in the discoveries in Ghana. None of these papers ever applied these techniques to the field under study. This research therefore seeks to contribute information to that effect by successfully integrating seismic attributes such as volume attribute of minimum amplitude extraction (VATMIN) and coherency attribute coupled with well logs information to characterize the Tweneboa Enyenra Ntomme field within the Deep Water Tano Basin.

### **CHAPTER THREE**

### **GEOLOGY OF THE TANO BASIN OF GHANA**

### 3.1 Introduction

Nearly half of Ghana's total area of about 135,000 km<sup>2</sup> is covered by sedimentary rocks with four main sedimentary basins namely: Accra-Keta Basin (cretaceous, offshore with onshore extension), Tano-Cape Three Points or the Western Basin (cretaceous, offshore with onshore extension), Voltaian Basin (Neo-Proterozoic, inland) and Saltpond or Central Basin (Paleozoic, offshore). The proterozoic and cretaceous basins constitute Ghana's continental margin, which expands from the Ghana -Togo border in the east to the Ghana-Cote D'Ivoire border in the West. This margin is part of the main Gulf of Guinea Province (Brownfield and Charpentier, 2006).

Approximately 125 Ma ago in the early cretaceous, Southern part of West Africa and the Northern part of South America began to rift and small basins opened as the thick continental crust was stretched and thinned (Brownfield and Charpentier, 2006). Basin infill was sourced from eroded upland continental areas. The tectonism caused both block and transforms faulting, and newly formed basins deformed along the transform faults which later became the fracture zones after active movements. As the continental crust was further thinned, sea floor spreading was initiated between late Aptian and Early Albian (~ 110 Ma). New oceanic crust formed at the trailing edges of the two continental plates as they began separating during late Albian (100 Ma). The two plates finally separated by late Santonian to Early Campanian (~85 Ma). The above movements were superimposed on an extensive Paleozoic basin, which existed along the margin prior to the extension and breakup. Figure 3.1 shows the locations of the four main sedimentary basins of Ghana.

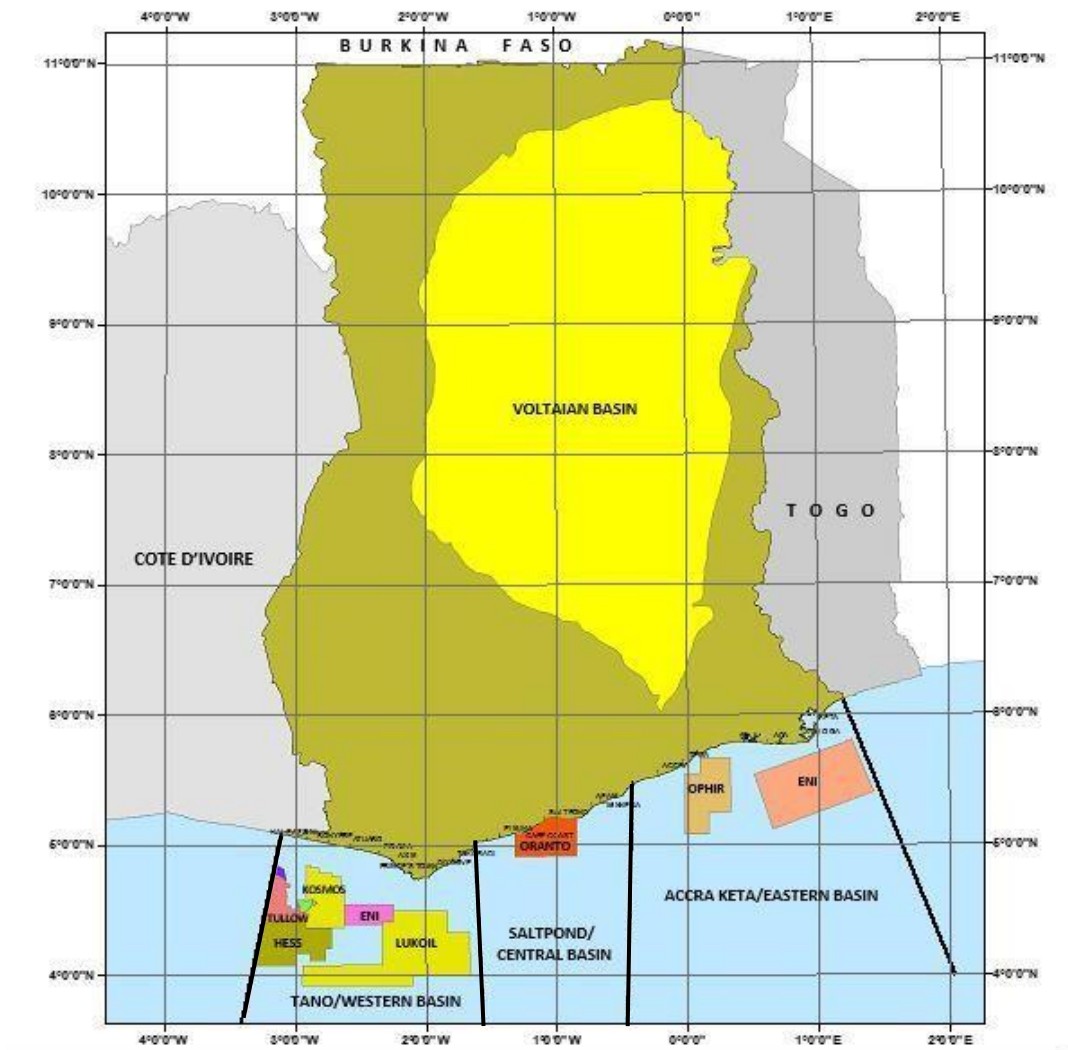


Figure 3.1: Map of Ghana showing the four sedimentary basins (GNPC, 2015)

### 3.2 The Tano-Cape Three Points Basin

The Tano-Cape Three Points Basin is a cretaceous wrench modified pull-apart basin confined by the St. Paul Fracture Zone in the west and the Saltpond Basin in the East. It is the eastern extension of the Ghana-Cote d'Ivoire Basin. The basin was formed as a result of trans-tensional movement during the separation of South America and Africa, and the opening of the Atlantic Ocean in the Albian which led to the deposition of rich thick organic shale in the Turonian and Cenomanian at the time. Clastic sediments were also funnelled into the basin from several rivers. As a result, large turbidites fan channel system were created. Cretaceous play is the main petroleum play

type of the Tano Basin with Albian and Turonian-Cenomanian shales serving as source rocks and the Albian sandstone in the sloped fault blocks as well as the turbidites slope fan sandstones of the Turonian also serving as the reservoirs. Trapping of hydrocarbons is both structural and stratigraphic. Based on onshore oil seeps, the hydrocarbon potential in the Tano basin has been known since the 1890s (Brownfield and Charpentier, 2006).

### **3.3 Stratigraphic Setting of the Tano Basin**

The stratigraphic setting of the Tano Basin within which the study area is located and its associated geology as shown in Figure 3.2 and Figure 3.3 have been described as follows:

#### **3.3.1 Aptian-Lower Albian (Kobnaswaso Formation)**

The lower Aptian sediments of the Kobnaswaso formation overlie the Carboniferous with an angular unconformity. Two mega-sequences are identified in the North and the South Tano areas. Fine to poorly sorted coarse grained sandstones with poor porosity forming thin to medium interbedded sandstones constituted the lower mega-sequence. It is also characterized by dark to olive grey, very micaceous and carbonaceous shales (Davies, 1986).

The upper Aptian mega-sequence is made up of 200 m thick shale unit interbedded with sandstone and siltstones. According to Davies (1986), the sandstones are made up of fine to medium grained, poorly sorted calcareous, dolomitic and argillaceous sediments. The shales are also medium to dark grey, sub fissile to fissile, silty and sometimes calcareous in nature (Ghana National Petroleum Cooperation, 1998).

Marginal marine depositional conditions are attributed to the upper mega-sequence.

### **3.3.2 The Lower-Middle Albian**

The lower-middle Albian is the major long term open marine transgression in the Tano Basin. It is dark grey, non-calcareous and micro-micaceous silts and sand. It ranges in thickness between 84 m and 262 m in the north Tano (Davies, 1986). The prevailing deposits were of marginal to shallow marine coupled with terrestrial depositions. In the south Tano the shale is medium to dark grey, sub fissile, micro-micaceous interbedded with silts to sands (Davies 1986).

### **3.3.3 The Uppermost Lower Albian-Middle Albian**

A study conducted by Ghana National Petroleum Cooperation (1998) assigned this formation an uppermost early Albian to middle Albian age. The thickness section in North Tano is penetrated by two different wells in the North Tano intersected thickness of 431 m and 436 m respectively.

Occasional fine sands, silts and non carbonates form the dark grey micro-micaceous shales of the formation. The lower section of the formation has medium grained calcareous sandstones with grey shaly partings. Depositional settings of the sediments are attributed to near shore marine to intertidal environments. However, the presence of planktonic foraminifera in the wells suggests occasional open marine influence, at inner neritic water depths (Ghana National Petroleum Cooperation, 1998).

### **3.3.4 Upper Albian (Domini Formation)**

The Upper Albian comprises of interbedded thin sandstones, carbonates, shales and siltstones. The sandstones in this formation are fine to moderate grained. Calcite cements are common in the formation yielding to the presence of poor porosity limestones interbeds which are micritic in texture. The depositional environment in the

North Tano area was more of near shore depositions and becoming more marine at the later period of deposits (Ghana National Petroleum Cooperation, 1998). The base of this formation is placed at the top of the shale in a projecting sandstone marker which can be interrelated within other wells in the Tano basin (Davies, 1986). The formation thickness of the upper Albian ranges between 431 m and 436 m. Angular unconformity exists between the top of the upper Albian and the base of the Cenomanian.

### **3.3.5 Cenomanian Formation**

The Cenomanian formation shows a wide disparity in thickness and lithology with the Tano sub-basin. It has a dominant condensed carbonate section which overlain the Cenomanian unconformity in the South Tano area. The base of the Cenomanian in the North Tano was picked at the top of the sequence of interbedded limestone and sandstones overlain by the thin sequence of black shale. In the Tano sub-basin, the Cenomanian have two limestones facies: deeper shelf oligostigmoid limestone which overlies shallow-water shaly limestones. Both facies are of late cretaceous age (Ghana National Petroleum Cooperation, 1998). In the North Tano area, the lower to middle Cenomanian is characterized by interbedded fine to coarse grained sands with occasional calcite cement and grey, variable silty mudstones. This unit was deposited under shallow, near shore and fully marine inner neritic conditions though slight open marine influence was also noticed (Ghana National Petroleum Cooperation, 1998).

In the South Tano, the unit is a representation of a condensed sequence which overlies an eroded upper Albian. Thin interbedded sands to oligostigmoid limestones, sandstones and shale characterized the middle to upper Cenomanian sequence. The sandstones are of fine to very coarse grains which are carbonaceous and calcareous in some sections with minor limestones and mudstones identified in the middle-upper Cenomanian in

the South Tano. This is an indication of offshore marine lower energy depositional conditions (Ghana National Petroleum Cooperation, 1998).

### **3.3.6 Turonian**

In the North Tano area, the top of the Turonian is picked at the top of series of thinly interbedded sandstones, limestones and shales. The Turonian shale is about 45 m to 90 m thick and is overlain by coarsening-up sandstones (Davies, 1986). At the South Tano, the Turonian is picked at the top of a shale section which overlain the Cenomanian limestones. The lithology through the Turonian interval consists of claystones with thinly interbedded siltstone and limestone. According to Davies (1998), the lithology was described as follows:

- 1. Claystone:**

Grey, dark grey, hard, platy, fissile in part, angular, earthy, slightly calcareous and silty.

- 2. Siltstone:**

Grey, pale grey, moderately soft, sub blocky, blocky, calcareous cement

### **3.3.7 Coniacian-Santonian**

This formation extends from the Turonian to the Campanian and is about 412 m thick. Sediments are predominantly dark grey shales with interbedded grey siltstones. Unconsolidated sands are prominent particularly towards the base of the formation. The sequence of depositions of sediments shows a fining upwards succession which is an indication of a marine deposition (Davies, 1986).

### **3.3.8 Uppermost Santonian to Intra Lower Campanian**

This formation represents a sandstone unit with two thick shale sequences. The sequences are well developed in the offshore Tano Basin. Their compositions are of

mudstones with thin carbonate stringers (Davies, 1986). Deposition of sediments were of marine shelf in South and North Tano (Davies, 1986).

### **3.3.9 Lower Campanian to Upper Campanian**

Deposition of sediments in this formation were predominantly made up of mudstones and minor carbonate-rich layers. The upper unit found in the Tano North, is characterised by the presence of sandstone. In the Tano North, initial short-lived transgressive episodes attaining outer neritic water depths were followed by deposition in a mainly middle to inner neritic setting. The Tano South has low energy depositional setting in a mainly distal shelf at outer neritic water depths (Ghana National Petroleum Cooperation, 1998).

### **3.3.10 Maastrichtian**

The Maastrichtian sequence is about 138 m to 178 m thick in the Tano basin. The Maastrichtian has two main sub-divisions: lower and upper units (Davies, 1986). The units comprise of coarse grain, unconsolidated, poor to well sorted sandstones interbedded with glauconitic and fossiliferous mudstones. Depositions occurred in inner neritic setting at North Tano while low energy conditions dominated the deposition in the South Tano. According to Davies (1986), the uppermost Maastrichtian sub-unit lies on top of the sandy Maastrichtian sequence which is made of shales and claystones. The upper to the middle part of the Maastrichtian sequence is characterized by the occurrence of glauconitic mudstones. The depositional environment, as stated by Davies (1986) for the middle to upper Maastrichtian at the North Tano is an offshore marine setting within neritic water depth.

### 3.3.11 Tertiary Sequences

The sediments in the Tertiary sequence belong to the upper Miocene to Paleocene age. The Paleocene lies unconformable on the Cretaceous which accounted for the absence of the lower Paleocene in the Tano basin (Ghana National Petroleum Cooperation, 1998). However sediments of upper Paleocene have been identified at North and South Tano. Glauconitic shales are in abundance in the top of the Paleocene at the Tano South. The Paleocene sediments represent the first transgressive-regressive cycle of sedimentation initiated during the Thanetian times. Deposition is in the deep marine low energy settings at inner neritic to bathyal water depths. The lower and the middle Eocene sediments were also identified in the Tano basin. The upper Eocene is absent due to regional unconformity in the area. Organic rich pyrites and glauconitic sediments constitute the lower Eocene mudstones (Ghana National Petroleum Cooperation, 1998). Figure 3.3 and Figure 3.4 below show the stratigraphic formations of the Tano Basin with the associated descriptions respectively.

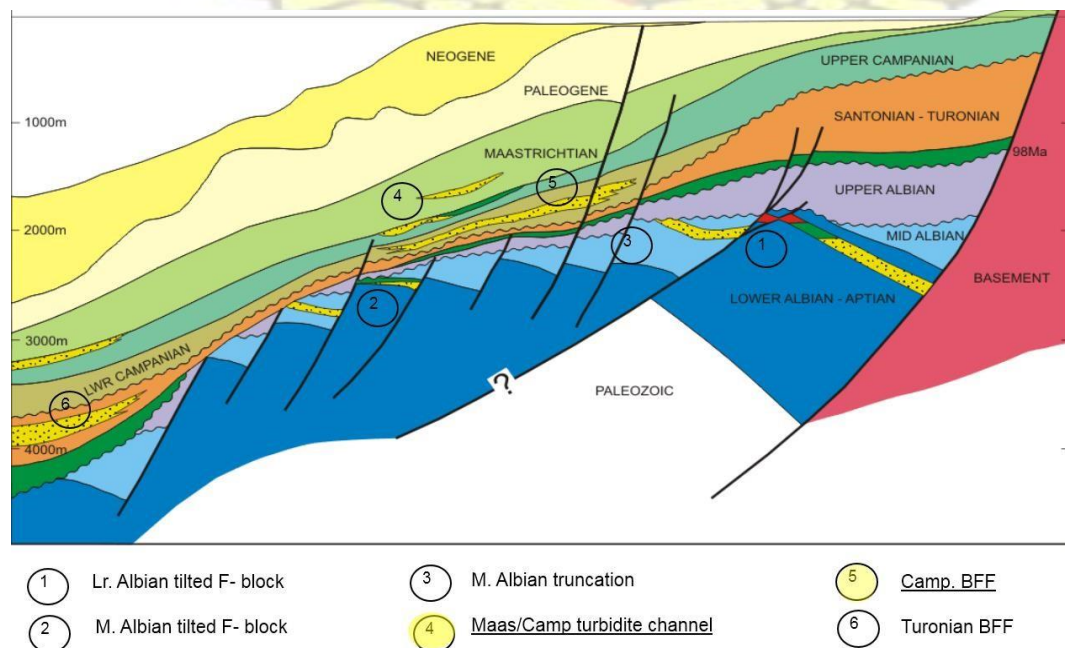


Figure 3.2: Stratigraphic section of the formations in Tano Basin (Sutherland, 2008)

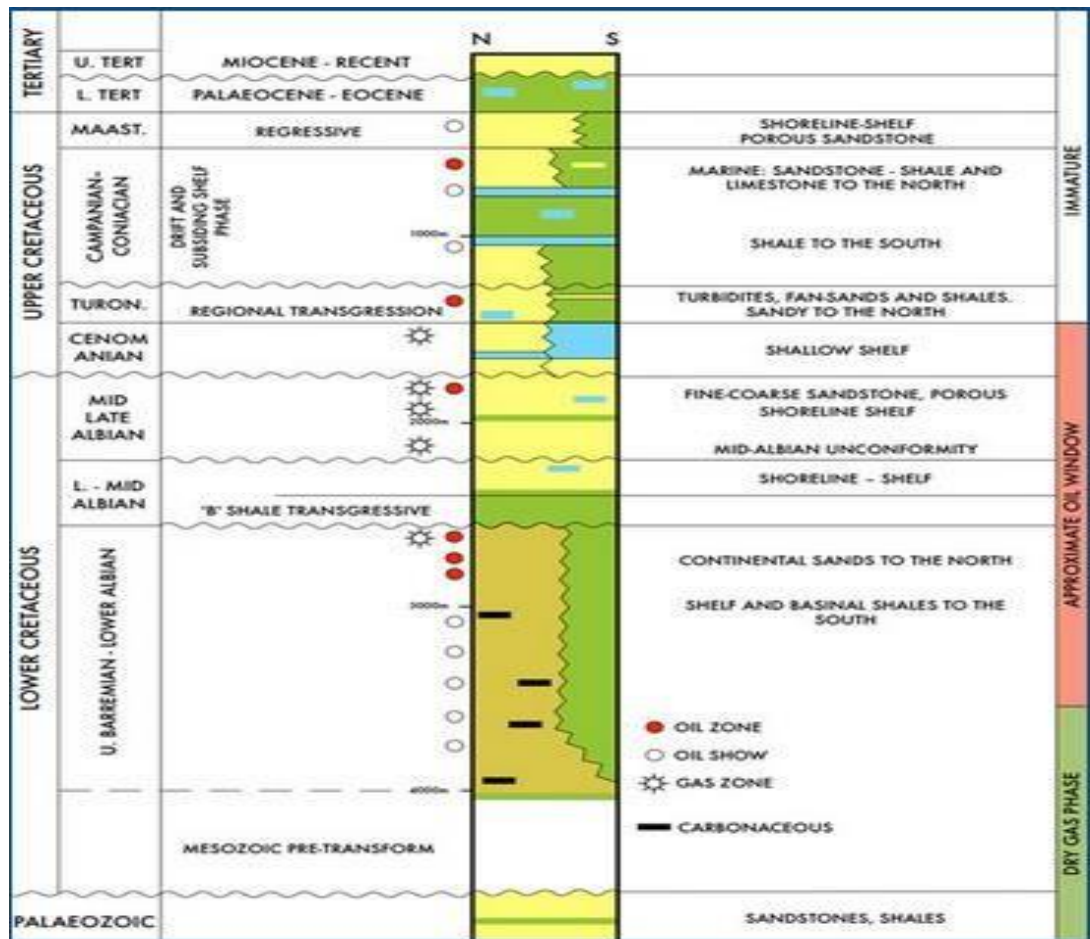


Figure 3.3: General Geology and Stratigraphy of the Tano Basin (Anadarko, 2011)

### 3.4 The History of Hydrocarbon Exploration in the Tano Basin

Hydrocarbon exploration of the Tano sedimentary basin started onshore way back in 1896 in today's administrative Western region. This was due to the discovery of onshore seepages of hydrocarbon found by early explorers. It is important to note that twenty one wildcats were drilled between 1896 and 1957 as part of the exploration expedition in Ghana (Ghana National Petroleum Cooperation, 2015).

In 1970, the offshore exploration begun with the drilling of the Volta Tano well. Subsequently, the first deep water exploration well named the South Dixcove-1X well was drilled by Phillips Petroleum in 1979 in water depth of about 900 m. Effort for

exploration and production activities intensified and in the 1980s, the government of Ghana established a new statutory and legal framework which yielded to the birth of GNPC in 1983. Consequently, 2D and 3D seismic over blocks onshore and offshore Tano were acquired which attracted foreign giant oil industry players into Ghana's exploration activities (Ghana National Petroleum Cooperation, 2015).

Over the past 15 years, the search for hydrocarbons in commercial quantities in the Tano basin was still on the rise. Giant industry players such as Tullow, Hess, Hunt oil, Kosmos and ENI Exploration and Production Company have entered the offshore Tano basin and have undertaken several exploration activities. In June 2007, the first commercial oil was discovered in the Jubilee field offshore Ghana by Kosmos Energy. Consequently, the Hyedua-1 appraisal well was drilled in August 2007 by Tullow oil in the neighbouring deep water Tano basin which confirmed continuous accumulation of hydrocarbon between the two concessions. Several blocks in the Tano Basin are undergoing prospecting and appraisal awaiting production (Ghana National Petroleum Cooperation, 2015).

### **3.5 The Petroleum System of the Tano Basin**

The petroleum system of the Tano basin is a Cretaceous System, dating from Aptian to Maastrichtian.

#### **3.5.1 Source Rocks (Aptian 120Ma – Turonian 93Ma)**

The use of paleogeographic maps and intercepted wells help to predict the deposition of source rocks in the Aptian, Albian, and Cenomanian and Turonian times. Small divergent basins developed during rifting in the Aptian were ideal for the deposition of lacustrine source rocks and coal. Prevailing conditions at the Cenomanian and Turonian also favoured the deposition of thick organic rich shales which followed later burial, generated hydrocarbons (Adda, 2013).

### **3.5.2 Reservoir Rocks (Aptian 113Ma – Maastrichtian 60Ma)**

Several paleo river systems such as the paleo Tano River that drained the western parts of Ghana and Cote d'Ivoire have funnelled significant clastic sediments into the deep basin which led to the formation of large turbidites channel complexes. Four possible reservoir rocks have been identified; namely the Albian, Turonian, Campanian and Maastrichtian sandstones (Adda, 2013).

### **3.5.3 Seals (Turonian 91 Ma – Maastrichtian 60 Ma)**

Turonian shales, Santonian shales, Maastrichtian mudstones and other intraformational mudstones serve as potential lateral, top and bottom seals for the hydrocarbon accumulations in the Tano Basin (Atta-Peters and Garry, 2014).

### **3.5.4 Traps**

The trapping mechanisms in the Tano basin are both stratigraphic and structural. A combination of both has been proved to be effective in the Jubilee field. The prominent trapping mechanism in this study area is stratigraphic. The reservoir sands are stratigraphically trapped by a combination of up dip and lateral pinch out (Atta-Peters and Garry, 2014).

# KNUST

## CHAPTER FOUR BACKGROUND THEORY

### 4.1 Introduction

This chapter provides a summary of seismic data, well logs and reservoir characterization concepts and other background topics necessary for understanding this thesis work.

### 4.2 Seismic Method

The development of the theory of seismic wave propagation in elastic, acoustic and anisotropic media was to permit modelling of seismic waves in complex 3-D earth models. One dimensional (1-D) and two dimensional (2-D) basic modelling have been employed within the hydrocarbon companies for exploration purposes for over 25 years (Doligez *et al.*, 1986). In this method, elastic waves are sent into the subsurface, and subsequently the energy that arrives back at the surface is recorded. This recorded energy is due to reflection, diffraction and refraction at subsurface boundaries. These boundaries are interfaces between layers of the earth that have different acoustic and elastic properties (Kearey *et al.*, 2002).

Much of the seismic theory was developed prior to the availability of instruments that were capable of sufficient sensitivity to permit significant measurement. In 1845, Mallet tried to measure the velocities in an experiment using artificial earthquakes (Telford *et al.*, 1990). In 1889, Knott developed the theory of reflection and refraction and in 1907 the wave theory was published by Zoeppritz and Wiechert. In the early 1920's Karcher developed a reflection seismograph that saw field use in Oklahoma (Telford *et al.*, 1990). The use of seismic method in petroleum exploration began in the United States Gulf Coast where Orchard Salt Dome field was discovered in 1924 (Telford *et al.*, 1990). The refraction seismic method was applied on this field. Its application is based on the ability of seismic energy to travel along interfaces between lithologies of different acoustic properties.

In 1927, three years after the application of the refraction method, a reflection seismic survey was also employed to aid the description of the Maud field in Oklahoma (Telford *et al.*, 1990). The reflection methods are the commonly used in the petroleum industry. The seismic data are combined with any available geological information and well data to determine as accurately as possible the subsurface structure and the material properties of the subsurface layers. The seismic methods, involving the application of various advanced data processing techniques, had developed into one of the most valuable tools for finding accumulations of oil and gas.

#### **4.2.1 Seismic Survey**

In seismic survey, controlled seismic source waves are generated and propagated through the subsurface. These waves will then return to the surface as result of reflection or refraction when they encounter subsurface geological boundaries. Geophones are then used to record the motion of the ground caused by the returning

waves. The arrival times of the waves at different ranges from source are measured which contain geological information about the subsurface (Kearey *et al.*, 2002).

#### **4.2.2 Seismic Waves**

Seismic waves are parcels of elastic energy generated by a sound source at the earth's surface or earthquakes. The sources appropriate for the seismic survey usually produce short-lived waves that encompass wide range of frequencies. The strains that accompanied the passage of a seismic wave are assumed to be minute and elastic except in the immediate vicinity of the source. Based on this postulate, the velocities of propagation of seismic pulses depend on the densities and the elastic moduli of the material through which the pulses propagate (Kearey *et al.*, 2002).

#### **4.2.3 Seismic Reflection Method**

Seismic reflection method is a geophysical method that applies the principles of seismology in order to estimate the earth's subsurface properties from seismic waves. A controlled seismic energy source such as air gun, vibroseis and dynamites are required in this method. For all exploration environments, the principle is to propagate sound energy into the subsurface where the different strata within the crust of the earth reflect this energy back. These reflected waves are recorded over a predetermined time period (called the record length) by using hydrophones in water and geophones on land. The reflected waves are stored onto a magnetic tape. Once the data is recorded, it can be processed using special software resulting in production of processed seismic profiles. This data sets are then interpreted for to ascertain the presence of hydrocarbon (Kearey *et al.*, 2002).

By knowing the seismic wave velocities in the rock and the measured travel time estimation of the depth to the reflector can be made. For example, the travel time of a reflected ray from a single horizontal reflector at depth  $z$ , beneath the top layer of velocity  $V$ , and with the detector-shot separation,  $x$ , can be calculated using the relation below (Kearey *et al.*, 2002).

$$t = (x^2 + 4z^2)^{1/2} / V \quad (3.1)$$

A series of apparently related reflections on several seismograms is often referred to as a reflection event. By correlating reflection events, a geoscientist can generate a cross section of the geological structures. High three dimensional computer graphics with special software are used in interpretation of large survey data.

#### **4.3 History of the Extended Elastic Impedance (EEI)**

Whitcombe (2002) was the first to introduce the Extended Elastic Impedance (EEI) as a seismic attribute for fluid and lithology prediction in his effort to refine the definition of elastic impedance. Whitcombe main aim is to broaden the definition of elastic impedance to remove the dependence of its dimensionality on the angle  $\theta$ . Whitcombe *et al.* (2002) estimated the water saturation and gamma ray logs from EEI using data from the Forties field in the central North Sea. Naves *et al.* (2004) equally estimated gamma ray logs for a gas play in central Saudi Arabia. Both authors calculated the correlation coefficients between appropriate petrophysical logs with the EEI logs between  $-90^\circ$  and  $+90^\circ$ .

The Extended Elastic Impedance was introduced to improve the limitation on Elastic Impedance theory for rock properties prediction. In the Elastic Impedance theory, some

properties of rock cannot be predicted from existing seismic gather due to limitations on incidence angles. Hence, the EEI concept was introduced to extend the angle from 0-30 degrees to -90 to 90 degrees in theory (Hicks and Francis, 2006) as shown in Figure 4.1. Consequently, the rock properties that are associated with higher angles can be predicted.

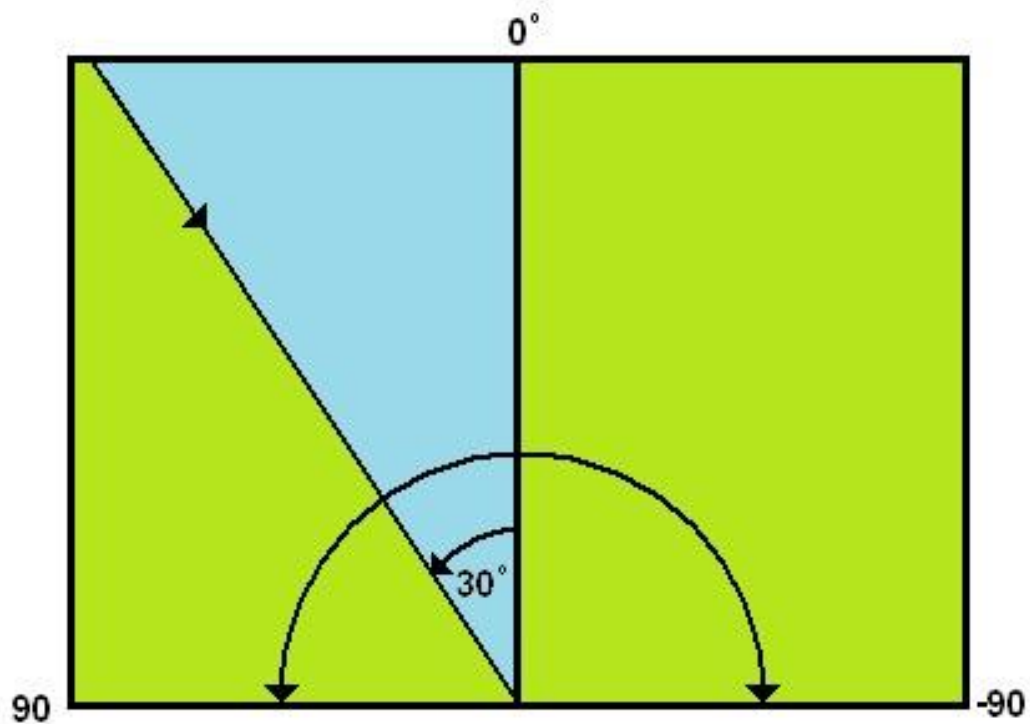


Figure 4.1: Extended elastic impedance angles ranging from  $-90^\circ$  to  $+90^\circ$ , at which values  $\sin^2\theta$  is physically impossible (adopted from Hampson-Russell, 2006).

According to Francis and Hicks (2006), the distinct difference between the extended elastic impedance and normalized version of elastic impedance is the change of variable. EEI is a function of  $\chi$  (an angle in an abstract construction) and EI is a function of  $\theta$  (an angle in a physical experiment). It is important to notice that new variable ( $\chi$ ) allows calculation of impedance value beyond physically observable range of angle  $\theta$  (including imaginary angles not necessarily recorded in the gathers). A clear example of this situation happens when shear impedance corresponds to  $\sin^2\theta = -1.25$ . It is

obvious, negative angle is not physically recordable but can be projected from angle gathers by linear extrapolation (Francis and Hicks, 2006).

It is easy to show that the EEI log at  $\chi = 0$  is similar to EI log at  $\theta = 0$ , which is simply the acoustic impedance (AI). Under certain approximation, the EEI log at various  $\chi$  angles is proportional to different rock elastic parameters. In other words, the  $\chi$  angle can be selected to optimize the correlation of the EEI curves with petrophysical reservoir parameters, such as  $V_{\text{shale}}$ , water saturation and porosity or with the elastic parameters such as bulk module and shear module. Therefore, the EEI for specific angles from these parameters can be produced by using EEI equation which is suited for tie well data directly to seismic data (Shahri, 2013).

For instant the EEI data for this study is Tano EEI Chi80 which is the degree to which the well logs correlate with the seismic data which is 80 degree. This data is lithology conditioned.

#### **4.4 Seismic Attributes**

All measurements derived from the seismic data are called seismic attributes (Sheriff, 2002). Seismic attributes are used to help interpreters at all levels, ranging from analysis of regional depositional systems to details mapping of structures, stratigraphic and rock properties. From 1970s where seismic attributes were first introduced, they have become very important tool in reservoir characterization for geoscientists.

According to Chopra and Marfurt (2007), seismic attributes such as amplitude, root mean square (RMS) amplitude, envelope, minimum amplitude, elastic impedance, acoustic impedance, spectral magnitude and amplitude versus offset (AVO) are directly

sensitive to seismic impedance changes. Other seismic attributes such a peak frequency, bandwidth and peak-to-trough thickness are sensitive to layer thicknesses. Both classes of attributes can be correlated quantitatively to well control by using geostatistics, multivariate analysis or neural networks. Coherency, amplitude gradients, level cooccurrence matrix measures, dip- azimuth, curvature and sobel filter-based edge detectors attributes are directly sensitive to the seismic morphology and textures. Geologic facies analysis are also predicted qualitatively by incorporating geological depositional model, seismic geomorphology, seismic stratigraphy principles and structural deformation.

Subrahmanyam and Rao (2008) classified seismic attributes into two categories namely; Physical and Geometrical attributes. Attributes that are directly linked to the propagated waves and lithology are defined as physical attributes. They are further classified as post-stack and pre-stack attributes with each sub-classified into wavelet and instantaneous attributes (Subrahmanyam and Rao, 2008). Instantaneous attributes are computed sample by sample and indicate continuous change of attributes along the time and space axis. The wavelet attributes, on the other hand represent wavelet and their amplitude spectrum characteristics (Subrahmanyam and Rao, 2008).

The geometrical attributes include azimuth, dip and discontinuity. The dip attribute or amplitude of the data corresponds to the dip of the seismic events. The dip amplitude is important in delineating faults because it makes faults more discernible. The amplitude of the data on azimuth attribute corresponds to the azimuth of the maximum dip direction of the seismic feature. Figure 4.2 shows a summary of seismic attributes computed from seismic data (Herron 2011).

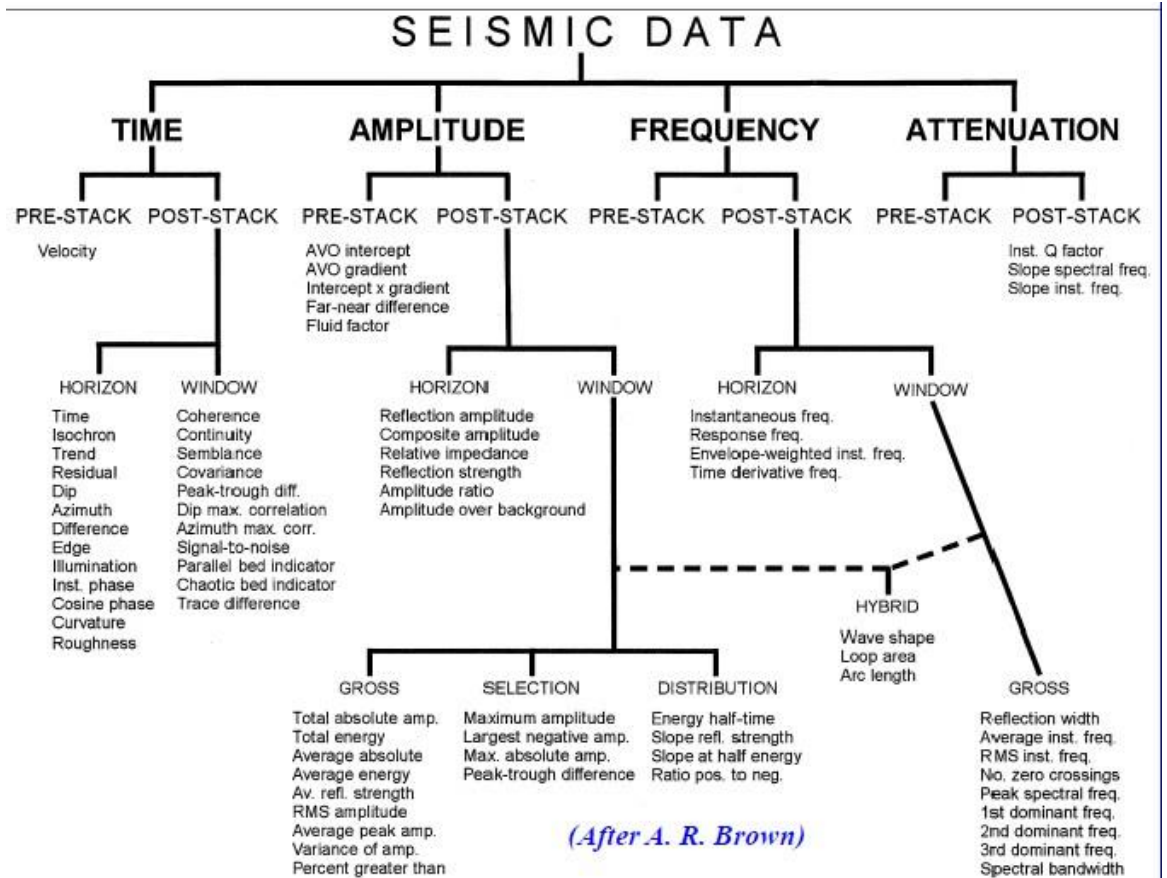


Figure 4.2: Summary of seismic attributes (After Brown A. R., 1996)

For the purpose of this research work, the two seismic attributes, amplitude and Coherence are described below.

#### 4.4.1 Amplitude

Amplitude is simply the measure of the strength of the reflected signal. That is the reference for the amplitude reflection seismic data is zero; so amplitude are positive or negative in accordance with agreed polarity and display conventions. In terms of a simple two layer model, the magnitude and algebraic sign (positive or negative) of the amplitude of a reflection from a single isolated acoustic impedance boundary is directly proportional to the magnitude and algebraic sign of the reflection coefficient (RC) at that boundary (Herron, 2011).

Seismic amplitudes are manifestation of geology because they can measure rock fluids and estimate pore fluid type (Herron, 2011). Standard procedures for amplitude extraction of individual reflection as well as of user-specified intervals of interest are used in most modern workstation systems. Such standard extractions include; amplitude, maximum positive amplitude (VATMAX), average absolute amplitude, root mean square (RMS) amplitude, volume attribute of minimum amplitude (VATMIN) and many more. For the purpose of this work, the amplitude extractions used for the reservoir studies are described below.

#### **4.4.1.1 Volume Attribute of Minimum Amplitude (VATMIN)**

The VATMIN is a volume attribute of minimum amplitude (VATMIN) that retains the most negative amplitude in the depth range of the formation of interest. This attribute is computed only on a window. The use of VATMIN is to delineate the sand prone area which are recognized as trough (negative polarity on the seismic data) as compared to shale which are recognized as peak (Beaupretre, 2015).

#### **4.4.1.2 Coherency Attribute**

Coherency attribute is a seismic volume attribute which is computed only on 3-D seismic data. It compares the trace similarities of the seismic wave forms within a small analysis window (Herron 2011). This technology was first developed by Amoco (Bahorich & Farmer, 1995) to help in more complete use of the enormous information contained in 3-D seismic volume to complement standard interpretation techniques. Because important geological elements like faults and depositional features like channels, fans are recognized as discontinuities in seismic data, coherence attribute is very useful in identifying and visualising the features which are used in describing the depositional environment in reservoir characterization (Herron, 2011).

## 4.5 Seismic Data in Reservoir Characterization

The travel time, the character of events, amplitude, and the patterns of events are the measurable parameters from the seismic data. From these parameters, we can obtain the following geological information (Sheriff, 1992):

1. Depth maps of important horizons from travel times and velocity information.
2. Contrast in rock properties from measurements of reflection amplitude.
3. Locations of faults and stratigraphic changes from reflection discontinuities patterns.
4. Dip and discontinuities from differences in travel times along a surface.
5. Estimation of lithology, porosity and fluid content from internal velocity;
6. Hydrocarbon locations, changes in porosity, lithology and thickness from lateral amplitude changes.
7. Depositional environments, or faults and fractures from seismic data patterns;

## 4.6 Reservoir Maps

The reservoir maps generated and used in general sense in understanding the geology of reservoir. In reservoir characterisation process, reservoir maps are used to determine particulars such as thickness, oil water contact, and net pay of a specific formation. These maps include isochron maps, depth structure maps, isopach maps and isochore maps. The depth structure maps and Isopach maps are described below for the purposes of this research work (Baker Hughes, 1999).

### 4.6.1 Depth Structure Maps

These show contours of a particular horizon, with the contour representing depths to that horizon from sea-level or ground level. They are derived from depth conversion of two way travel times of the seismic data. Subsurface structure maps are often

constructed for specific stratigraphic horizons to show three dimensional geometric shapes of these horizons. Accurate structural interpretation is required to ensure that the geology has correctly been determined and this required interpretation of closures and faults (Baker Hughes, 1999).

#### **4.6.2 Isopach Maps**

Isopach maps illustrate the true stratigraphic thickness of a unit. An isopach unit may be as small as just a few metres thick or as large as a thousand metres thick covering a number of sand units. These maps are extremely used in determining the structural relationship responsible for a given type of sedimentation, the shape of a basin, the position of the shoreline, areas of uplift, and in some circumstances the amount of vertical uplift and erosion, can be recognized by mapping the variations in thickness of a given stratigraphic interval (formation). Isopach maps are also used for depositional environment studies, depositional fairway studies, and calculation of hydrocarbon volumes. They can identify the concentrations of sands and hopefully provide insight to delta channel location (Baker Hughes, 1999).

#### **4.7 Depositional environment**

According to Slatt (2006) depositional environment is a geomorphic setting in which a set of biological, chemical and physical processes operate to produce a certain kind of sedimentary deposit. Three main classification was propounded by Slatt (2006) namely:

1. Continental deposits
2. Marginal-marine or Transitional deposits
3. Marine deposits.

#### 4.7.1 Continental Deposits:

Continental deposits include the following:

##### A. Fluvial deposits

1. Alluvial fan: Alluvial fans are sedimentary deposits developed in areas of high relief, where there is an abundant supply of sediment. They can pass downward through a variety of sedimentary environment, or build into lakes, alluvial or deltaic plains, tidal flats, and deep water basins.
2. Braided River: Braided sedimentary depositional environments are those areas in which river flow diverges and rejoins around bars within a more or less defined channel. They have higher clay to sand ratio with the sandstone having greater lateral extent. The geometry of deposits due to meandering and braided deposits are quite different and have a strong significance in their value as petroleum reservoirs (Baker Hughes, 1999).
3. Meandering river deposits have more developed distribution of channel processes and greater distinction between channel and over bank deposits.

B. **Desert:** These are sediments accumulated by the action of wind, wash from upland slopes and ephemeral streams.

#### 4.7.2 Transitional Deposits

These deposits include:

1. **Deltas:** Deltas are distinct extensions from the shoreline where rivers enter marine or fresh-water depositional basins and supply sediments faster than the basin processes can redistribute them. The morphology of deltas is dominated by fluvial processes like lobate and birdsfoot resulting in crevasses splays, channels and sand bars (Baker Hughes, 1999)

2. **Lagoons:** shallow elongate body of water between the mainland and barrier island where circulation is commonly restricted and access to marine waters.

### 4.7.3 Marine Deposits

Marine sediments depositions occur at different section of the marine body. Marine environments include continental shelf (Shallow Marine), continental slope and rise (intermediate seas) and deep sea floor (Deep Marine). Coarser sediments are deposited near shores in shallow marine environment. At continental slopes, sediments are mostly fine materials. Sediment depositions are mainly from meteoric, volcanic and pelagic organic with poorly sorted siliceous and calcareous oozes. Figure 4.3 below is an illustration of the various depositional environment (Pyles, 2007).

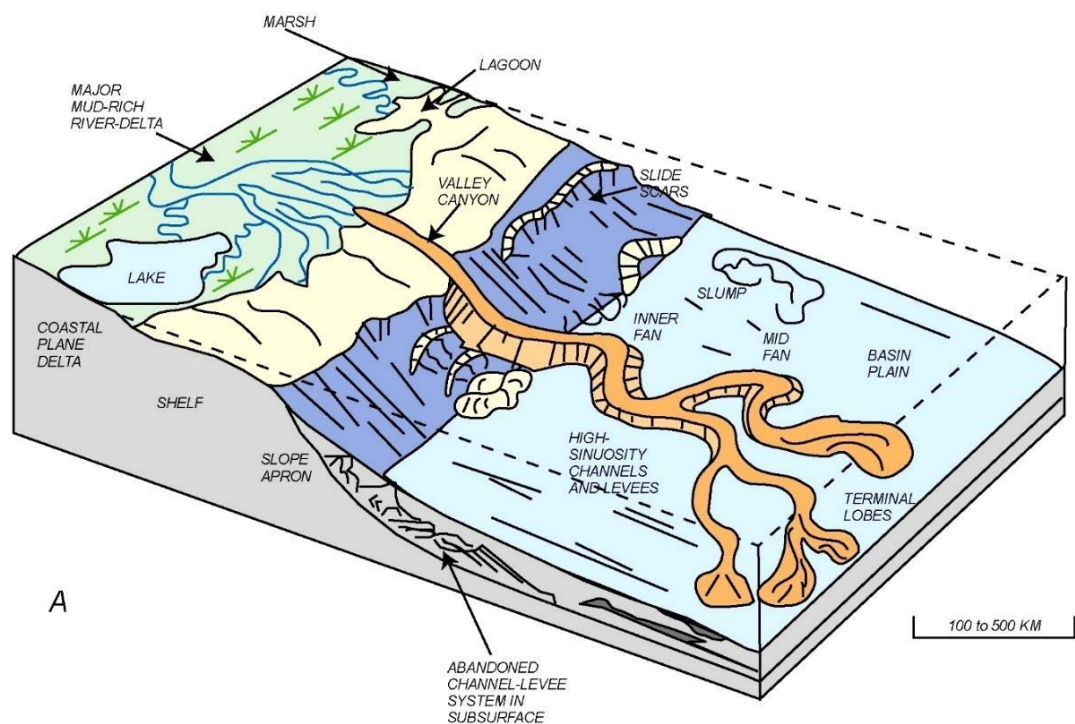


Figure 4.3: A Schematic diagram showing depositional environments (Pyles, 2007).

### 4.8 Architecture Elements.

Many authors have studied the concept of architectural elements. Miall (1985) defines architectural elements as “a lithesome” characterized by its geometry, facies composition, and scale, and represents a particular process or suite of processes occurring within depositional fairways. According to Pyles (2007) these elements act as a fundamental building block for larger stratigraphic units including trapping system and are considered the host of good sand bodies. The principal architectural elements in submarine or deep water system include channel, sheet, lobes, canyon and levees as seen in Table 4.1. Knowledge about the depositional system of a reservoir helps in enhancing recoverability of oil and in reservoir stimulation model.

**Channel elements** are submarine conduit for sediment to be transmitted into the deeper water environments (Pyles, 2007). They host coarse deposits in fluvial systems with geometry of channels is defined by depth sinuosity and sand body thickness. They are characterized by channel margins which become gentle in slope with increasing channel width (Baker Hughes, 1999). This can be seen in Figure 4.4.

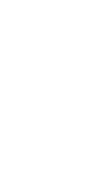
**Lobe element or frontal splay** described depositional elements that are formed at the terminal end of channels, and tend to form a lobe shape in plain view (Posamentier and Walker, 2006). Normark *et al.* (1979) described a lobe as an element located basinward of a submarine channel which is composed of sediments that are eroded and transmitted through channel.

**Levee elements** are described by Posamentier and Walker (2006) as “overbank”, spillage which is composed of levees or crevasse splays. **Levees** are sedimentary deposits formed on concave or steep bank channel due to sudden loss of the strength of

streams as they overlap their banks. Sediment deposits are coarser and thickest closed to the channel sand and gets thinner and finer toward the flood basin (Boggs Jr, 1995)

**Crevasse splay** are thin sandstones deposits within floodplain claystones and siltstones, deposited by meandering rivers that have breached their banks when turbidity currents within the channel spill are higher than the channel wall (Miall, 1996). Table 4.1 shows the principal architectural elements; the shapes and the trends of the various architectural elements.

Table 4.1. Principal Architecture elements of deep water clastic systems (Reading and Richard, 1994).

SYSTEM TYPE	WEDGES	CHANNELS	LOBES	SHEETS	CHAOTIC MOUNDS
GRAVEL-RICH SYSTEMS		CHUTES 			
SAND-RICH SYSTEMS		BRAIDED 	CHANNELIZED-LOBES 		
MUD/SAND-RICH SYSTEMS		CHANNEL-LEVEE 	DEPOSITIONAL LOBES 		SLUMPS & SLIDES 
MUD-RICH SYSTEMS		CHANNEL-LEVEE 	DEPOSITIONAL LOBES 		SLUMPS & SLIDES 

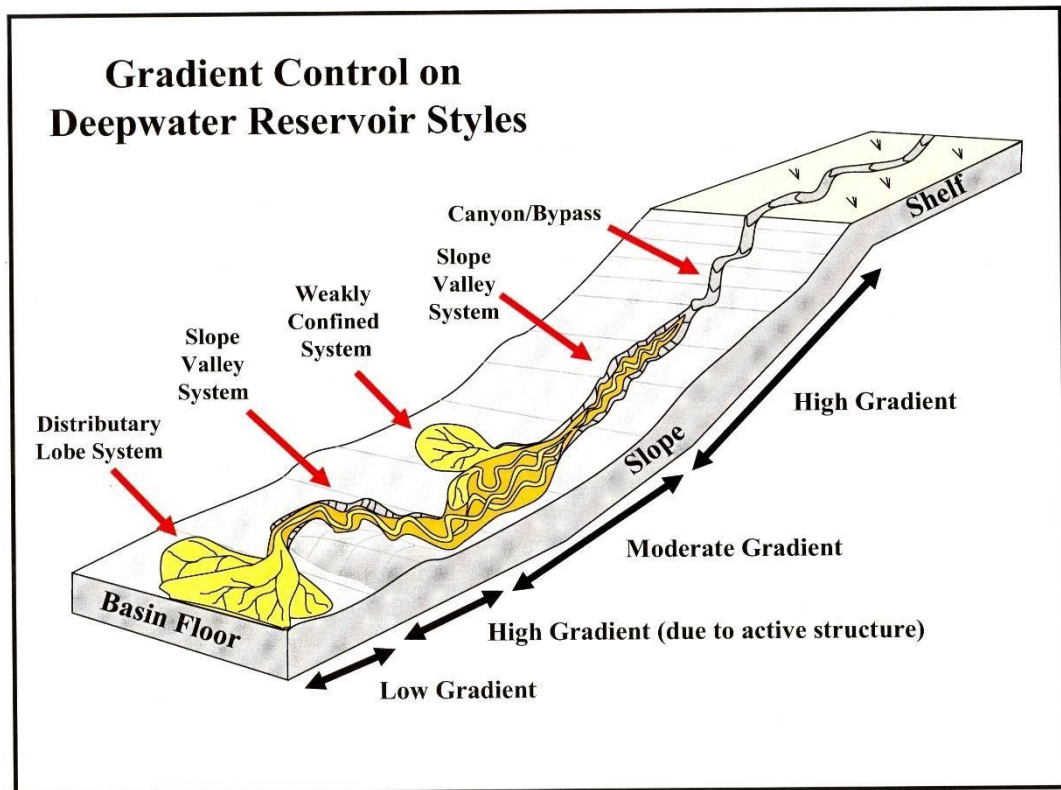


Figure 4.4: Slope Control Architectural Elements of Deepwater Reservoirs (Posamentier and Kolla, 2003).

#### 4.9 Borehole logging

Wireline logging refers to the practice within the oil and gas industry of lowering a logging tool attached to a wireline into an oil well to measure the rock and fluids properties of the formation. The measurements obtained are then interpreted and used to determine the depths and zones where oil and gas can be found. The continuous recording of a geophysical parameter along a borehole produces a geophysical well log. The value of the measurement is plotted continuously against depth in the well (Ryder, 2002). In 1931, Henri George Doll and G. Dechatre who were working for Schlumberger, discovered that the galvanometer wiggled even when no current was being passed through the logging cables down in the well. This led to the discovery of the spontaneous potential (SP) which was as important as the ability to measure resistivity. The SP effect was produced naturally by the borehole mud at the boundaries

of permeable beds. By simultaneously recording SP and resistivity, loggers could distinguish between permeable oil-bearing beds and impermeable nonproducing beds (Telford *et al.*, 1990).

In 1940, Schlumberger introduced the spontaneous potential dipmeter; this instrument allowed the calculation of the dip and direction of the dip of a layer. The basic dipmeter was later enhanced by the resistivity dipmeter in 1947, and the continuous resistivity dipmeter in 1952 (Schlumberger, 1991). Oil-based mud (OBM) was first used in Rangely Field, Colorado in 1948. Normal electric logs require a conductive or waterbased mud, but Oil-based muds are nonconductive. The solution to this problem was the induction log, developed in the early 1950s (Schlumberger, 1991). The introduction of the transistor and integrated circuits in the 1960s made electric logs vastly more reliable. Computerization allowed much faster log processing, and dramatically expanded log data-gathering capacity. The 1970s brought more logs and computers. These included combo type logs where resistivity logs and porosity logs were recorded in one pass in the borehole. The two types of porosity logs (acoustic logs and nuclear logs) date originally from the 1940s. Sonic logs grew out of technology developed during World War II. Nuclear logging has supplemented acoustic logging, but acoustic or sonic logs are still run on some combination logging tools (Telford *et al.*, 1990).

Nuclear logging was initially developed to measure the natural gamma radiation emitted by underground formations. However, the industry quickly moved to logs that actively bombard rocks with nuclear particles. The gamma ray log, measuring the natural radioactivity, was introduced by Well Surveys Inc. in 1939, and the Well Survey Incorporation neutron log came in 1941 (Telford *et al.*, 1990). The gamma ray log is

particularly useful as shale beds which often provide a relatively low permeability cap over hydrocarbon reservoirs usually display a higher level of gamma radiation. These logs were important because they can be used in cased wells (wells with production casing) (Schlumberger, 1991). Many modern oil and gas wells are drilled directionally. At first, loggers had to run their tools somehow attached to the drill pipe if the well was not vertical. Modern techniques now permit continuous information at the surface. This is known as logging while drilling (LWD) or measurement-while-drilling (MWD). Measurement while drilling logs use mud pulse technology to transmit data from the tools on the bottom of the drillstring to the processors at the surface (Schlumberger, 1991).

#### **4.10 Well logs in Reservoir Characterization**

Well logs analyses are used in estimation of petrophysical parameters such as porosity, permeability, water and hydrocarbon saturations and detection of lithology. Different reservoir properties are determined by different logs.

Gamma Ray log in reservoir characterization is useful for identifying lithologies, calculating shale volume and correlating between formations. The gamma ray log normally reflects the shale content of the formation because of the concentration of radioactive elements in the shale/clays. Shale free sandstones have low gamma ray value unless they are contaminated by radioactive elements. High gamma ray values are indication of shale zones (Baker Hughes, 1999).

Neutron logs are used as porosity logs in estimating porosity. This can be combined with density log for estimation of porosity. Neutron logs measures the hydrogen concentration in a formation. In a clean reservoir filled with oil and gas the log measures liquid filled porosity (Baker Hughes, 1999). The Density log in formation evaluation

measures the electron density of the formation. It consists of a radioactive source that emits gamma rays into the formation and one or more gamma ray detectors located at fixed distance from the source (Baker Hughes, 1999).

#### **4.11 Petrophysical Parameters**

To have a producing hydrocarbon reservoir, certain properties must exist. These properties help to assess the commercial viability of the reservoir. There must be rocks having sufficient porosity to accommodate the reservoir fluids and permeability to permit their movement. The rocks must contain hydrocarbons in commercial quantities (Baker Hughes, 1999). The petrophysical parameters are described below.

##### **4.11.1 Porosity**

Porosity is the measure of the portion of rock that is composed of non-rock voids and may be filled with hydrocarbon. Porosity can vary from less than 5 percent in tight sandstones to more than 30 percent in unconsolidated sands.

##### **4.11.2 Water Saturation**

Natural pore water is a good conductor of electricity due to the presence of dissolved salts. Hydrocarbons are poor conductors and cause an increase in the measured resistivity of a rock relative to that with water. Hydrocarbons displace pore water and cause it to be reduced to an irreducible level. Archie (1942) came out with a method of estimating water saturation based on laboratory measurements of resistivities for sandstone core of varying degree of hydrocarbons. The Archie's equation is given as  $S_w = (R_f / R_h)^{1/n}$ , where n is assumed to be 2,  $R_f$  and  $R_h$  are resistivity of matrix + pore water

$R_h$

and matrix + pore water + hydrocarbon respectively.

#### **4.11.3 Permeability**

Permeability is the capacity of a rock to transmit fluids. The degree to which the rock transmits fluid depends on the shape and size of pores, the shape and size of their interconnections, and the extent of interconnections. It is measured in milliDarcy (mD) (Baker Hughes, 1999).

#### **4.11.4 Net to Gross Ratio**

According to Dean and Mireault, (2008), net-to-gross ratio is the fraction of the net pay sand of a reservoir from which oil and gas can be produced at economic rate to the gross pay sand (zone) of a reservoir which is the overall interval within the pay sand exists.

#### **4.12 Volumetric Estimation**

Volumetric estimation is the only means available to assess hydrocarbons in place prior to acquiring sufficient pressure and production information to apply material balance techniques (Dean and Mireault, 2008). Recoverable hydrocarbons are estimated from in place estimates, and a recovery factor that is estimated from analogue pool performance and/or simulation studies. Therefore, volumetric methods are primarily used to evaluate in-place hydrocarbons in new, non-producing wells and pools, and new petroleum basins (Dean and Mireault, 2008).

Volumetric estimation is based on cores, analysis of wireline logs, and geological maps. Knowledge of the depositional environment, the structural complexities, the trapping mechanism, and any fluid interaction is required. Information such as Trap Gross Rock Volume (GRV), Net-To-Gross (N/G), Porosity, Hydrocarbon Saturation, Formation Volume Factor (FVF), Type of Fluid, Recovery Factor (RF), and the area extent of the accumulation (A) are considered when assessing the volume of hydrocarbon in place. For

oil reservoirs the original oil in place (OOIP) volumetric calculation is:  $OOIP (m^3) = \text{Rock Volume} \times \Phi \times (1 - S_w) \times (1/B_o)$  and in API Stock tank conversion  $STOIPP (Bbl.) = RV \times (N/G) \times (1 - S_w) \times (1/B_o) \times CF \times RF$  (Dean and Mireault, 2008).

Where:

STOIPP = Stock Tank Oil Initially In Place

Rock Volume ( $m^3$ ) =  $A \times h$

$A (m^2)$  = Drainage area (lateral extent of the reservoir)  $h$

$(m)$  = Gross pay thickness, metres

$\Phi$  = Porosity, fraction of rock volume available to store fluids

$S_w$  = Volume fraction of porosity filled with interstitial water

$B_o$  = Formation volume factor ( $m^3/m^3$ ) (dimensionless factor for the change in oil volume between reservoir conditions and standard conditions at surface)

$1/B_o$  = Shrinkage (Stock Tank  $m^3$ / reservoir  $m^3$ ) = volume change that the oil undergoes when brought to the earth's surface due to solution gas evolving out of the oil.

Conversion factor (CF) converts cubic metre to stock tank barrels ( $1 m^3 = 6.29$  barrel). To calculate recoverable oil volumes the OOIP must be multiplied by the Recovery Factor (fraction). The recovery factor is one of the most important, yet the most difficult variable to estimate. Fluid properties such as formation volume factor, viscosity, density, and solution gas/oil ratio all influence the recovery factor. In addition, it is also a function of the reservoir drive mechanism and the interaction between reservoir rock and the fluids in the reservoir. Some industry standard oil recovery factor ranges for various natural drive mechanisms are listed below:

1. Solution gas drive 2 – 30%
2. Gas cap drive 30 – 60%
3. Water drive 2 – 50%
4. Gravity Up to 60% (Dean and Mireault, 2008).

# KNUST



## CHAPTER FIVE

### METHODOLOGY

#### 5.1 General Overview of Workflow

The method of approach in this study was catalogued into four main components. The first component dealt with the generation of structural maps for structural interpretation.

The steps involved: Loading of formation tops, generation of the synthetic seismograms, picking of horizons (interval of interest), picking of faults on seismic section, generating of depth structural maps and isopach maps.

The second component dealt with delineation of the reservoir sand occurrence zones using Volume Seismic Attribute (amplitude, Volume Attribute of Minimum Amplitude-VATMIN) computed on the horizons of interest.

The third component looked at the general depositional environment using coherency rock solid attribute maps. The detailed architectural elements of the reservoirs were also analysed by computing VATMIN on the generated ISO-proportional intervals on the EEI data (lithology conditioned EEI Chi80) within the Turonian and Santonian.

The final section looked at the integration of the seismic and well logs for the reservoir characterization. This includes five main parts:

- (i) Well correlation to find reservoir units or zones within the delineated reservoirs using gamma ray logs,
- (ii) Seismic to well tie using the gamma ray logs, the EEI data (EEI Chi80 lithology conditioned) and the ISO-proportional interval.
- (iii) Computation of petrophysical parameters of each reservoir units i.e. estimation of porosity of the identified reservoirs, permeability, water saturation volume, net and gross thickness, etc.
- (iv) Reservoir quality analysis using porosity permeability cross plots.
- (v) Estimation of volume in-place hydrocarbon using the computed petrophysical parameters, and the area extent from the seismic attributes maps.

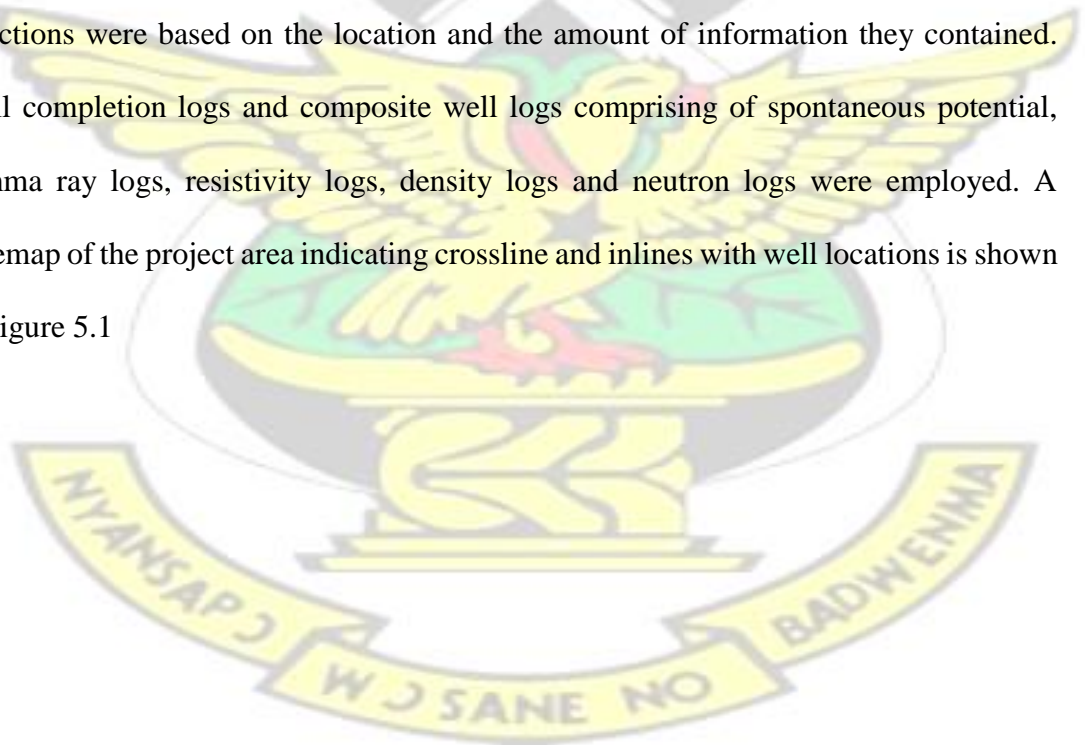
## 5.2 Data Sets

### 5.2.1 Seismic Data

Two main 3-D seismic data sets namely the normal reflectivity Deep Water Tano Prestack Depth Migrated (PSDM) and Extended Elastic Impedance (Tano EEI chi80 lithology conditioned) data from Ghana National Petroleum Cooperation were used for this research. The data covers an area of about 650 km<sup>2</sup>. Literature on the data sets revealed that amplitude versus offset (AVO) is unreliable indicators of reservoir oil water contact or gas oil contact, rather, relatively high negative seismic amplitude are however hydrocarbons sand depositional fairways in this block.

### 5.2.2 Well data.

Five (5) wells namely W1, W3, W4, W5, and W6 were engaged in the study. Well selections were based on the location and the amount of information they contained. Well completion logs and composite well logs comprising of spontaneous potential, gamma ray logs, resistivity logs, density logs and neutron logs were employed. A basemap of the project area indicating crossline and inlines with well locations is shown in Figure 5.1



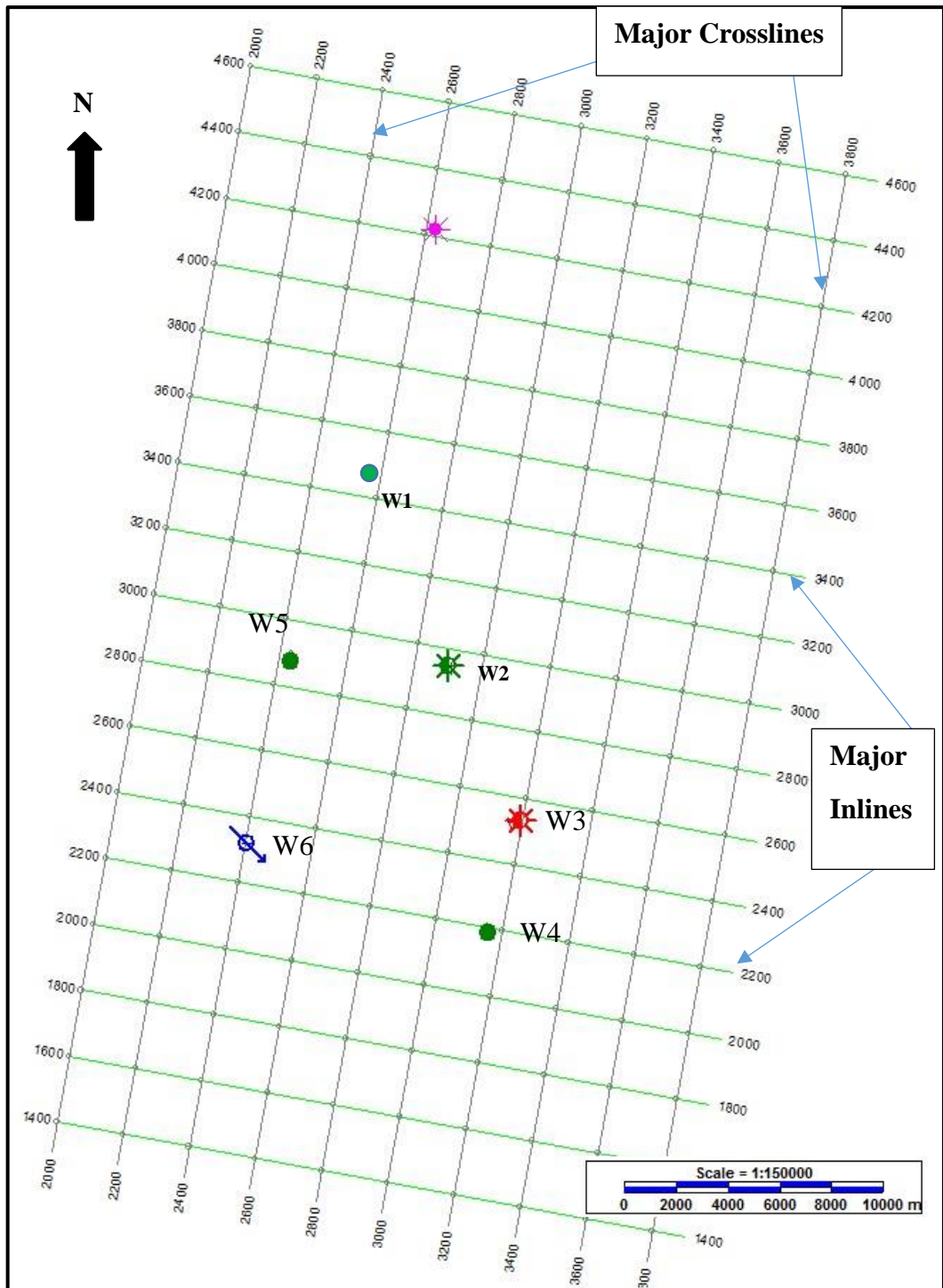


Figure 5.1: Base map of the survey Area showing principal Inlines and Crosslines

### 5.3 Software Package

Kingdom Suite Package software (2D/3D-EarthPak, EarthPak) was the main software employed for both seismic data interpretation and well log analysis. The Kingdom SynPak was used for constructing synthetic seismograms and the seismic matching. The 2D/3D-

EarthPak was used for the horizons interpretations and to create structural maps as well as extraction of amplitudes. Interactive Petrophysics (IP) was used for computation of petrophysical properties.

#### **5.4 Data Quality Check**

Both seismic data sets were quality checked for misties. This data has polarity with the peak (+) in black coloration and red colour represents the trough (-). End of Well Reports (EOWR) were used to verify the well locations in relation with the seismic data in the study area as well as the use of the formation tops to check the correlations of the tops with the seismic events and synthetic seismograms to correct and achieve a proper tying. Further review of the seismic volume revealed that the high amplitude signature at the far north may be due to processing error which was not real signatures with the original seismic data. Despite this assertion a well through that section confirmed the existence of hydrocarbon accumulation at this part of the study area and I am of the view that taking out the processing artefacts, there is still some signatures of importance at that part of the data. This effect as highlighted in Figure 6.5 did not affect other parts of the data in anyway and results from these parts were highly authentic.

#### **5.5 Loading Formation Tops**

Formation Tops are time-depth charts that are entered into the Kingdom Suite Software to place the tops of the major formations and their subdivisions in their right geological time. This was obtained from the End of Well Report. It helps to locate where the base and top horizons of a formations should be picked. Figure 5.2 shows the software window.

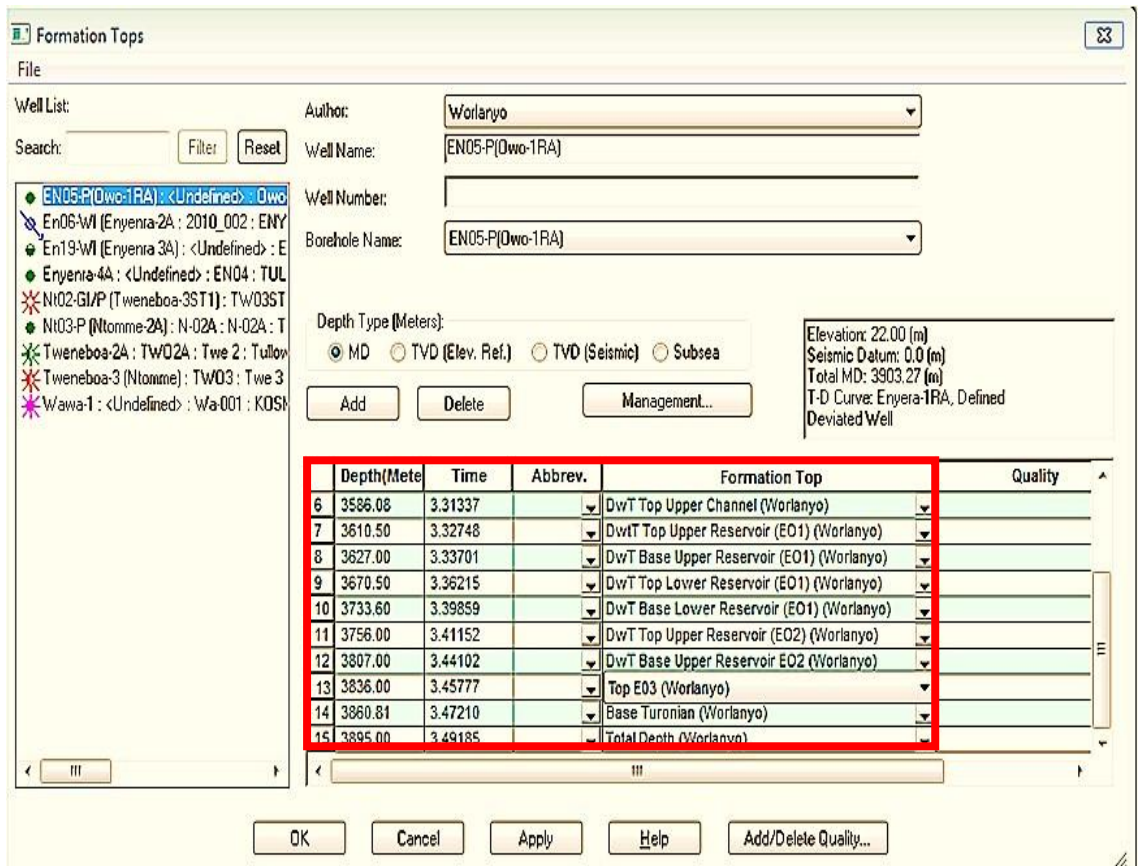


Figure 5.2: GNPC SMT Software window interface showing the Formation Tops in red Polygon for the study area.

### 5.5 Generation of Synthetic Seismograms.

Synthetic seismograms are practical approximation to actual seismic records and are therefore useful in correlating reflection events with horizons. The comparison of real seismic data with synthetic seismograms may help to determine which events represent primary reflections and which ones do not. This also helped to indicate the polarity of the target horizons. Time to depth charts for the wells were imported from EOWR. Their sonic logs were converted into velocity logs. Minimum phase wavelets were created by extracting matching frequency contents from traces in the seismic data, within a radius of 100 m. The frequency spectra of these minimum phase wavelets were examined for average maximum frequency contents. These maximum frequencies were

used to generate zero phase Ricker wavelets that were convolved with reflectivity coefficients to produce the synthetic seismograms as shown in Figure 5.3.

The correlation obtained is 0.618 which gives a good match between the Synthetic seismograms and the real seismic data.

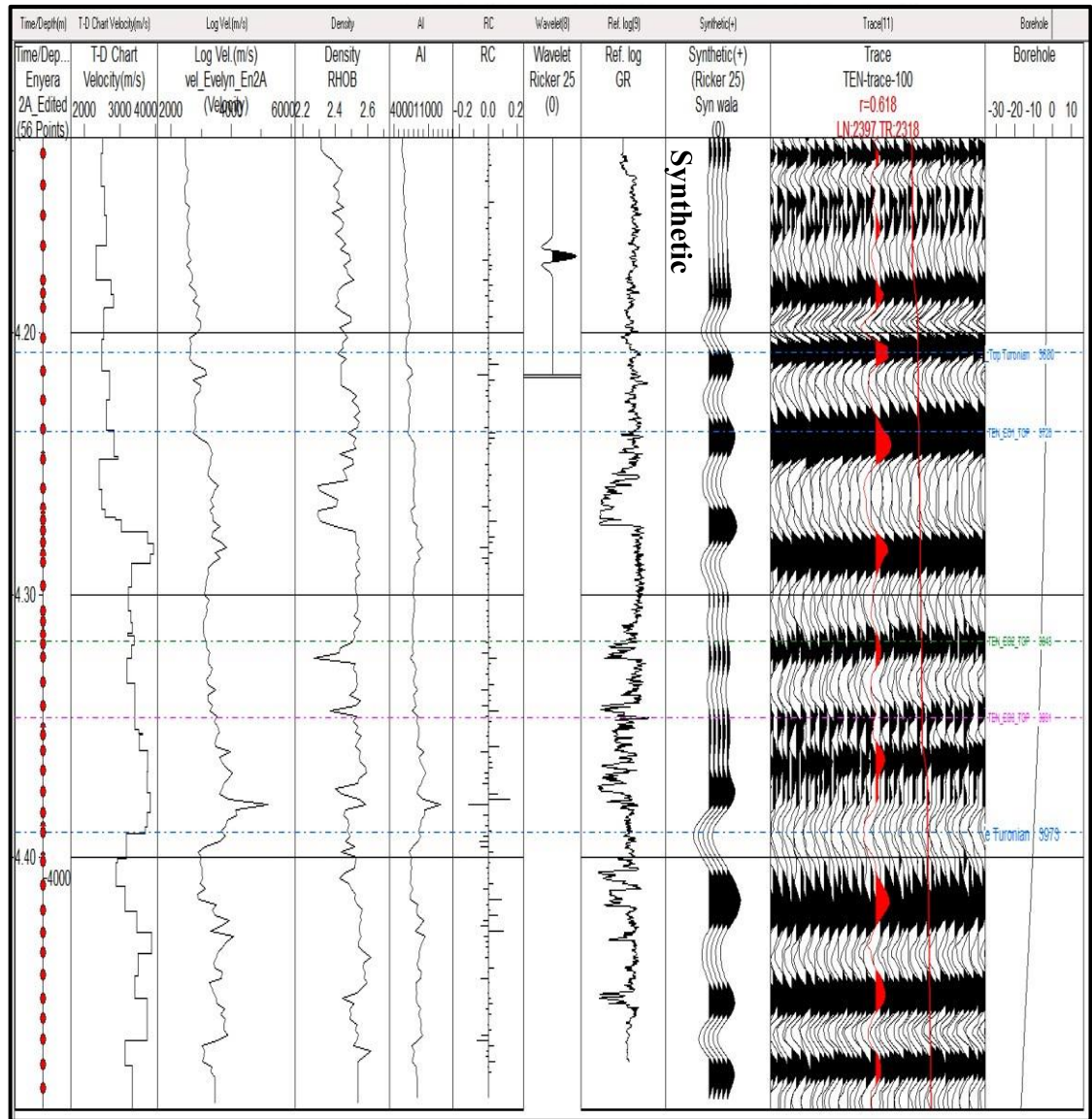


Figure 5.3: Synthetic Seismograms generated using seismic and well data of the Study Area

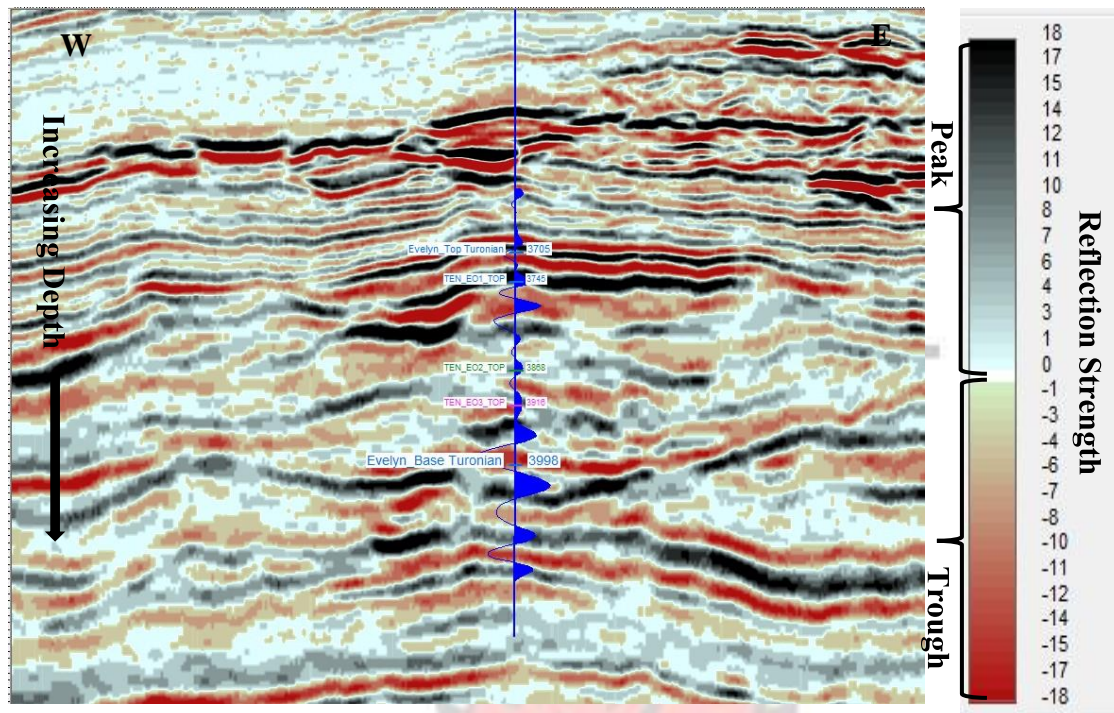


Figure 5.4: Seismic section showing well to seismic tying using synthetic seismogram.

Figure 5.4 above shows the correlation between the real seismic data with the generated synthetic seismogram of a good correlation of 0.618 and this helped to mark the top Turonian as peak (+) and the Base Turonian as trough (-). It gives an indication of a reliable well to seismic tie.

### 5.5.1 Horizon Picking

According to Sheriff (2002), a horizon is the surface separating two different rock layers which gives rise to a seismic reflection according to the acoustic impedance contrast between the two layers. Four horizons namely, Base and Top Turonian, Base and Top Santonian, were picked and correlated. For each of the horizon, a total of 90 inlines and 160 crosslines in incremental step of 20 for both crosslines and inlines were correlated. The inlines direction is in N-S whiles the crosslines is in W-E direction. The choice of these intervals was based on earlier studies of the Tano Basin which revealed that good sands possible of hydrocarbons accumulations were possible in the Turonian, Santonian

and Albian formations. Figure 5.6 shows a seismic section of the mapped (picked) horizons. On the average the Turonian interval is within the depth of 2700 m to 4000 m from the seismic reference datum.

### 5.5.2 Top Turonian and Base Turonian Picking

The top Turonian surface is characterised by a sub-continuous strong peak reflection. The top Turonian event can be seen to pinch out toward the west. The base Turonian is marked by a sub-continuous reflection. Figure 5.5 shows seismic section before interpretation while Figure 5.6 shows seismic section after horizon interpretation (picking).

### 5.5.3 Top Santonian and Base Santonian Picking

The top Santonian was picked with a 20×20 grid on a peak with a strong peak reflection. The base Santonian was conversely picked on the trough with mixed strong and sub weak reflections. Portion of the reflectors were subtle and demanded extremely cautious mapping.

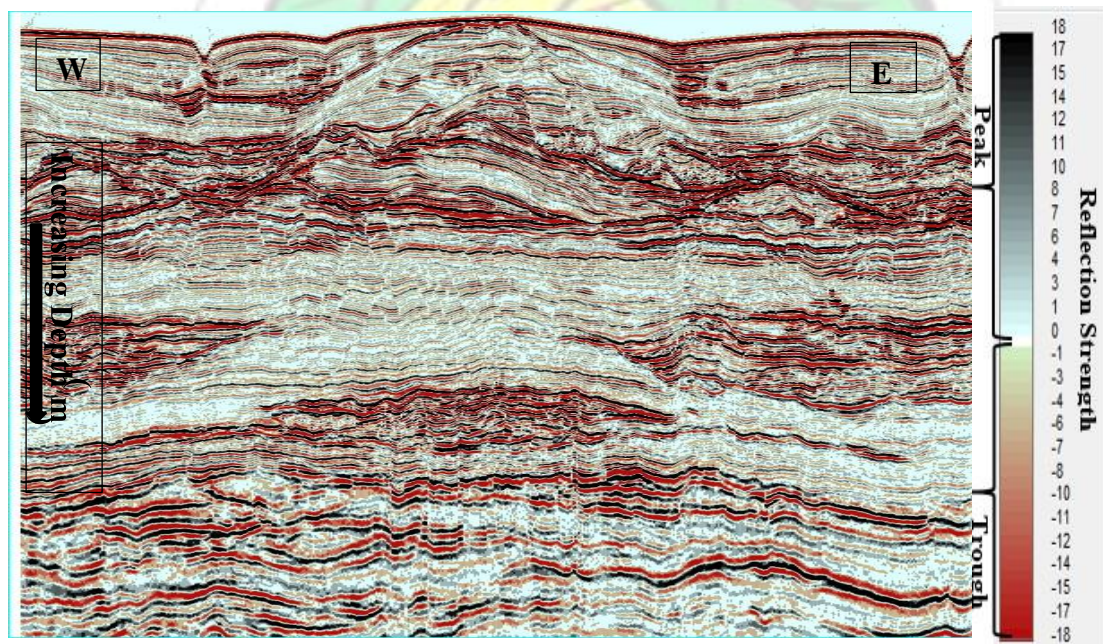


Figure 5.5: Seismic Section before Interpretation (Picking of Horizons).

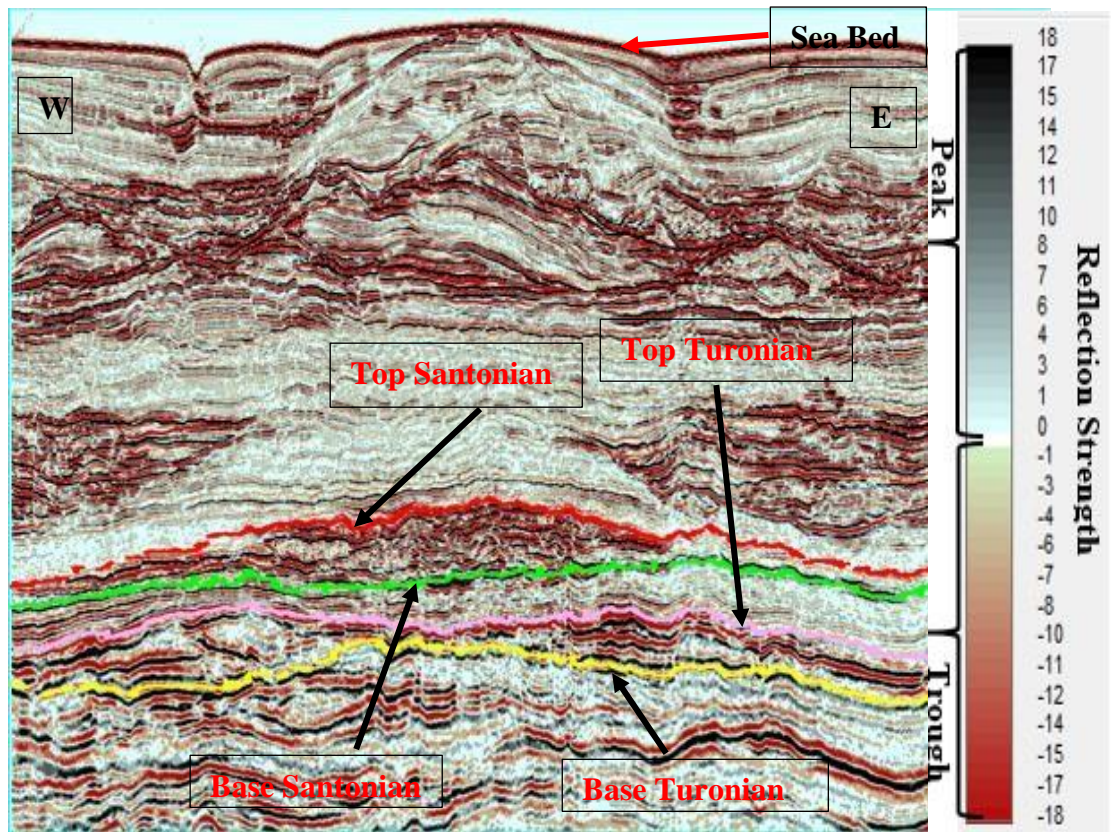


Figure 5.6: Seismic Section after Interpretation of Horizons

### 5.6 Fault Picking

Faults in the Turonian and Santonian intervals were picked based on the abrupt termination of reflection events or displacements. The fault picking was done on crosslines and inlines set to line grid of 20. The Turonian interval as well as the Santonian interval lacks major faults. The result of the delineated faults is shown in Figure 6.3.

### 5.7 Generating Depth Structural Maps

This is done by gridding the horizons (top and base) and creating contour maps. Fifty (50 m) contour interval surface maps were generated from the grids created for each of the four horizons picked. These maps were produced for identification of closures

(anticlinal features possible for accumulation of hydrocarbons) that may be of interest in this research study. Isopach maps of the Turonian and Santonian Intervals were also created using the Kingdom SMT to study the interval thicknesses between the Top and Base of the Turonian and the Santonian respectively. The generated maps were shown under the results section in Figure 6.2a and Figure 6.2b.

## **5.8 Seismic Volume Attributes Analysis**

After the generation of the structure maps, seismic volume attributes were computed to study the Turonian and Santonian intervals. This was done in three major steps. In the first step, Volume Attribute of Minimum Amplitude (VATMIN) maps were created on the Turonian and Santonian intervals respectively. This was done to delineate the sand depositions which could be related to the potential reservoirs in the study area. In the second step, Coherency attribute slices were generated to aid in describing the depositional environment and the morphology of the channel that might have existed. In the third step, VATMIN was computed on the ISO proportional intervals to create Architecture Element maps. This was done to study the internal architecture of reservoirs delineated by studying the trend of amplitudes and their importance and make geological meaning out of them. The architecture maps within which each reservoir unit existed was used to compute the lateral extent using polygon (planimeter). Again the architecture maps were combined to produce schematic hydrocarbon sand deposition maps. The VATMIN maps are shown in the result section in chapter six.

### **5.8.1 Generating VATMIN Maps**

VATMIN which retains the most negative amplitude in the depth range were generated to assess amplitude distribution within the volumes of interest in order to decipher the distribution of the potential hot sand and shale. The volume attribute calculator of the

SMT software was used to generate the VATMIN maps. Figure 5.7 shows the SMT software interface for calculating VATMIN. The VATMIN amplitude maps are shown in the result section in chapter six.

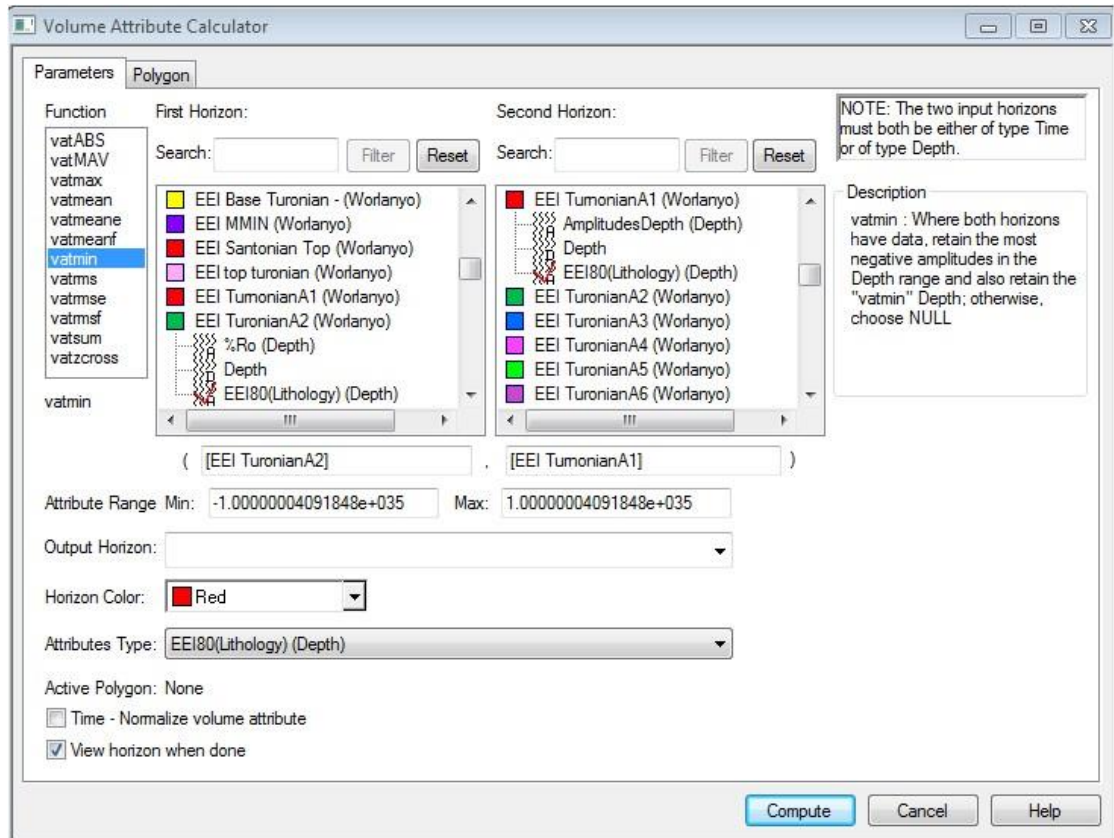


Figure 5.7: Kingdom Software window showing the interface for extracting VATMIN Amplitude

### 5.8.2 Generating Coherency Slices

This component looked at the analysis of plane view images that can significantly enhance predictions of the spatial and temporal distribution of the subsurface lithology. The Coherency slices were computed to delineate distinctive depositional features depicting buried deltas, river channels, crevasse splays, reefs, and levees using the Kingdom Software. Figure 6.7a, Figure 6.7b, Figure 6.7c, Figure 6.28a and Figure

6.28b are the results of the generated coherency attribute maps shown and discussed in chapter six.

### 5.8.3 Generating Architecture Element Maps.

The architecture maps were generated by creating ISO-Proportional intervals and computing VATMIN on each ISO-Proportional interval created using the Extended Math Calculator toolbar of the Kingdom SMT software as shown in Figure 5.8a.

#### 5.8.3.1 ISO-Proportional Slices

In generating ISO-proportional slices, the Kingdom SMT software allows to do arithmetical operation on the surfaces using user defined equations. The equations below were inputted into the Extended Math Calculator toolbar of the SMT software to generate the ISO-proportional slices. The A and B are in depth (m).

$$A1 = A + ((B-A)/6)$$

$$A2 = A + 2((B-A)/6)$$

$$A3 = A + 3((B-A)/6)$$

$$A4 = A + 4((B-A)/6)$$

$$A5 = A + 5((B-A)/6)$$

$$A6 = A + 6((B-A)/6)$$

A is the Top (Top Turonian and Top Santonian) and B represents Base (Base Turonian and Base Santonian) of the interval. The tops of the Turonian and Santonian were used as the reference surfaces to create Six (6) ISO-proportional surfaces A1, A2, A3, A4, A5, A6 each with their corresponding VATMIN maps computed for Turonian intervals (T1, T2, T3, T4, T5 and T6) and Santonian intervals (SI, S2, S3, S4, S5, S6) using the EEI data set. Figure 5.8a shows the software window for calculation the ISOproportional intervals and Figure 5.8b shows the various slices generated within the Turonian and the Santonian intervals on the seismic section.

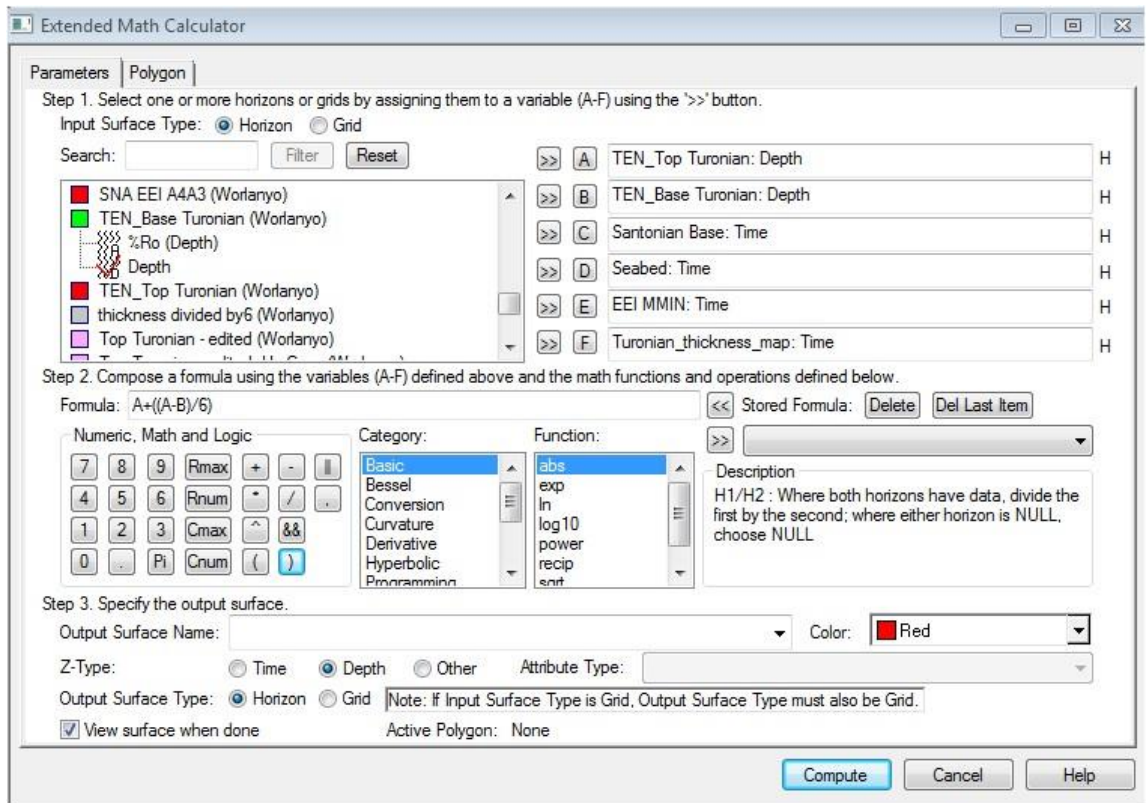
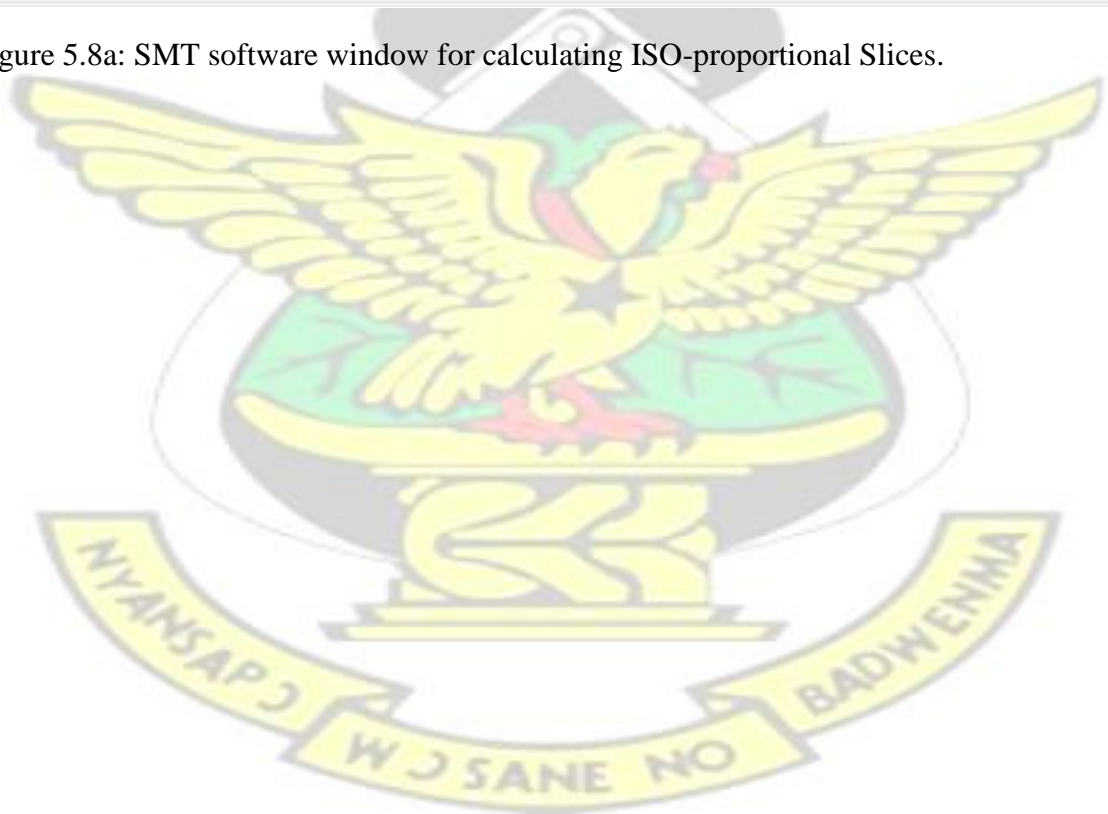


Figure 5.8a: SMT software window for calculating ISO-proportional Slices.



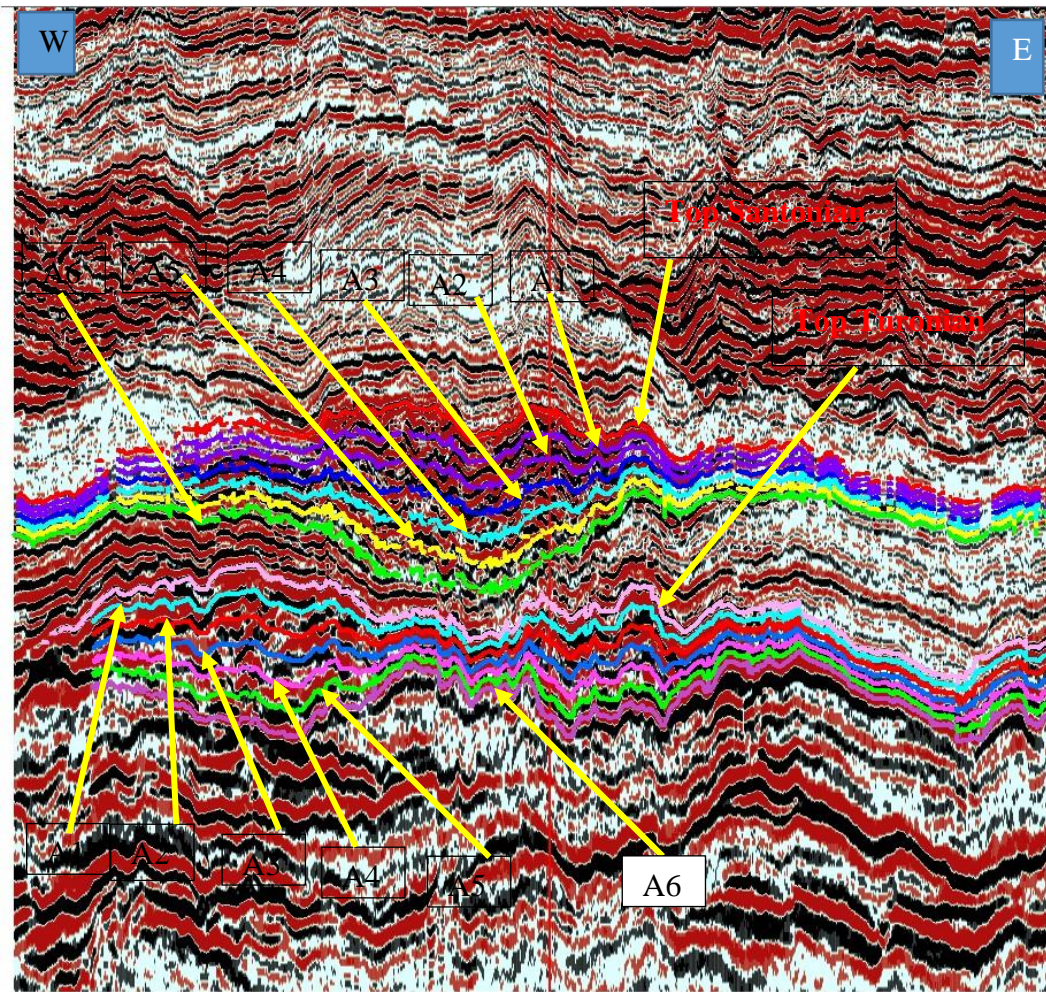


Figure 5.8b: Seismic Section showing the ISO proportional slices in Turonian and Santonian.

### 5.9 Well Logs Analysis

This aspect was divided into five main components: correlation of the wells, well to seismic tie to locate the various oil pools (reservoirs) within the interval of interest from the wells (Figure 6.15 and Figure 6.16 in the results section) were done using the GNPC Kingdom SMT software. These were followed by the estimation of petrophysical properties (shown in Table 6.1 to Table 6.4 ) using the Interaction Petrophysics software, reservoir quality analysis using permeability- porosity crossplot (Figure 6.24), and volumetric estimation (shown in Table 6.5 and Table 6.6).

### **5.9.1 Well Correlation**

Well correlation was done using the gamma ray log (Figure 6.15 and Figure 6.20) on the Kingdom Software Package. The results are displayed in Figure 6.15 and Figure 6.20.

### **5.9.2 Estimation of Petrophysical Parameters.**

Interactive Petrophysics (IP) software provided by GNPC was used to compute the petrophysical properties of the wells. Gamma ray log, resistivity log, Density log and the Neutron-Porosity logs, formation tops and survey deviation data were the input data used. The computation was based on automatic computer algorithms in the Interactive Petrophysics software as explained below and the estimated values displaced in chapter six (results and discussions) in Table 6.1, Table 6.2, Table 6.3 and Table 6.4.

#### **Gross Reservoir thickness Estimation**

The gross reservoir thickness (H) was obtained from the Gamma ray logs using the top and base of reservoir units.

#### **Net Pay thickness Estimation**

Computation of net pay thicknesses were obtained from Gamma ray logs. The net thickness which is the thickness of the reservoir was determined by defining the basis for non-reservoir and reservoir sands.

#### **Net/Gross Reservoir Thickness Estimation**

The gross reservoir thickness H, was determined by looking at tops and bases of the reservoir sands across the well. The net thickness which is the thickness of the reservoir was determined by defining the basis for non-reservoir and reservoir sands using the gamma ray log. This was carried out by drawing a shale baseline and sand baseline on

the gamma ray log. The net-to-gross ratio ( $N/G = h/H$ ) is computed by IP software as the ratio of the net pay thickness (h) to the gross reservoir thickness (H).

### Volume of Shale Estimation

The lithologies (sandstone and shale) were identified using the gamma ray log with reference to sand/shale baseline. The volume of shale is computed from the gamma ray log. The software computation of volume of shale is based on the linear method algorithm using the relation below.

$$V_{sh} = \frac{GR - GR_{matrix}}{GR_{shale} - GR_{matrix}}$$

Where: GR = Gamma Ray reading from log

GR<sub>matrix</sub> = Gamma Ray reading from clean sand zone

GR<sub>shale</sub> = maximum Gamma Ray reading from Shale zone

V<sub>sh</sub> = Volume of Shale

### Porosity Estimation

The input parameters for computation of effective porosity using the Interactive Petrophysics (IP) software provided by GNPC were the density log and the resistivity logs. The algorithm for the computation was based on the relation below (Baker Hughes, 1999).

$$\Phi = \frac{\rho_{matrix} - \rho_b}{\rho_{ma} - \rho_f}$$

Where :  $\rho_{ma}$  = matrix density

$\rho_b$  = bulk density read from log

$\rho_f$  = average density of fluid = 0.85

$\Phi$  = computed porosity

## Water Saturation Estimation

The Water Saturation was computed using the Archie's relation (Archie, 1942).

$$S_w = \left( \frac{aR_w m^{1/2}}{R_t \phi} \right)$$

Where  $a = 1$ ,  $n = 2$ ,  $m = 2$ ,

$S_w$ : water saturation,

$R_t$ : total resistivity,

$R_w$ : resistivity of water.

Hydrocarbon saturation ( $S_{hc}$ ), is the percentage of pore volume in a formation occupied by hydrocarbons. It is determined by subtracting the value obtained for water saturation from 100% i.e.  $S_{hc} = (100 - S_w) \%$ , where  $S_{hc}$  is the hydrocarbon saturation and  $S_w$  is the water saturation (Baker Hughes, 1999). The results are shown in chapter six.

### 5.10 Reservoir Quality

The quality of the reservoir was analysed using Permeability-Porosity cross plots of the wells in each delineated reservoir as shown in Figure 6.24.

### 5.11 Volumetric Calculation.

The equation below was used to calculate hydrocarbon in place (Dean and Mireault, 2008):

$$STOOIP = GRV \times (N/G) \times \phi \times S_{hc} \times (1/B_o) \times R_F \times C_F$$

Where STOOIP is the Stock Tank of oil originally in Place

Hydrocarbon Saturation ( $S_{hc}$ ), Porosity ( $\phi$ ), and Net to Gross ratio (N/G) were obtained from the petrophysical parameters computed for the delineated reservoirs. The following contact were also used.

**CF** is the Conversion Factor and is a constant = 6.29 ( $1 \text{ m}^3 = 6.29 \text{ oil barrels}$ )

**RF** is the Recovery Factor and is a constant = 0.3

**Bo** is formation Volume factor and  $(1/Bo)$  is a constant = 0.8

**GRV** is the gross rock volume = Reservoir thickness (m)  $\times$  area extent ( $\text{m}^2$ ). (Dean and Mireault, 2008). The area extent of each reservoir was obtained from the VATMIN extractions (Architecture element map) computed over each reservoir unit. The polygon (Planimeter) gives a computed area of the lateral extent of the reservoirs. The Polygons used are seen in appendix.



## CHAPTER SIX

### RESULTS AND DISCUSSION

#### 6.1 Seismic Interpretation of the Turonian

The 3D seismic data was interpreted on both inlines and crosslines. Horizon mapping were controlled by formation tops and also by correlation with well to seismic tie. Four main horizons namely: Top Turonian, Base Turonian, Top Santonian and Base Santonian were mapped. The results for Turonian formation were discussed followed by the results of the Santonian. Figure 6.1 shows the mapped horizons in the colours on the seismic section.

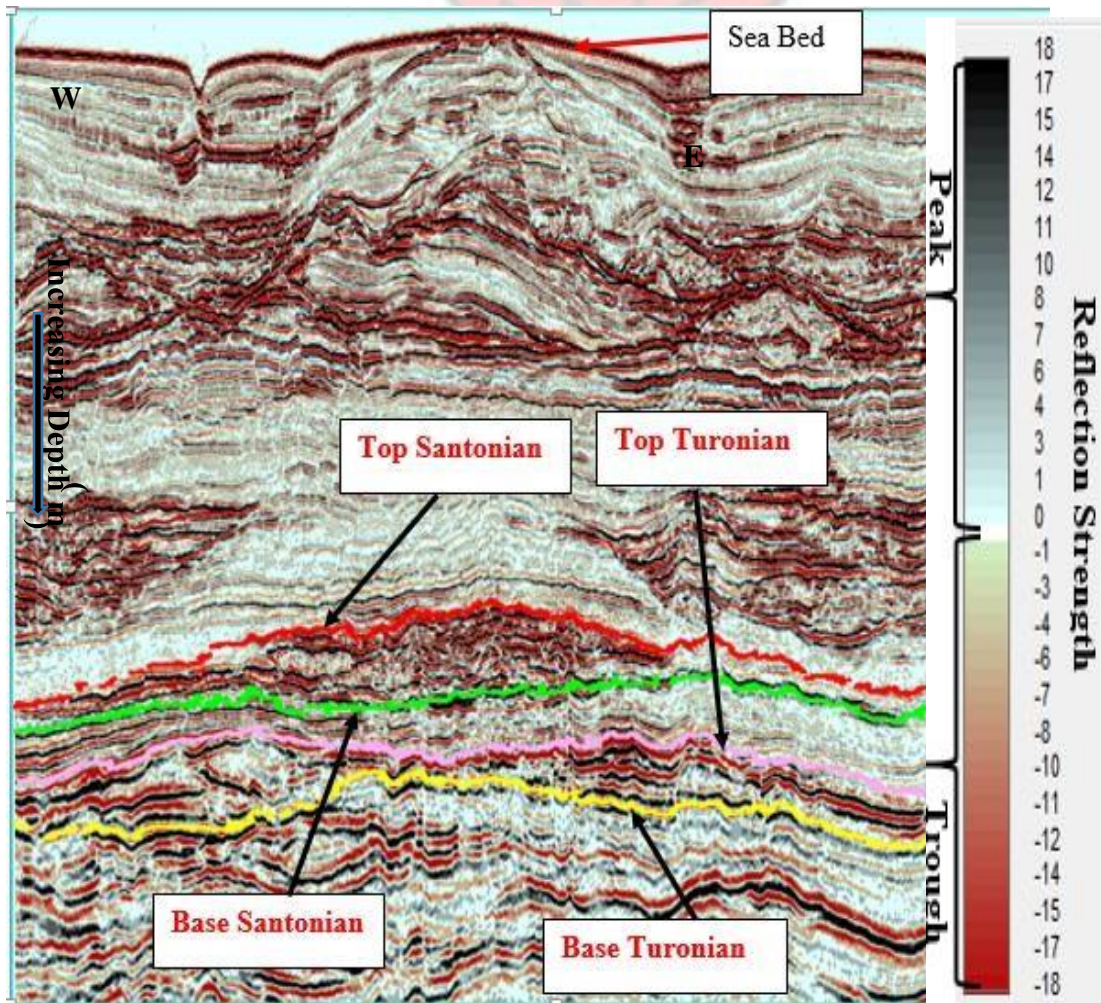


Figure 6.1: Seismic Section showing the mapped Horizons.

## 6.2 Structural Interpretation

### 6.2.1 Depth Structural Maps of the Turonian Formation

Figure 6.2a shows the depth structural map of the Top Turonian structural features. The depth ranges from 2601 m to 4204 m from the seismic reference datum. The map indicates a structural high at the northeast dipping towards southwest. Four way closures (anticlinal features) which may serve as hydrocarbon traps were identified at different locations and are indicated in the red circle.

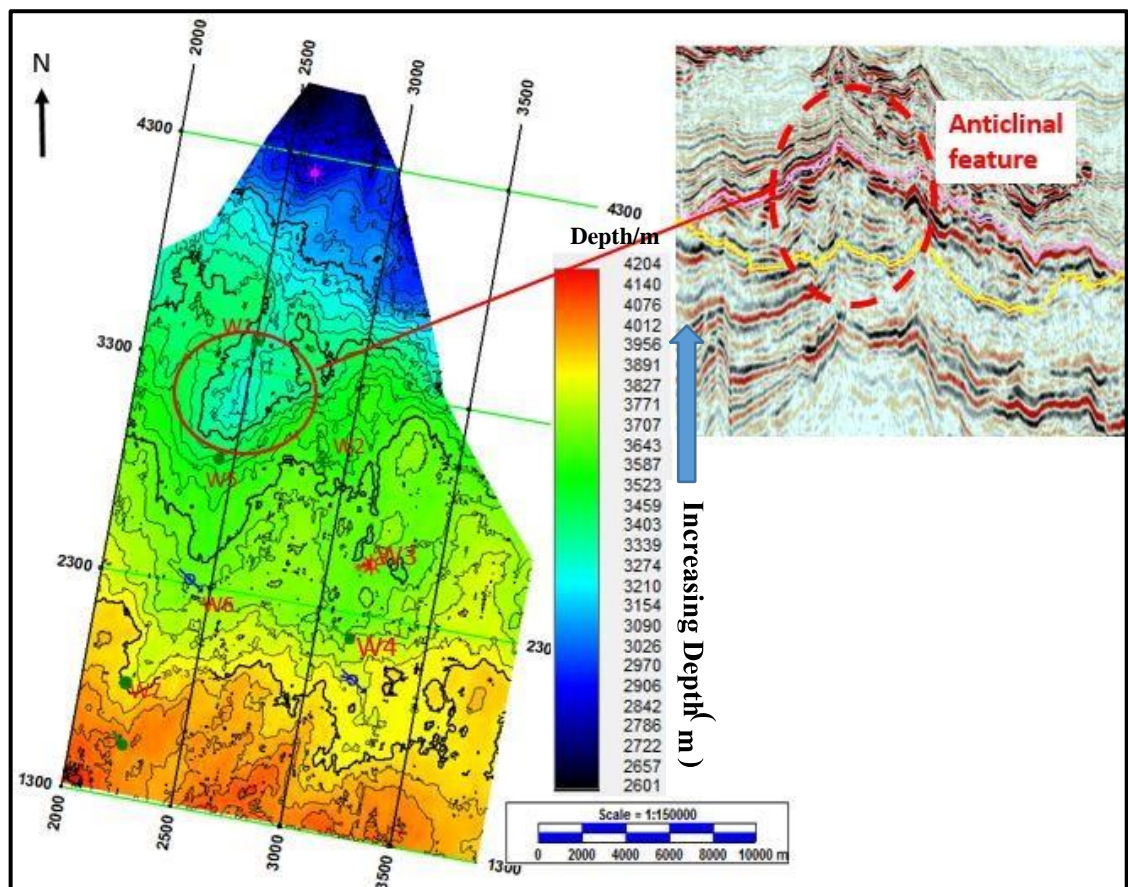


Figure 6.2a: Depth Structural map of the Top Turonian

Figure 6.2b shows the depth structural map of the Base Turonian. The map shows a gentle dipping surface trending in the southwest direction using the colouration. It ranges in depth between 2735 m at the north to 4392 m at south from the seismic reference datum. The green circles indicated possible four way closures (anticlinal

features). The Turonian structural maps (Figure 6.2a and Figure 6.2b) revealed a gentle slope topography dipping from northeast towards the southwest.

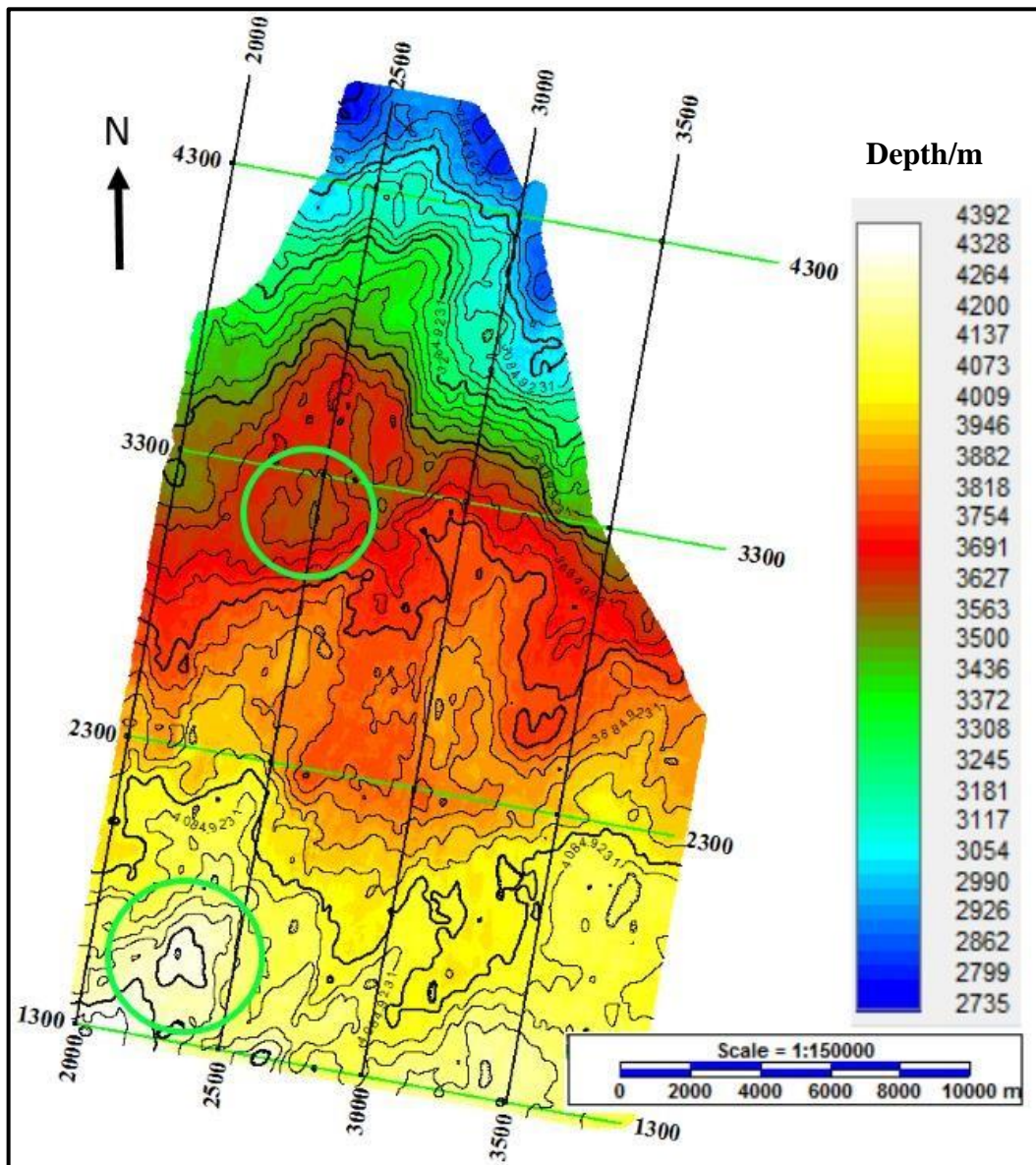


Figure 6.2b: Depth Structural map of the Base Turonian

### 6.2.2 Fault Interpretation of the Turonian

Figure 6.3 shows the faults in the Turonian formation. The Faults identified were minor faults occurrences. These faults can be generally classified as normal faults with little fault throws from their orientation. Therefore trapping of oil pools in the area can be

more likened to stratigraphic traps (inter-fingering of Sands and Shale) than structural traps (anticlines and faults).

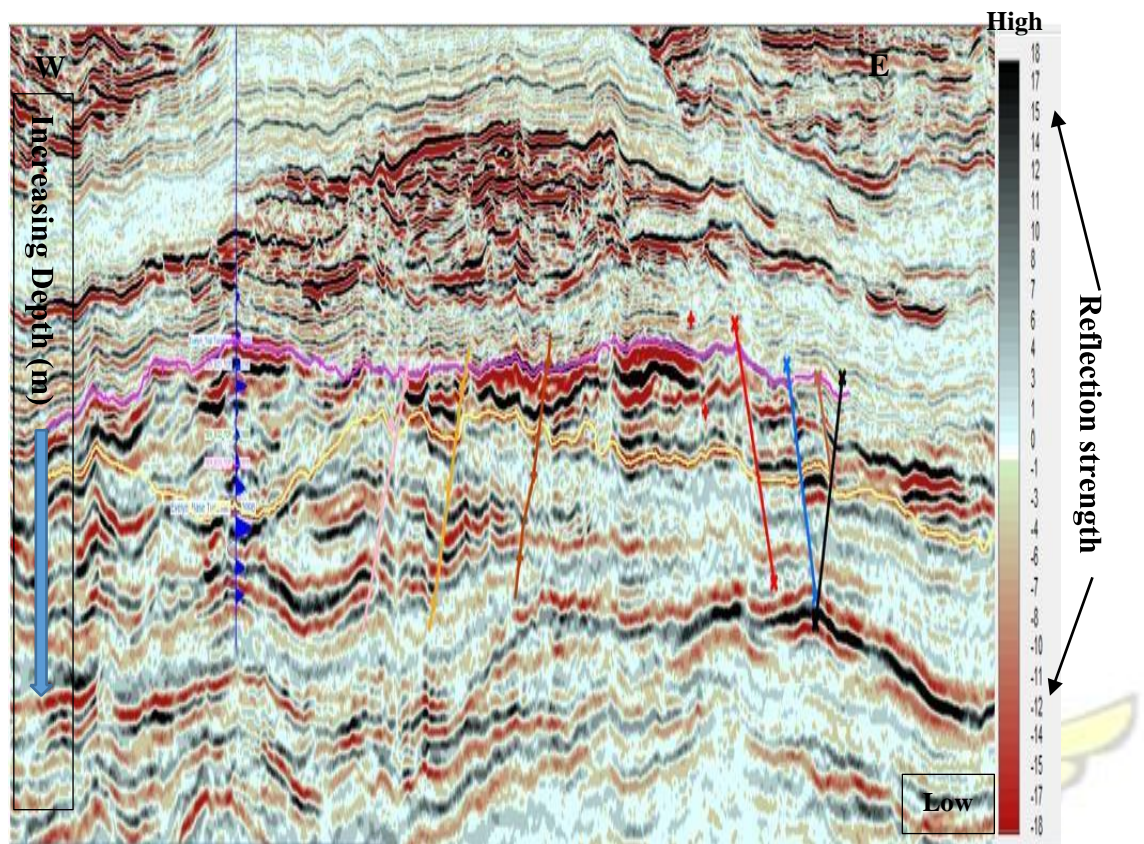


Figure 6.3: Seismic section showing faults in the Turonian formation

### 6.2.3 Isopach Map of Turonian

The Isopach map shows the lithology thickness variation of a formation (top to base). Figure 6.4 shows the Isopach map of Turonian formation. The thickest part is represented in yellow and the blue colour representing the thinnest portion using the colour scale. The sediment formation gets thinner towards the western and eastern flanks of the study area and thicker at the centre. The thickest portion is about 270 m to 400 m as seen on Figure 6.4.

The Isopach map also shows a two leg feature of the thickness trend. This could be indication of two channelized features. The existing wells in the area can be seen to be

situated in the thickest parts. This might be a lead to possible sand depositional fairways which may be hydrocarbon reserves in basin or fan system.

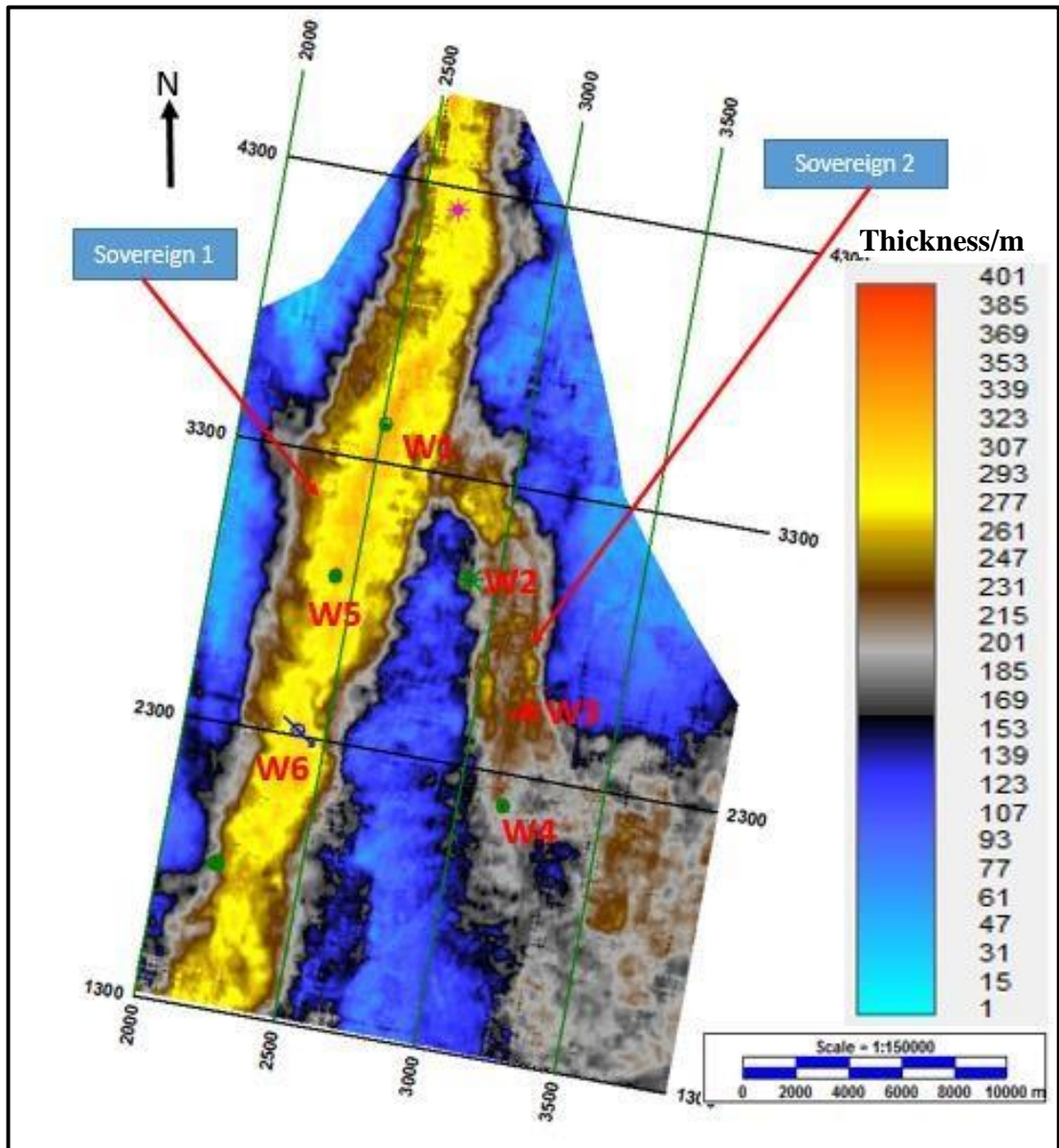


Figure 6.4: Turonian Isopach map

Combining the Isopach map with the structural maps in Figure 6.3a and Figure 6.3b, it can be inferred that, movement of sediments may be trending from the north (structural high) toward the South. Literature within the area showed that River Tano is likely to be the main suppliers of sediments for the sediment deposits.

### 6.3 Seismic Volume Attributes Analysis

#### 6.3.1 Interpretation of the Amplitude Map of the Turonian.

Utilizing amplitude for analysis is from the assumption that lithology, rock properties and fluid content should affect seismic character or amplitude. Figure 6.5 is the volume amplitude extraction map of the Turonian formation using the 3-D reflectivity data. The colouring is based on the amplitude content signature within the Turonian intervals.

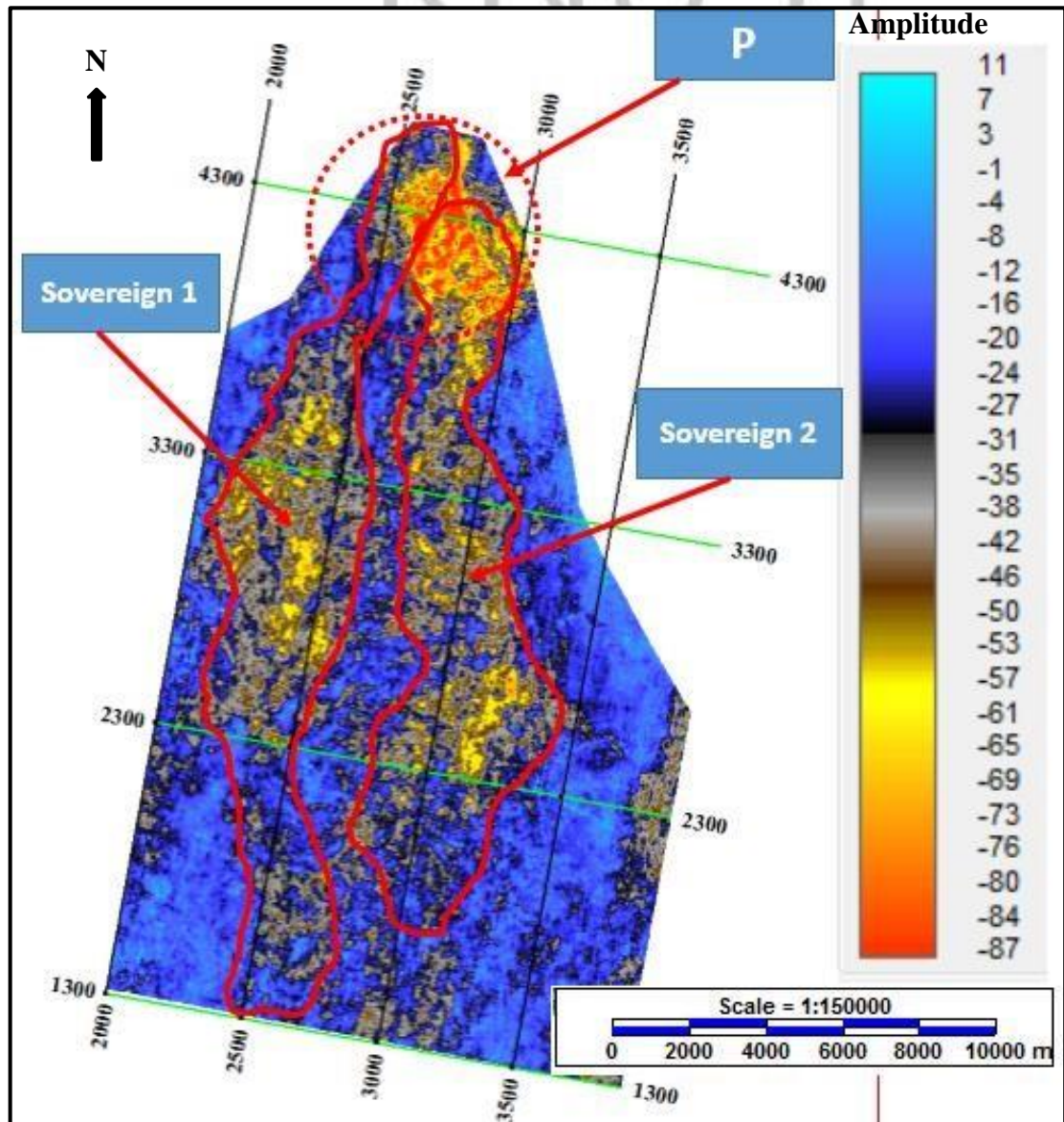


Figure 6.5: Amplitude Extraction Map (PSDM Seismic data) of the Turonian.

The yellow-red colour indicates the more negative amplitudes recognized as sand deposits. The less negative amplitudes highlighted in the blue colour indicates shale deposits.

Sovereign-1 and Sovereign-2 indicated in the red polygons are the sand accumulation areas delineated. The high negative amplitude labelled P on Figure 6.5 is attributed to processing artefact. The trend and shape of the minimum amplitude extraction as shown in Figure 6.5 could also suggest a meandering or sinuous channel system in Sovereign-1. Sovereign-2 could be likened to a channelized lobe system due to the broadening of the base of the system.

### **6.3.2 Interpretation of VATMIN Extractions for the Turonian**

The volume attribute of minimum amplitude (VATMIN) retains the most negative amplitude in the depth range. It is used to delineate the distribution of clean sands capable of hosting hydrocarbons. Figure 6.6 shows the VATMIN of the Turonian interval. More negative amplitudes indicated in black colour polygons are areas of clean sands. Two main sand fairways were delineated and denoted as Sovereign-1 and Sovereign-2. The bright negative amplitude located in the Sovereign-2 polygon seemed to suggest that Sovereign-2 has more clean sand than Sovereign-1. The delineated good sand packages (areas of bright negative amplitude) being labelled Sovereign-1 and Sovereign-2 at the western and eastern flanks were the two main sand zones characterised in the Turonian.

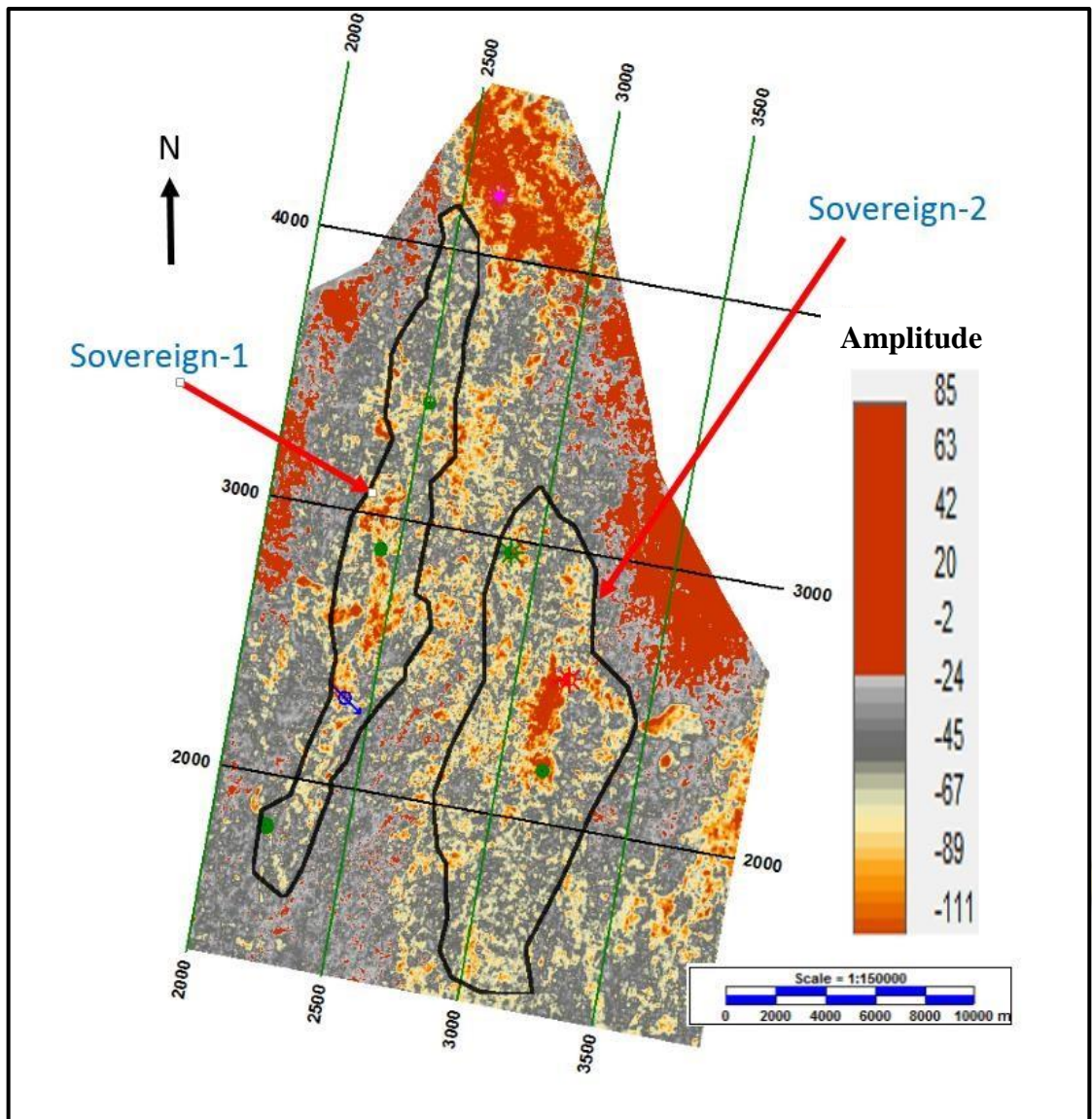


Figure 6.6: VATMIN Amplitude Extraction of the Turonian.

#### 6.4 Interpretation of the Coherence Slices

Coherency attributes enable structural and stratigraphic interpretation in analysing depositional environment of sediments. Outstanding features are mostly seen to stand out from the background. This attribute helps to verify the location and geomorphology of the channels that have been inferred. Below are the coherency slices of the Turonian interval.

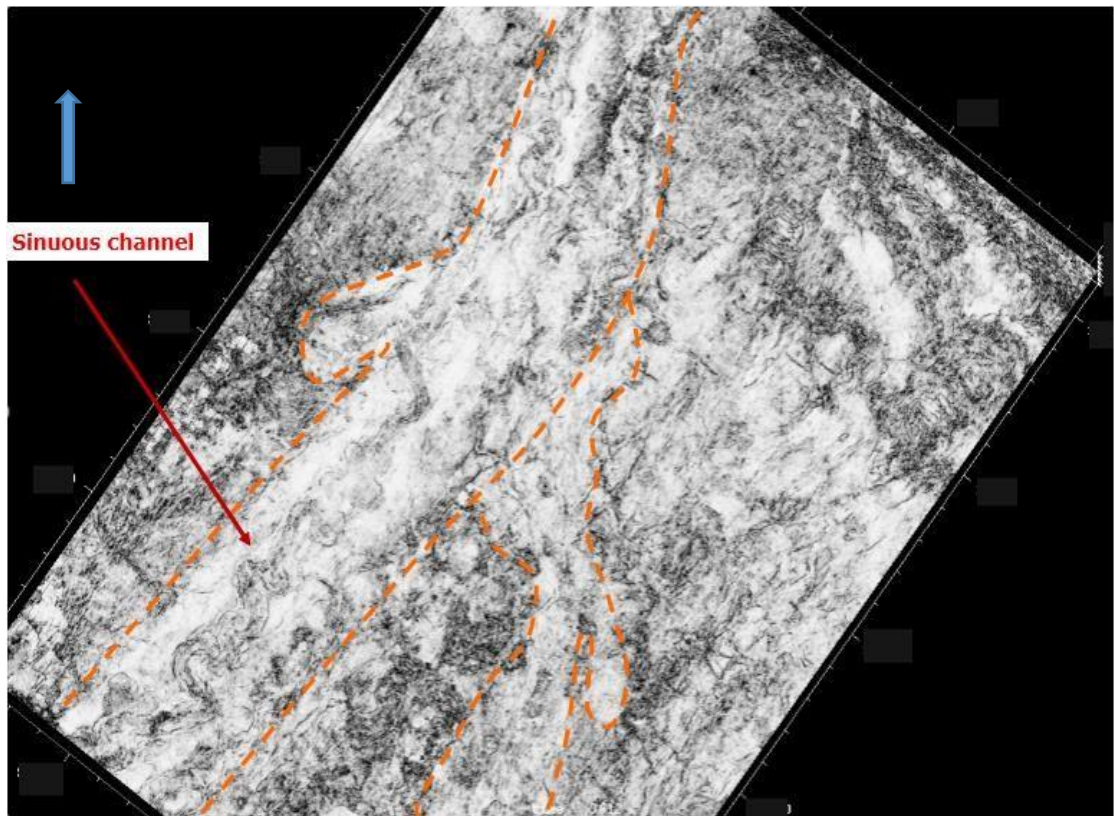
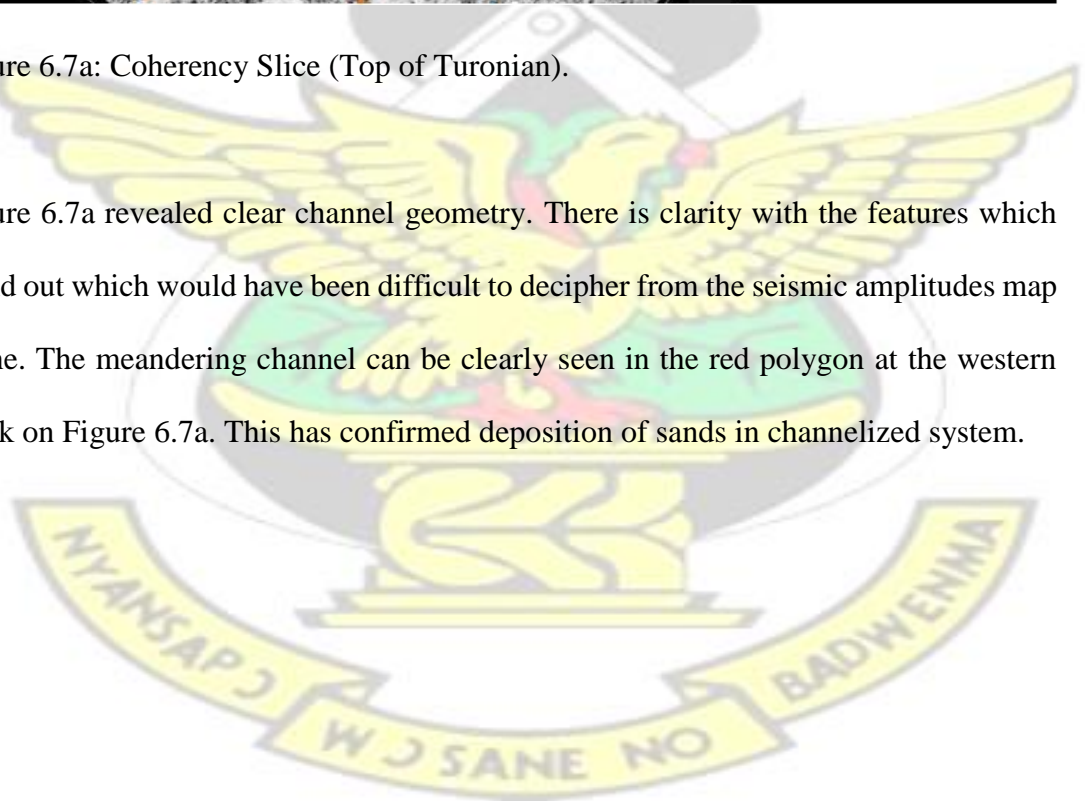


Figure 6.7a: Coherency Slice (Top of Turonian).

Figure 6.7a revealed clear channel geometry. There is clarity with the features which stand out which would have been difficult to decipher from the seismic amplitudes map alone. The meandering channel can be clearly seen in the red polygon at the western flank on Figure 6.7a. This has confirmed deposition of sands in channelized system.



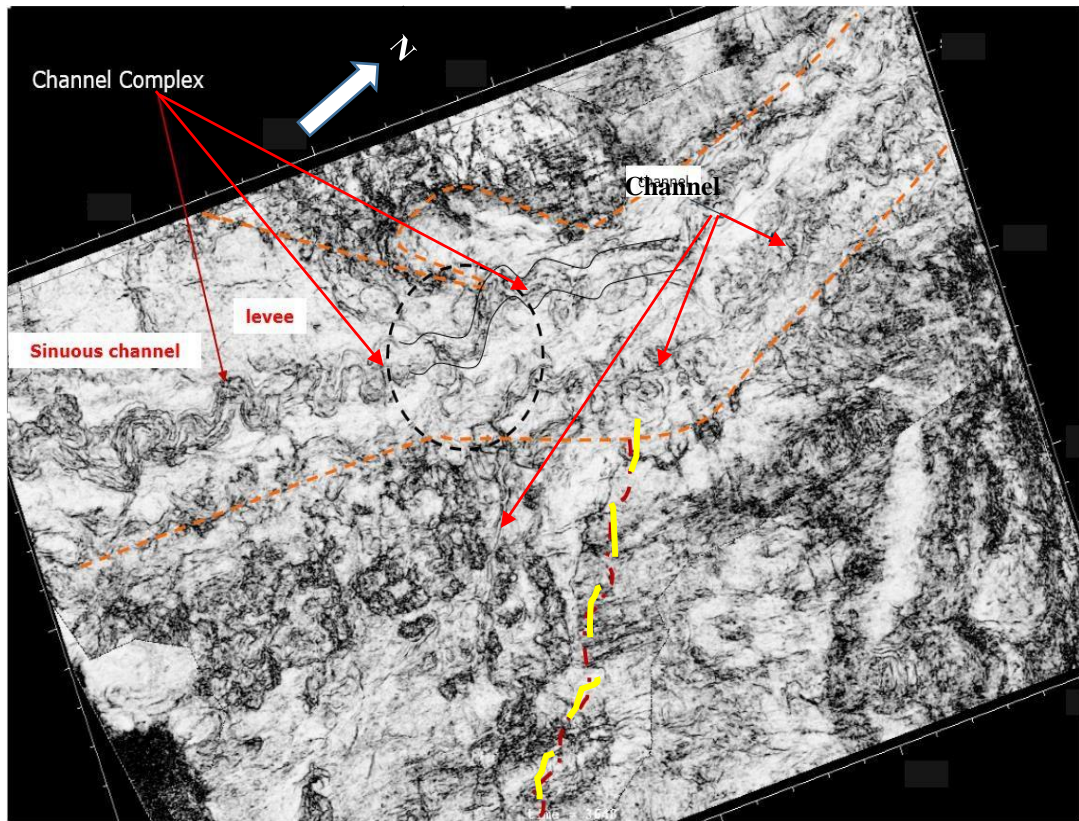
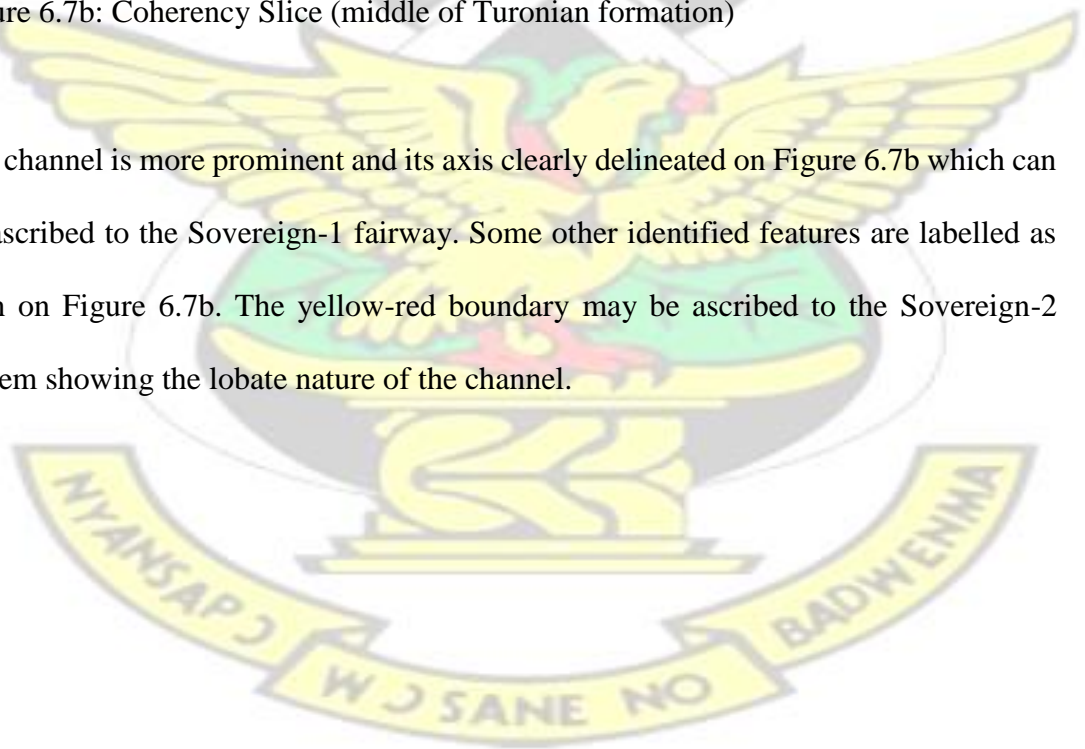


Figure 6.7b: Coherency Slice (middle of Turonian formation)

The channel is more prominent and its axis clearly delineated on Figure 6.7b which can be ascribed to the Sovereign-1 fairway. Some other identified features are labelled as seen on Figure 6.7b. The yellow-red boundary may be ascribed to the Sovereign-2 system showing the lobate nature of the channel.



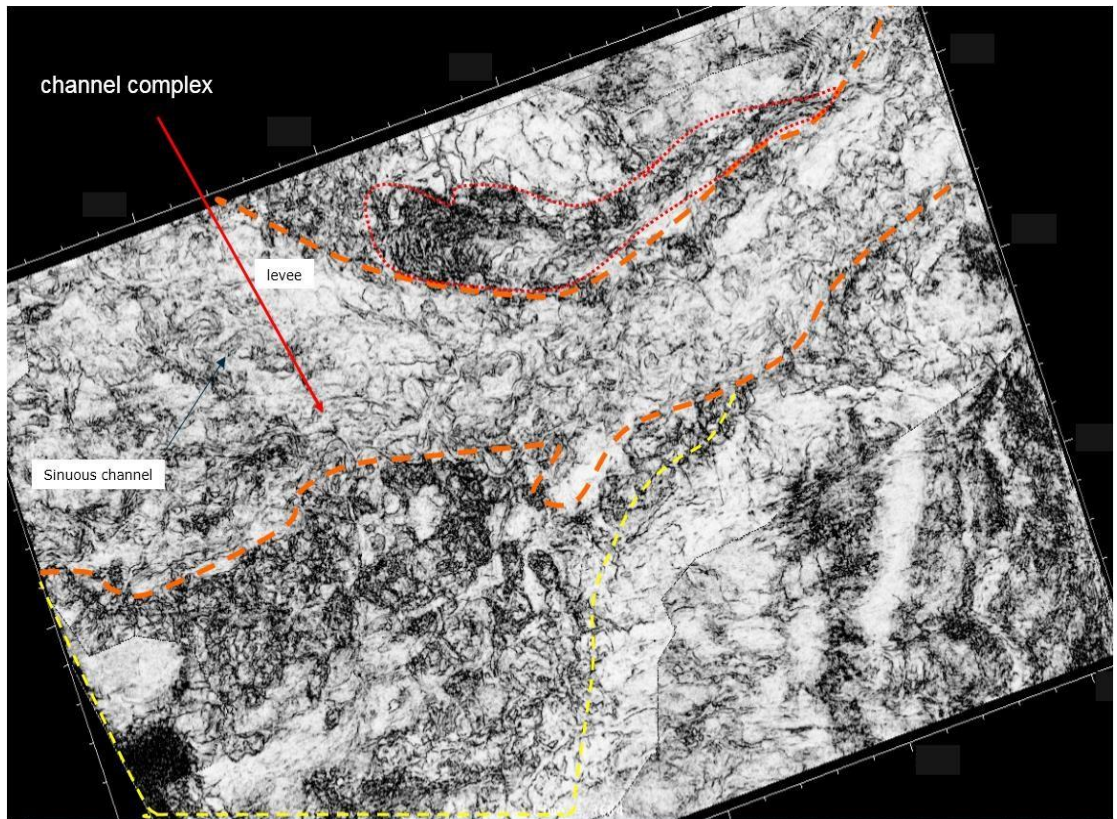


Figure 6.7c: Coherency Slice (near base of Turonian)

Figure 6.7c shows the coherency slice near the base of the Turonian. The demarcation in red dotted lines (Figure 6.7c) confirms the meandering or sinuous shape delineated as Sovereign-1 on Figure 6.5. Sovereign-2 sand fairway can be inferred to be situated in the yellow dotted polygon.

Figure 6.7a and Figure 6.7b gave clear delineation of the channel system for the Sovereign 1 and Sovereign 2. The Sovereign-1 as stated earlier is more confined with deposition of debris over the main axis forming the levees. Sovereign-2 on the coherency has no confined channel axis and can be associated with spill overs and thin gullies or channels indicated in the yellow-red polygon (Figure 6.7b and Figure 6.7c).

## 6.5 Interpretation of Architecture Element maps

The Architecture Element maps were obtained by extracting VATMIN on each ISOproportional interval. The purpose is to evaluate the internal seismic geomorphology (structures) of the reservoirs demarcated. The hidden reservoir sand deposits which were not recognizable on the VATMIN extracted from the top/base Turonian interval were highlighted in the various colour polygons.

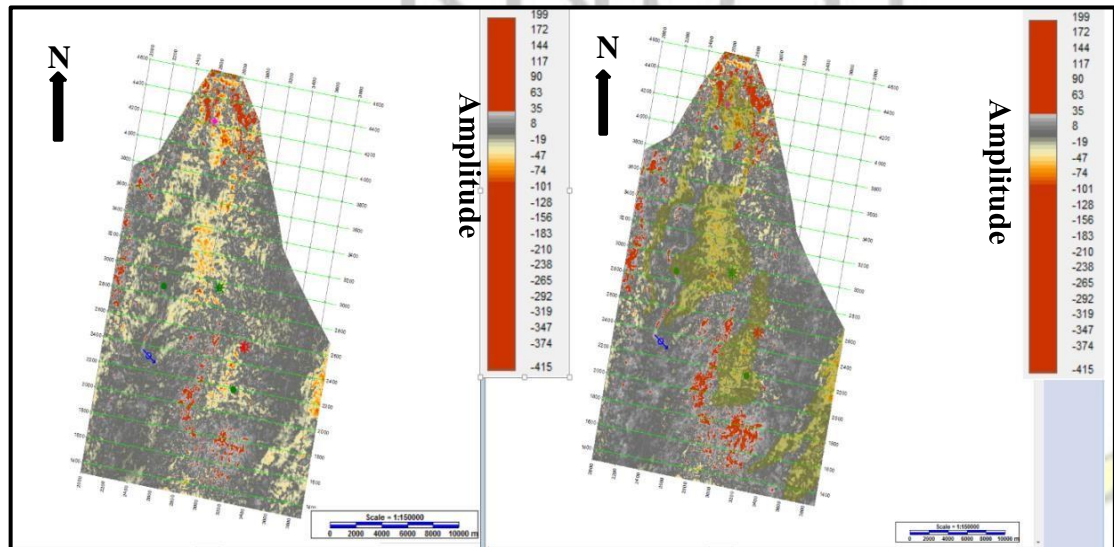


Figure 6.8: Architecture Element map (Interval T1).

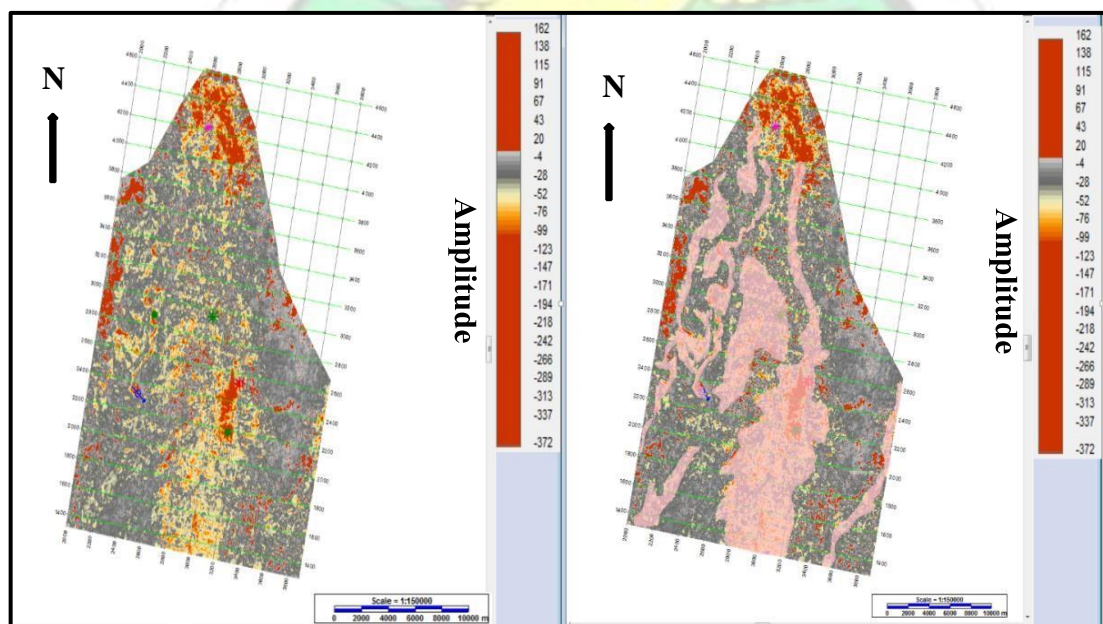


Figure 6.9: Architecture Element map (Interval T2).

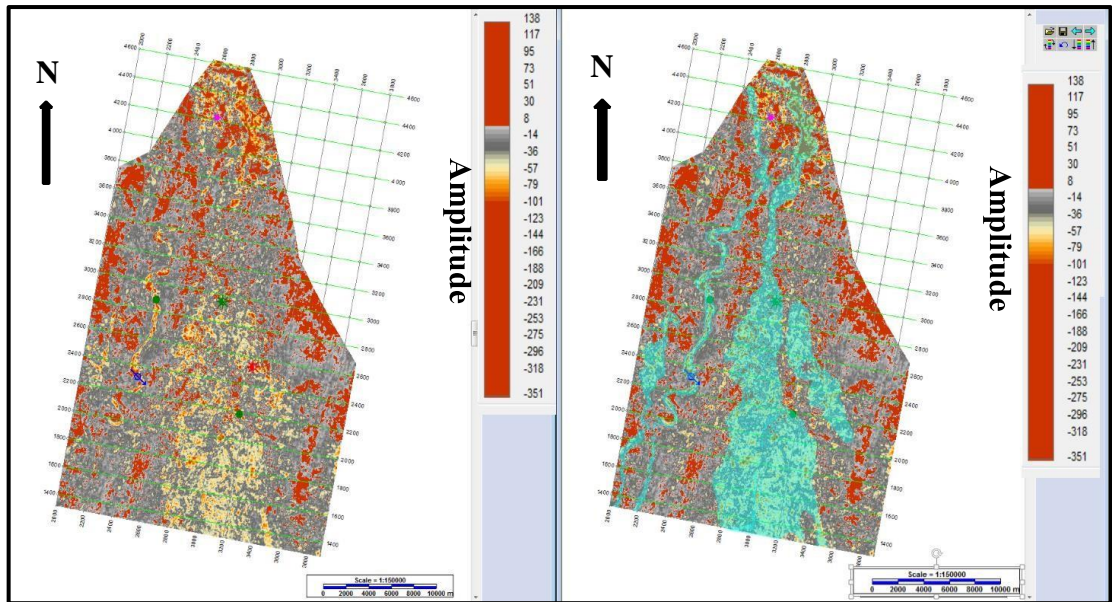


Figure 6.10: Architecture Element map (Interval T3).

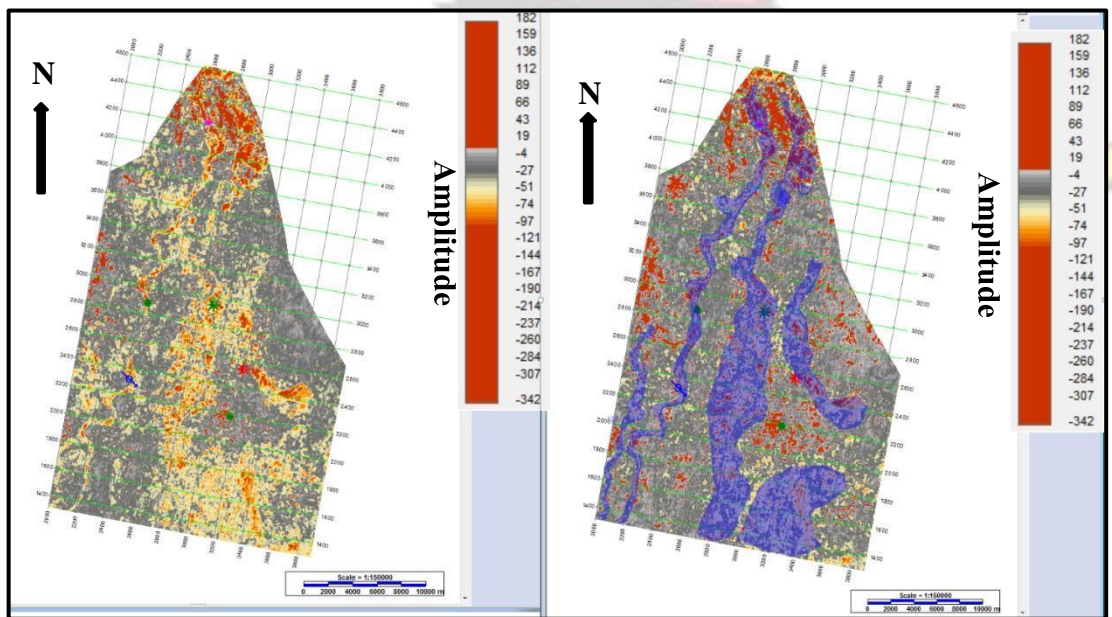


Figure 6.11 Architecture Element map (Interval T4).

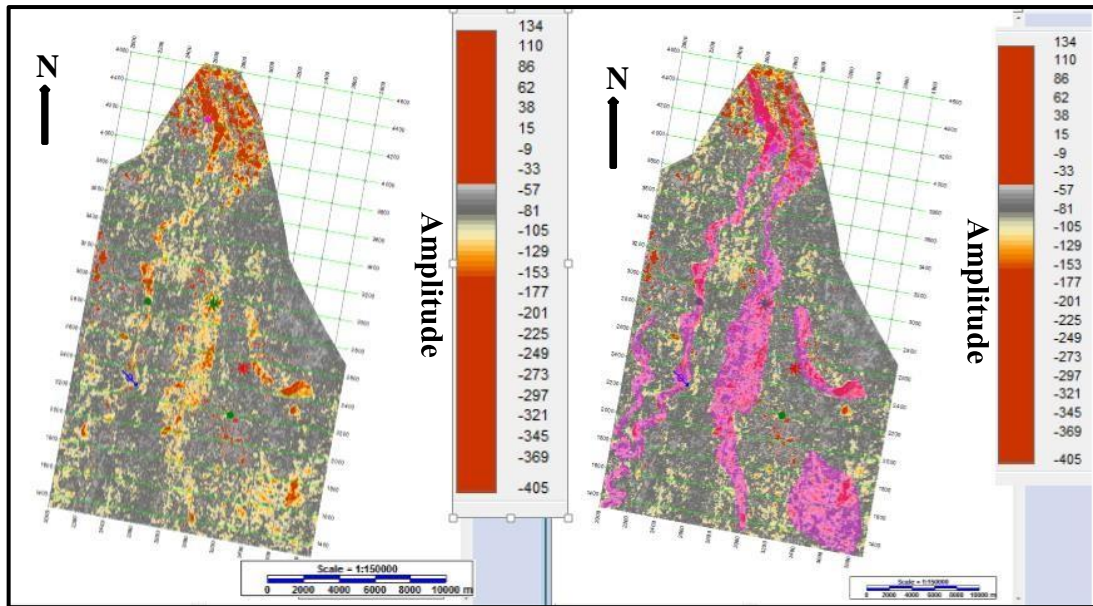


Figure 6.12: Architecture element map (Interval T5).

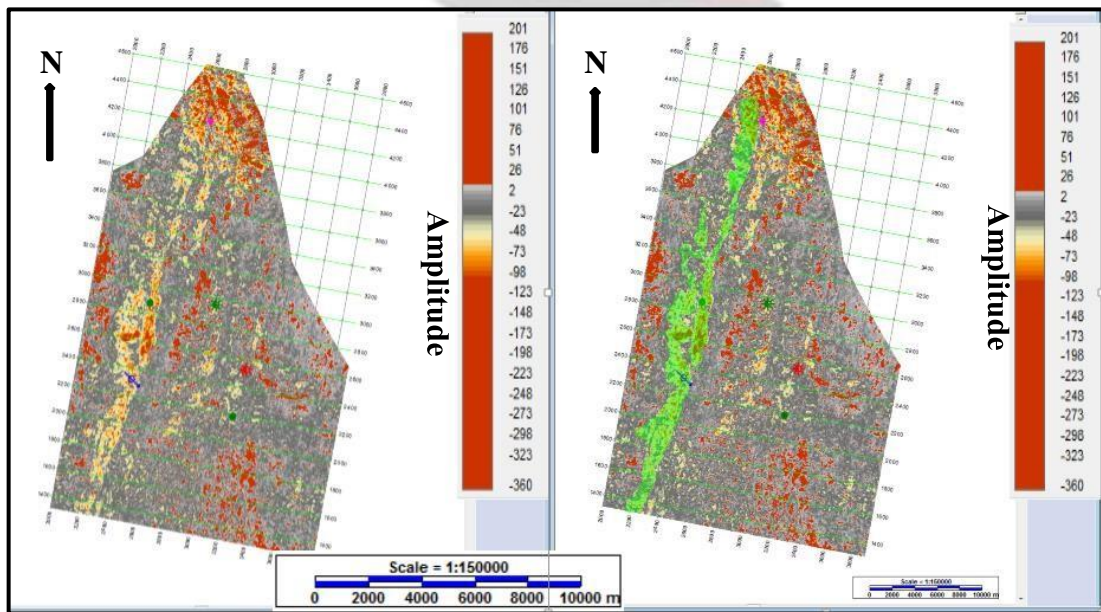


Figure 6.13 Architecture Element Map (Interval T6).

No clear channel axis is formed by the sand fairways in both western flanks (Sovereign1) and eastern flank Sovereign-2 systems on Figure 6.8. A confined and relative narrow meandering channel can be seen at the western flank, extending from northeast to southwest on Figure 6.9, Figure 6.10 and Figure 6.11.

The sand depositions in the channel at the eastern flank (Sovereign-2 system) can be interpreted to be less confined than those at the western flank (Sovereign-1 system). In Sovereign-2, Figure 6.9 revealed a typical channelized lobe with the channel at the proximal part and the lobe at the distal part indicated in the colours. This can also be seen on Figure 6.10. Deposition of sediments in the eastern flank (Sovereign-2 system) might have been in a mid-slope environment as proved by the lack of clear channel morphology (scattered deposition) on Figure 6.9, Figure 6.10, Figure 6.11 and Figure 6.12.

A clear straight channel geometry is inferred from Figure 6.13 at the western flank (Sovereign-1 system) with little or no sand deposition at the eastern flank (Sovereign-2 System). Moving from Top to base (Interval T1 to T6) the channelized lobate sand depositions at Sovereign-2 diminished but rather brighter within the Sovereign-1 sand fairway. This may be an indication that Sovereign-1 sand have been deposited before the Sovereign-2. Therefore Sovereign-2 channel system can be said to be stratigraphically older than the Sovereign-2 but of the same Turonian age. The various architecture elements were combined to produce a schematic hydrocarbon sand deposition map of the Turonian shown in Figure 14 below.

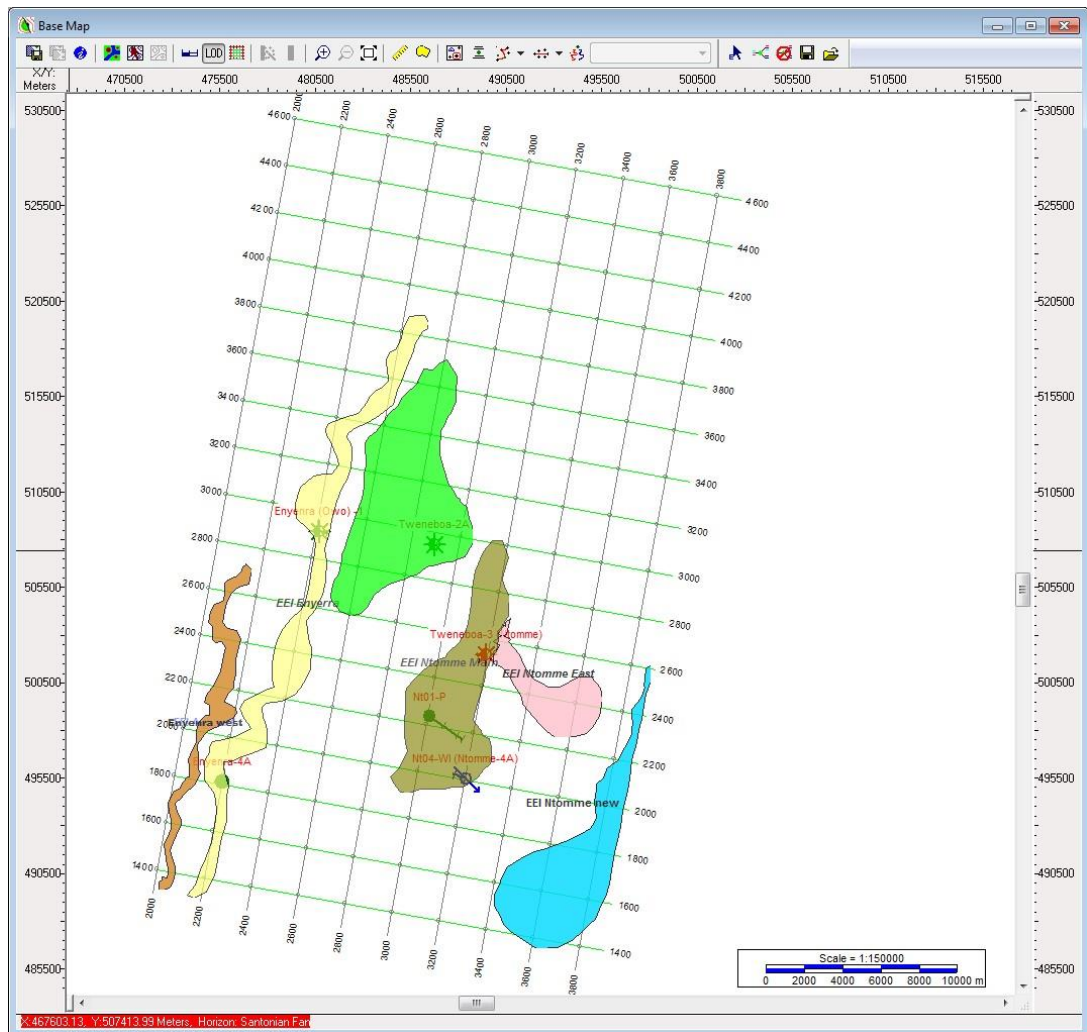


Figure 6.14: Schematic sand depositions map within Turonian Formation.

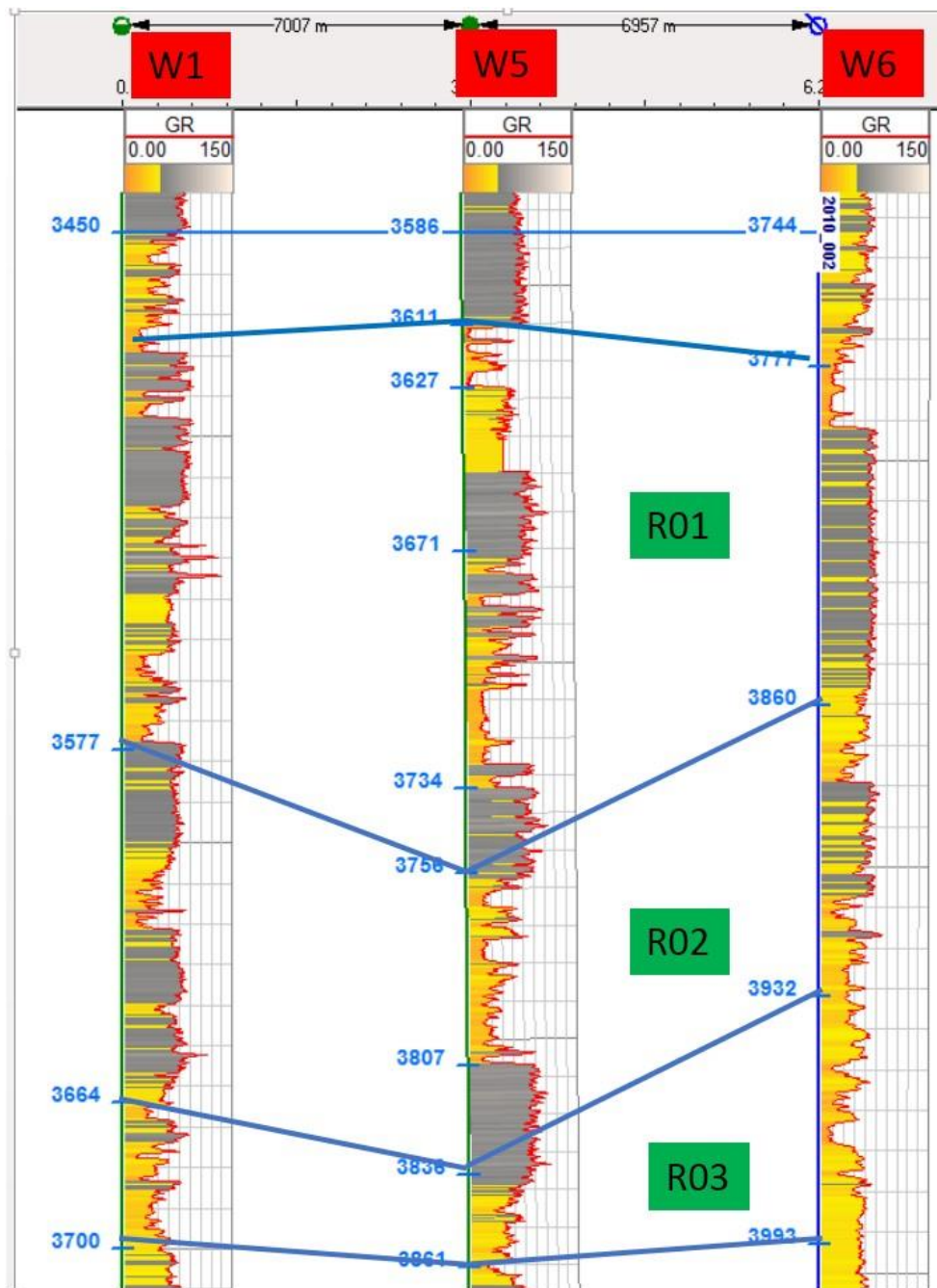
## 6.6 Well Logs Analysis of the Turonian

### 6.6.1 Correlation of Wells in Sovereign-1 fairway

Figure 6.15 below shows the result of the correlated wells using the gamma ray logs and the well tops loaded onto the Kingdom Suite Software. The grey colouration which is an indication of high gamma ray value represents the shale. The yellow colour, an indication of low gamma ray value represents the clean sand.

Shale

Sand



Legend

Figure 6.15: Well correlation within the Sovereign 1 channel complex.

The sand units of interest were mapped and correlated to give an idea of the continuity of the reservoirs at different depths within the sand prone Sovereign-1 channel system as shown on Figure 6.15. Three main reservoir units were identified on the wells logs

within Sovereign-1, namely R01, R02 and R03 (Figure 6.15) with the help of the formation tops of the wells.

### 6.6.2 Well to Seismic (EEI Chi80 data) Tie

In order to describe the reservoir units correlated, the gamma ray logs were superimposed on the EEI seismic data to show the gamma ray log behaviour with sands and shales and the ISO proportional intervals as shown in Figure 6.16. The trough (-) on the seismic section which indicates sand, matched with sand deposit of the gamma ray logs indicated in yellow. It also shows the ISO-proportional interval within which each reservoir unit falls and was also used to estimate the lateral extent of the reservoir units identified. Figure 6.16 also indicated the correlation of high negative amplitude with sands.



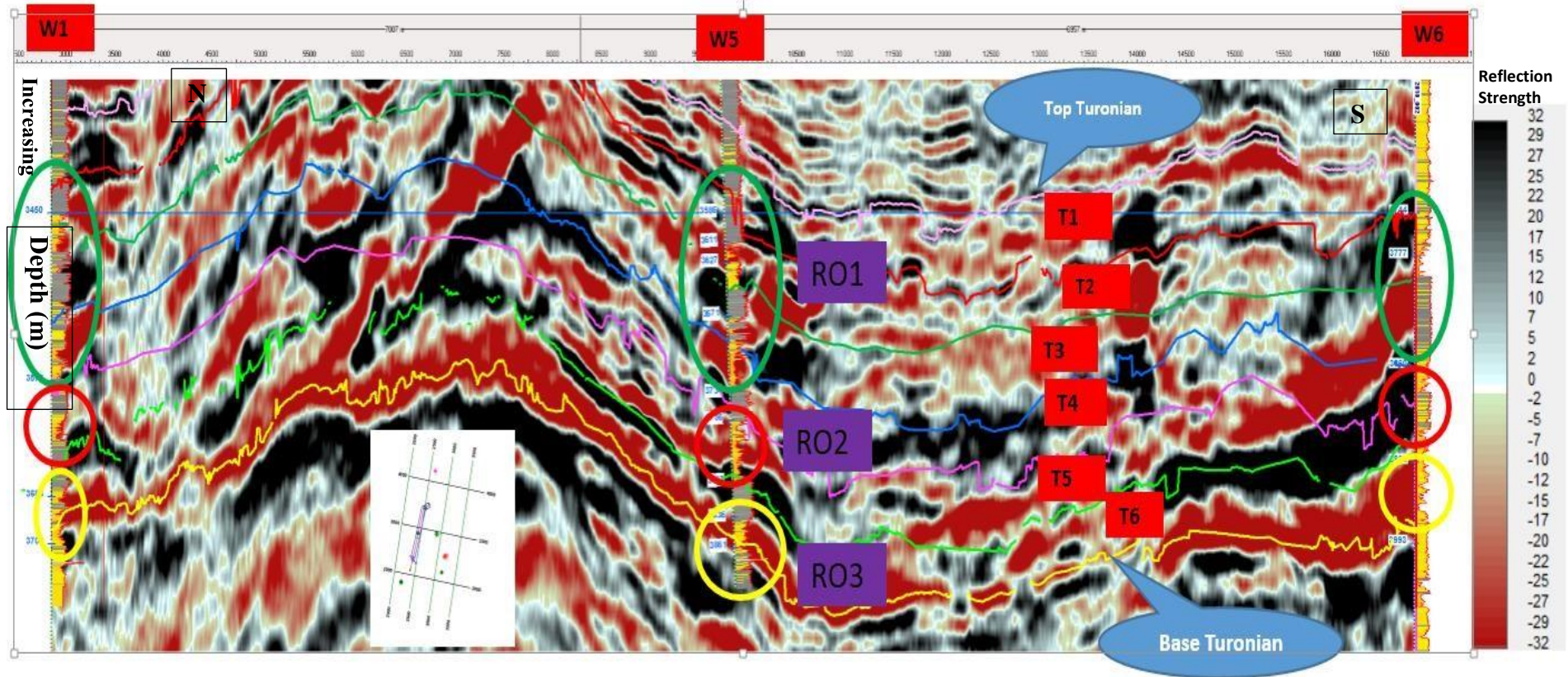
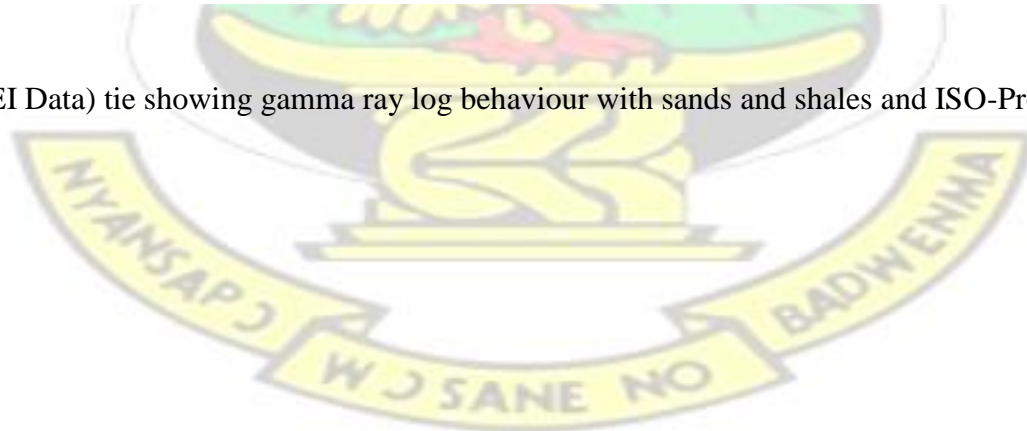


Figure 6.16: Well to Seismic (EEI Data) tie showing gamma ray log behaviour with sands and shales and ISO-Proportional Intervals.



# KNUST



R03 (sand deposit) lies in the internal T6 shown on (Figure 6.16). The trend of the amplitude extract seen on Figure 6.17 is similar to that of a straight channel which infers proximal channel source (close to channel source).

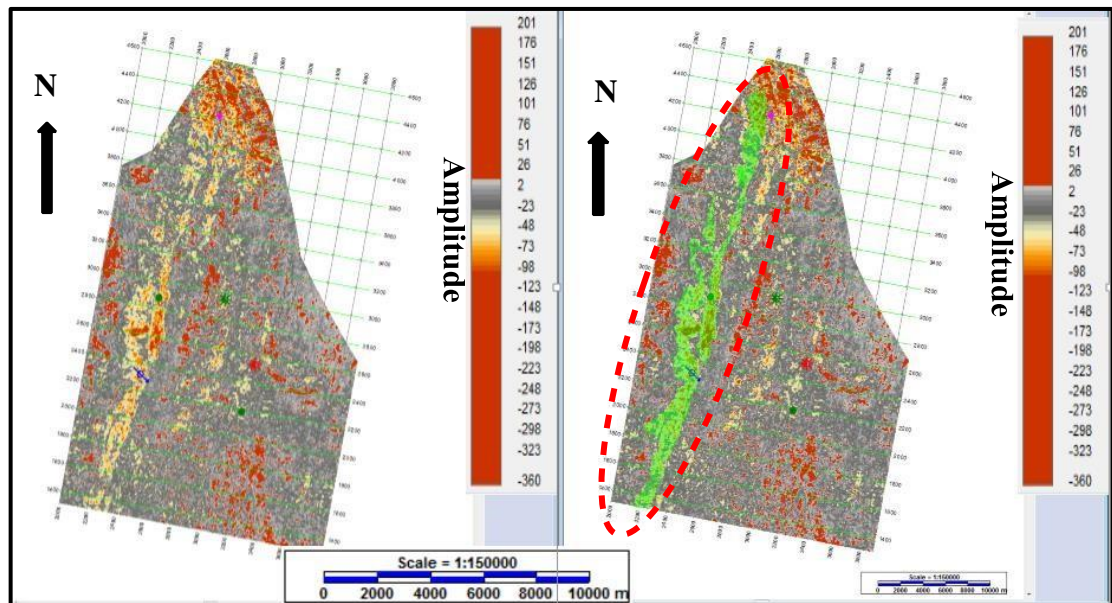


Figure 6.17: VATMIN extraction on R03 Interval.

The shale plug between R03 and R02 which is associated with increase in sea level will imply the channel source getting further landward. Therefore a braided or meandering channel morphology would be expected above the lower straight channel complex (R03). This is confirmed by the trend of VATMIN amplitude extraction on Figure 6.18 (Interval T5 and T4) within which R02 lies. The meandering morphology of the channel implies a relatively distal source (far from source).

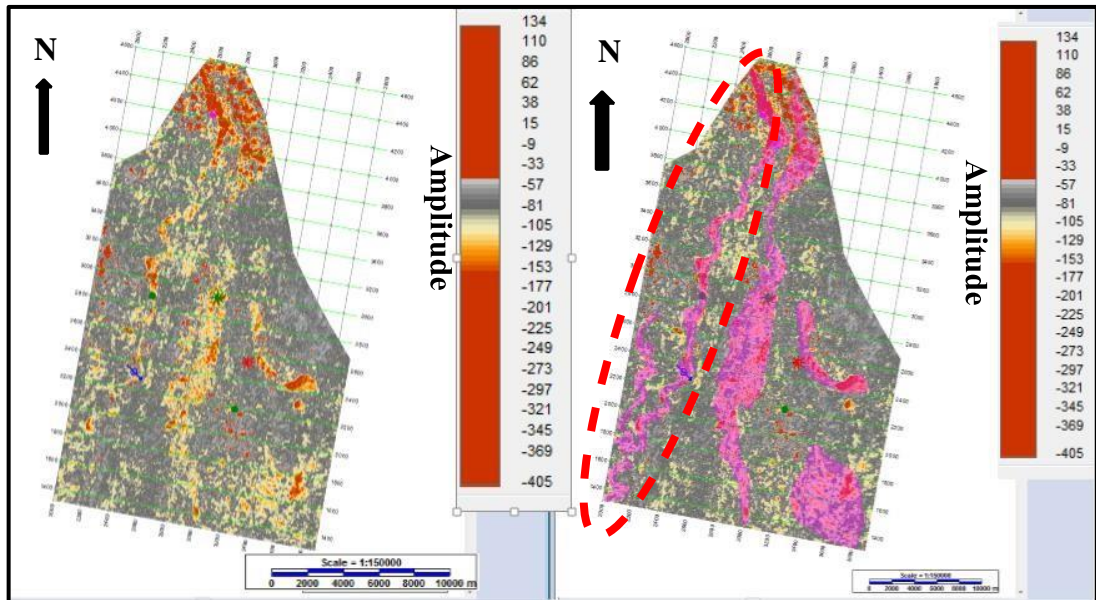


Figure 6.18: VATMIN extraction on R02 interval

R01 lies within three ISO-proportional intervals (T2, T3 and T4). The corresponding VATMIN (Figure 6.18) revealing no well-defined channel morphology but rather scattered short-lived channels. This could be formed as a result of ephemeral deposition that may result from flooding or short changes in sea level leading to the sheet-like shale-sand nature of R01.

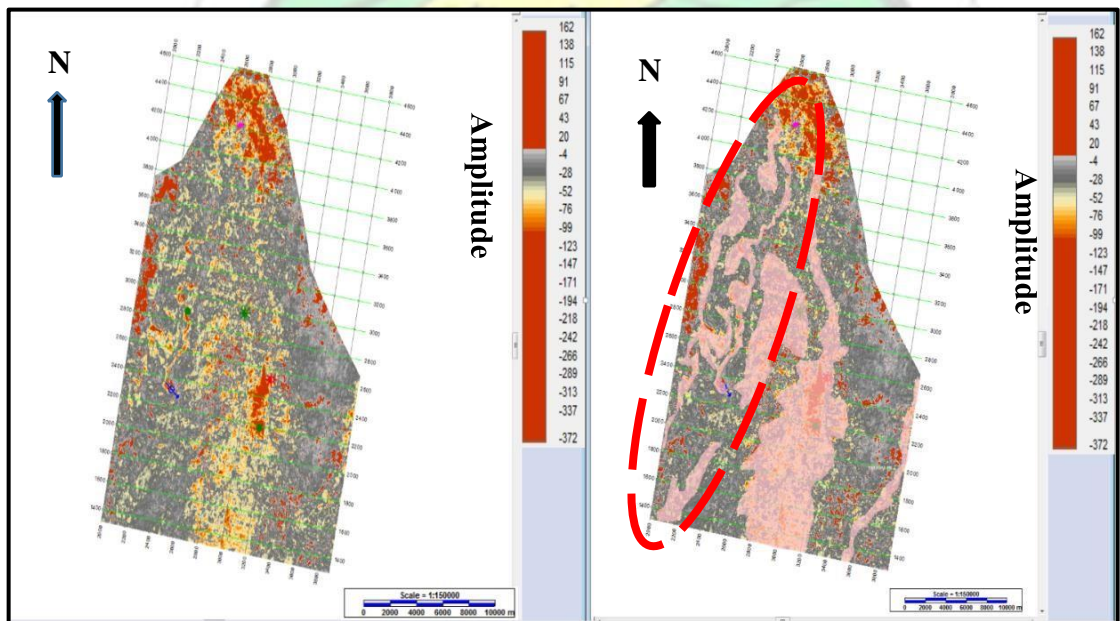


Figure 6.19: VATMIN Extraction on Reservoir R01 Interval.

### 6.6.3 Estimation of Petrophysical Parameters of Sovereign-1 Sand Fairway.

Table 6.1 shows the average petrophysical parameters of the Wells in Sovereign-1 computed for each reservoir unit. Table 6.2 also shows the estimated average petrophysical parameters of the delineated Sovereign-1 reservoir.

Table 6.1: Summary of Petrophysical Parameters of Wells within Sovereign-1

Well Name	Sand Bodies	Top (m)	Bottom (m)	Gross (m)	Net (m)	N/G	Av Phi (%)	Av Sw (%)	Av. K (mD)
<b>W1</b>	<b>R01</b>	<b>3745.0</b>	<b>3872.0</b>	<b>127.1</b>	<b>19.7</b>	<b>0.16</b>	<b>17.0</b>	<b>21</b>	<b>145.61</b>
	<b>R02</b>	<b>3872.0</b>	<b>3916.0</b>	<b>44.0</b>	<b>5.2</b>	<b>0.12</b>	<b>17.0</b>	<b>39</b>	<b>46.57</b>
	<b>R03</b>	<b>3916.0</b>	<b>3998.0</b>	<b>82.0</b>	<b>3.5</b>	<b>0.04</b>	<b>16.0</b>	<b>32</b>	<b>105.59</b>
<b>W5</b>	<b>R01</b>	<b>3575.0</b>	<b>3793.0</b>	<b>218.2</b>	<b>55.0</b>	<b>0.33</b>	<b>17.0</b>	<b>24</b>	<b>221.89</b>
	<b>R02</b>	<b>3793.3</b>	<b>3871.0</b>	<b>77.8</b>	<b>13.4</b>	<b>0.17</b>	<b>18.0</b>	<b>31</b>	<b>242.34</b>
	<b>R03</b>	<b>3871.0</b>	<b>3933.3</b>	<b>63.2</b>	<b>12.3</b>	<b>0.20</b>	<b>15.0</b>	<b>17</b>	<b>101.51</b>
<b>W6</b>	<b>R01</b>	<b>3985.8</b>	<b>4058.2</b>	<b>72.4</b>	<b>28.4</b>	<b>0.39</b>	<b>18.0</b>	<b>18</b>	<b>247.33</b>
	<b>R02</b>	<b>4058.2</b>	<b>4095.4</b>	<b>37.2</b>	<b>9.6</b>	<b>0.26</b>	<b>16.4</b>	<b>31</b>	<b>150.10</b>
	<b>R03</b>	<b>4110.7</b>	<b>4123.0</b>	<b>39.9</b>	<b>9.6</b>	<b>0.24</b>	<b>16.0</b>	<b>20</b>	<b>110.70</b>

Table 6.2: General Average Petrophysical Parameters of the Sovereign-1.

<b>Sovereign-1 Reservoirs</b>	Av. Gross (m)	Av. Net (m)	N/G	Av Phi (%)	Av. Sw (%)	Av. Shc (%)	Av. K (mD)
<b>R01</b>	<b>139.23</b>	<b>34</b>	<b>0.24</b>	<b>17.33</b>	<b>21.0</b>	<b>79.0</b>	<b>183.75</b>
<b>R02</b>	<b>79.50</b>	<b>9.4</b>	<b>0.12</b>	<b>17.13</b>	<b>35.0</b>	<b>65.0</b>	<b>144.45</b>
<b>R03</b>	<b>61.70</b>	<b>8.5</b>	<b>0.14</b>	<b>15.60</b>	<b>24.5</b>	<b>75.5</b>	<b>105.42</b>

An approximate net pay totals 51.9 m is distributed among three oil reservoirs, R01, R02 and R03 as shown on Table 6.2. Net oil pay of 34 m was intersected in the shallowest channel (R01 pool) which had an average porosity of 17.33 percent, water saturation of 21.0 percent and permeability of 183.75 mD. This is an indication of good hydrocarbon deposits with hydrocarbon saturation of 79 percent. Below the thick shale section is an average of 9.4 m of net oil pay in two stacked channels (R02 pool) with an average porosity of 17.13 percent, water saturation of 35 percent, hydrocarbon saturation of 65 percent and permeability of 144.45 mD. A further 8.5 m of net pay was intersected in (R03), which had an average porosity of 16 percent, water saturation of 24.5 percent, hydrocarbon saturation of 75.5 percent and permeability of 105.42 mD. Therefore the reservoir properties (porosity, permeability and hydrocarbon saturation) are generally good and the reservoirs are of good quality with high hydrocarbon contents.

#### **6.6.4 Correlation of Wells in Sovereign-2**

The sand units were mapped and correlated to give an idea of the continuity of the reservoirs at different depths along the sand prone Sovereign-2 fairway as seen in Figure 6.20.

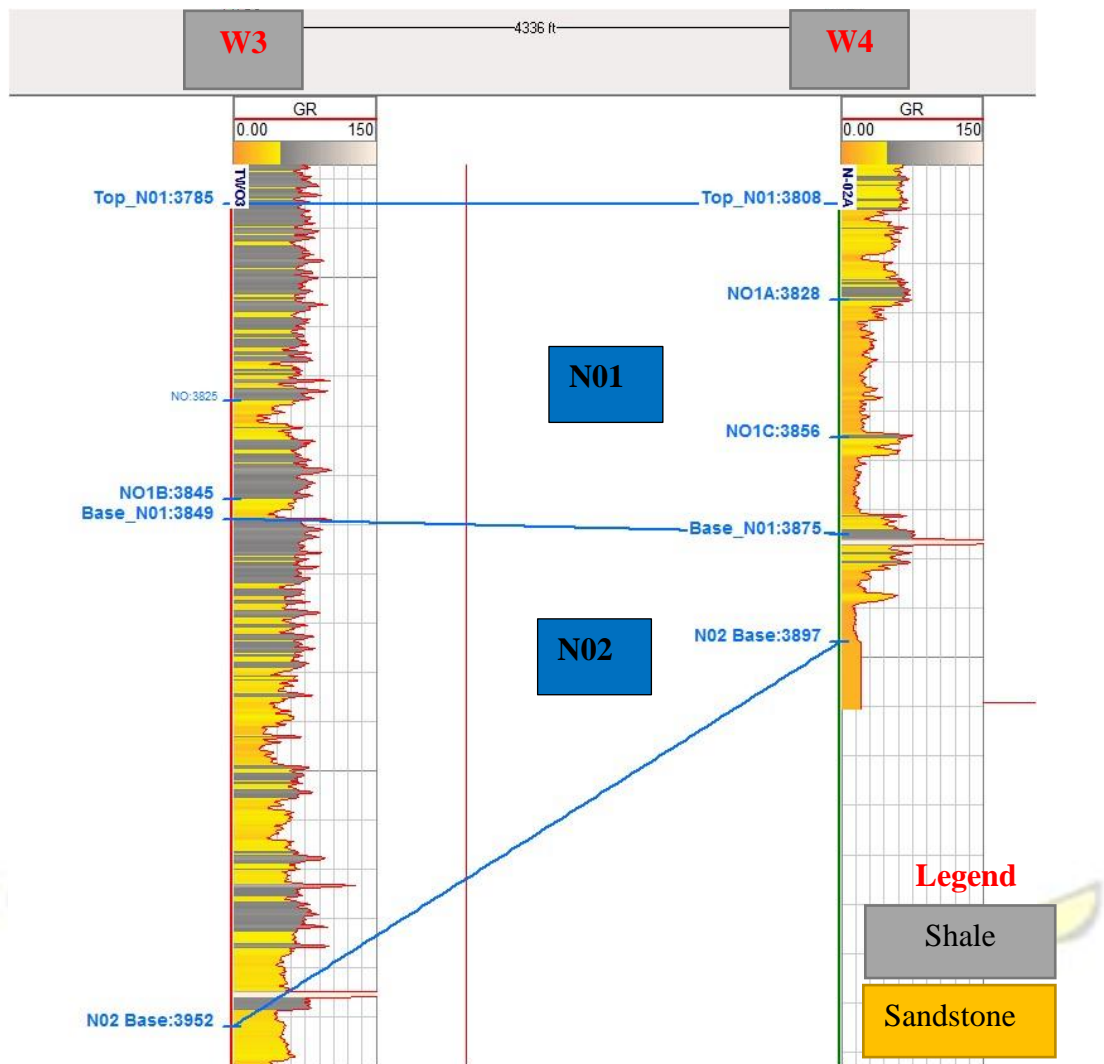


Figure 6.20: Well correlation within the Sovereign 2.

The yellow colouration represents the sandstones zones and the grey colour indicates the Shale. The shale regions can also be seen to have high gamma values and clean sand having low gamma values. This is characteristic of gamma ray log readings.

Two main reservoir units were identified in the Sovereign-2, namely N01 and N02 (Figure 6.20) with the help of the formation tops loaded into the Kingdom Suite Software.

#### 6.6.5 Well to Seismic (EEI Chi80) ties within Sovereign-2 Sand fairway

Figure 6.21 represents the gamma ray logs tie to seismic data showing the behaviour of the gamma ray logs with sands and shales with the ISO-proportional intervals. The

ISOproportional intervals give the depth range within which each reservoir unit (N01, N03) falls. In Figure 6.21 below, the low gamma values indicated as yellow colour on the gamma ray affirm the clean sands which are the trough (red) on the seismic section. This confirms the good correlation between the amplitude with the sands shown on W3 gamma ray log (Figure 6.21).

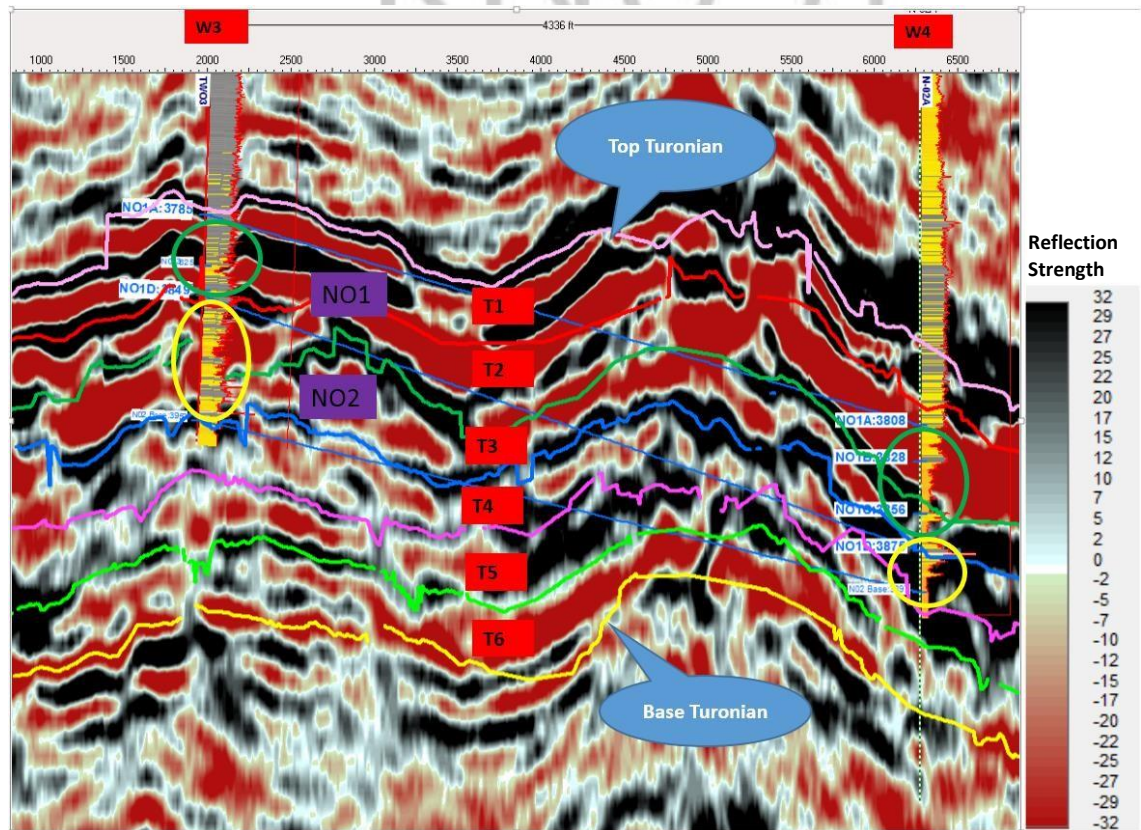


Figure 6.21 Well to Seismic (EEI data) tie showing gamma ray behaviour with sands and shales with the ISO-proportional intervals.

The N01 falls within T1 to T3 as shown on Figure 6.21. The extracted VATMIN amplitude for the N01 reservoir unit is shown in Figure 6.22. Inferred from VATMIN extraction on these intervals, sands deposition in N01 reservoir unit occurred in the channelized lobe with good sand quality as seen on Figure 6.22.

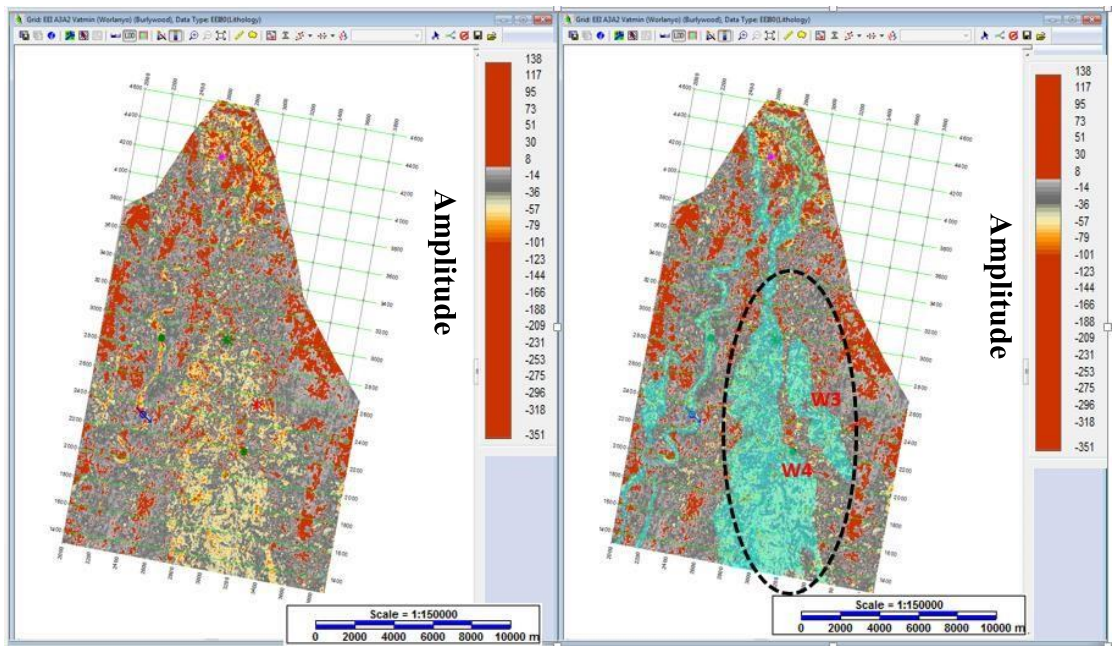


Figure 6.22: VATMIN Amplitude extraction on N01 Interval

N02 also lies within interval T4 and T5. The VATMIN amplitude extraction (figure 6.23) revealed diminishing of sand sediment deposition moving vertically from T4 to T6 as seen in Figure 6.23 below.

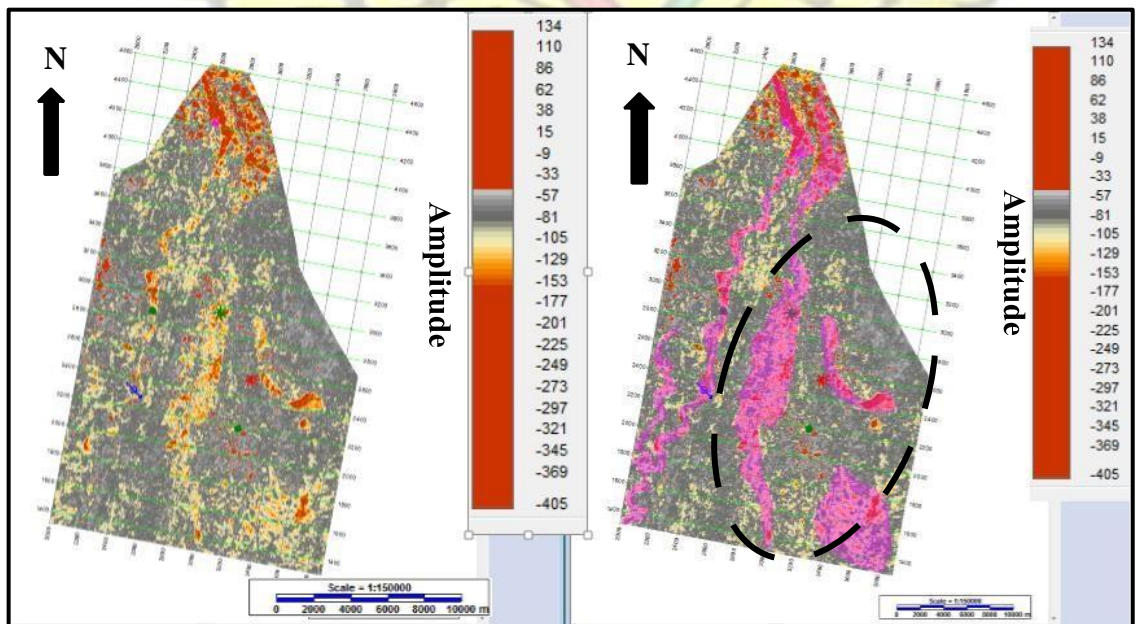


Figure 6.23: VATMIN Amplitude extraction on N02

### 6.6.6 Reservoir Properties of Sovereign -2 Sand Fairway

Table 6.3 gives summary of computed reservoir properties of the reservoir units of wells within Sovereign-2 and Table 6.4 gives the estimated averages of the reservoir properties of Sovereign-2 sand fairway.

Table 6.3: Reservoir Properties of the Wells within Sovereign-2

Well Name	Sand bodies	Top (m)	Base (m)	Gross (m)	Net (m)	N/G	Av. Phi (%)	Sw (%)	Av. K (mD)
<b>W4</b>	<b>N01</b>	3809.2	3887.3	78.1	41.8	0.54	19.0	23.70	252.70
	<b>N02</b>	3887.3	3897.0	9.7	2.3	0.23	19.4	93.00	13.00
<b>W3</b>	N01	3785.0	3849.4	64.4	4.0	0.06	14.5	71.20	49.00
	N02	3849.4	3952.5	103.1	10.9	0.11	16.4	69.40	49.90

Table 6.4: Summary of Petrophysical Parameters of Sovereign-2

<b>Sovereign 2 Reservoirs</b>	Av Gross (m)	Av Net	N/G	Av Phi (%)	Av Sw (%)	Av. Shc (%)	Av. K (mD)
<b>N01</b>	71.0	22.9	0.32	17.7	26.35	73.65	151.85
<b>N02</b>	56.4	6.6	0.12	17.9	81.20	18.80	31.45

The averages of the petrophysical parameters are summarised for Sovereign-2 reserve as follow (Figure 6.4); net pay thickness of 22.9 m, 17.7 percent porosity, 26.35 percent water saturation, hydrocarbon saturation of 73. 65 percent, and 151.85 mD permeability for N01. The N02 oil pool has 17.9 percent porosity, 81.20 percent water saturation, 18.80 percent hydrocarbon saturation and 31.45 mD permeability. The high water saturation of 81.20 percent in N02 reservoir unit is an indication of its low hydrocarbon

accumulation. It can be inferred from the reservoir properties that the reserve is prolific for development.

### 6.6.7 Reservoir quality comparison of Sovereign-1 and Sovereign-2 Fairways

Figure 6.24 below shows the analysis of the porosity and permeability cross plot of wells used within the Turonian interval.

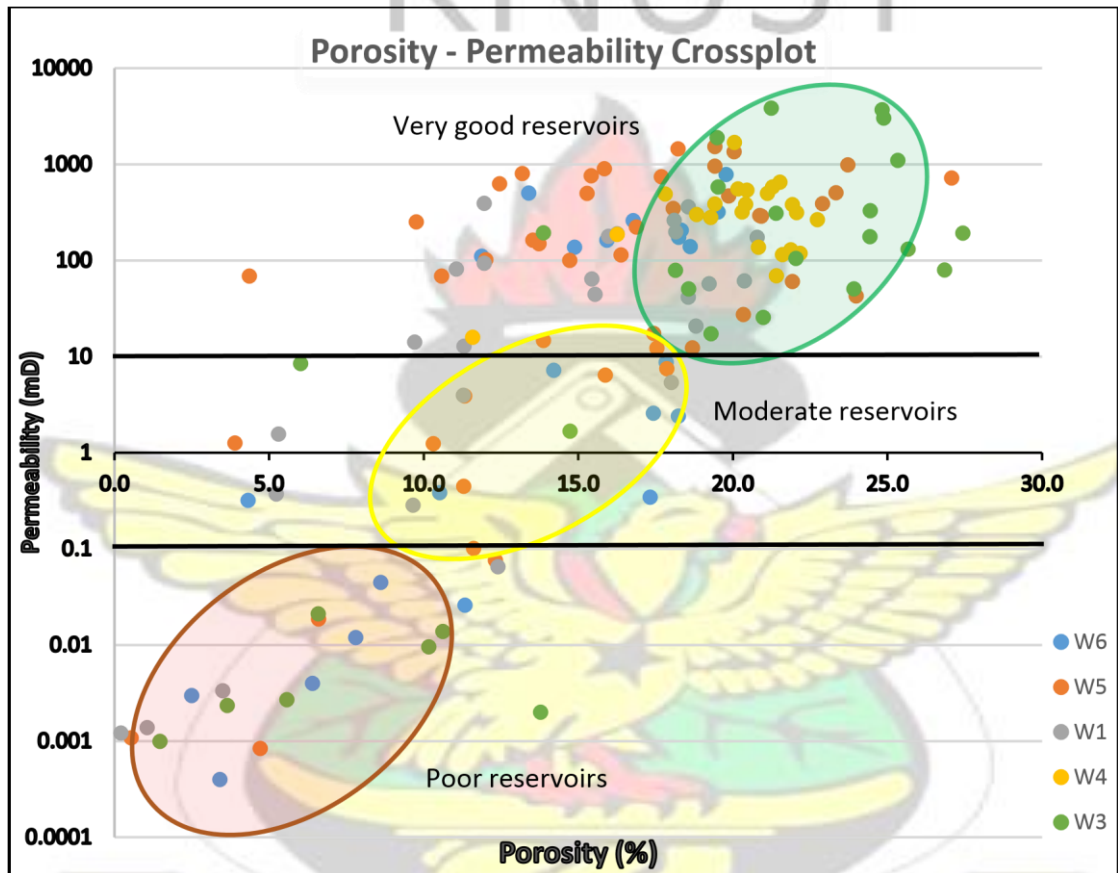


Figure 6.24: Porosity- Permeability Cross Plot

A clear partition can be observed from Figure 6.24. Sample displaying poor reservoir quality indicated in the red circle have porosity less than 10 percent and permeability less than 0.1 mD which may be attributed to shale or mudstone dominated regions.

Between 10-15 percent porosity and 0.1-10 mD is classified as moderately good reservoirs sands. Porosity range of 15-30 percent and permeability between 10-1000 mD representing very good reservoirs with very good sandstones.

From Figure 6.24, W4 and W3 can be inferred to have good porosity and permeability sands concentration in the very good reservoir region compared to the rest of the wells. These wells fall within Sovereign-2 reservoir, an indication that Sovereign-2 reservoir has more clean sands and of good reservoir quality than Sovereign-1.

## 6.7 Estimation of Volume of Hydrocarbon

The formula,  $STOIIP = \text{Gross Rock Volume} \times (N/G) \times (1-S_w) \times (1/B_o) * CF * RF$  as stated in the methodology was used to estimate the total in-place volume of hydrocarbon. The input parameters and the estimated results of in-place volume of hydrocarbon for Sovereign-1 and Sovereign-2 are shown in Table 6.5 and Table 6.6 respectively.

### 6.7.1 Estimation of Volume of Hydrocarbons in Sovereign-1

Table 6.5 gives the parameters used and the estimated in-place volume of hydrocarbon of the reservoir units (R01, R02 and R03) for Sovereign-1 reserve. The estimated volume of 254 MMbbl for R01, 67 MMbbl for R02, and 135 MMbbl contributed to a total of 456 MMbbl in-place hydrocarbons (STOIIP) in Sovereign-1 reserve.

Table 6.5: Volumetric Estimation of Sovereign-1 reserves

Petrophysical Parameters	R01	R02	R03
av. Area extent, A, (m <sup>2</sup> )	37546820.87	42174760.7	38045589.08

av. Height, h, (m)	139.23	79.5	61.7
av. Volume, GRV=A*h	5227643869	3352893476	2347412846
Net to Gross ratio (N/G)	0.24	0.12	0.34
Porosity (Phi)	0.17	0.17	0.15
Recovery Factor (RF)	0.30	0.30	0.30
Conversion Factor (CF)	6.29	6.29	6.29
Formation Volume Factor (1/Bo)	0.80	0.80	0.80
Hydrocarbon Saturation (Shc)	0.79	0.65	0.75
STOIIP (bbl.)	254363701.00	67115861.16	113554478.00
<b>STOIIP (MMbbl)</b>	<b>254.00</b>	<b>67.00</b>	<b>135.00</b>

### 6.7.2 Estimation of Volume of Hydrocarbon in Sovereign-2

Table 6.6 summarises the input parameters and the estimated in-place volume of hydrocarbon (STOOIP) of the Sovereign-2 reserve. N01 gives 365MMbbl and N02 gives 25 MMbbl with a total of 388 MMbbl in-place hydrocarbon for Sovereign-2.

Table 6.6: Volumetric Estimation of Sovereign-2 reserve.

<b>Petrophysical Parameters</b>	<b>N01</b>	<b>N02</b>
Av Area (m <sup>2</sup> )	84,102,006.40	73,322,124.96

Av Height (m)	71.00	56.00
Av Volume, GRV=A*h	5971242454.00	4106038998.00
Net-to-gross ratio (N/G)	0.32	0.12
Porosity ( $\Phi$ )	0.17	0.18
Recovery Factor (RF)	0.30	0.30
Conversion Factor (CF)	6.29	6.29
Formation volume factor (1/Bo)	0.80	0.80
Hydrocarbon Saturation (Shc)	0.74	0.19
STOIIP	362875136.40	25438547.44
<b>STOIIP (MMbbl)</b>	<b>363.00</b>	<b>25.00</b>

## 6.8 Structural Interpretation of Santonian

### 6.8.1. Depth Structural Maps of Santonian

Figure 6.25a and Figure 6.25b are structural maps of the top and base Santonian respectively. The top Santonian (Figure 6.25a) is in the depth range of 2435 m to 3798 m, dipping from the northeast towards the southwest. This has revealed a sloping subsurface topography of the top Santonian Formation.

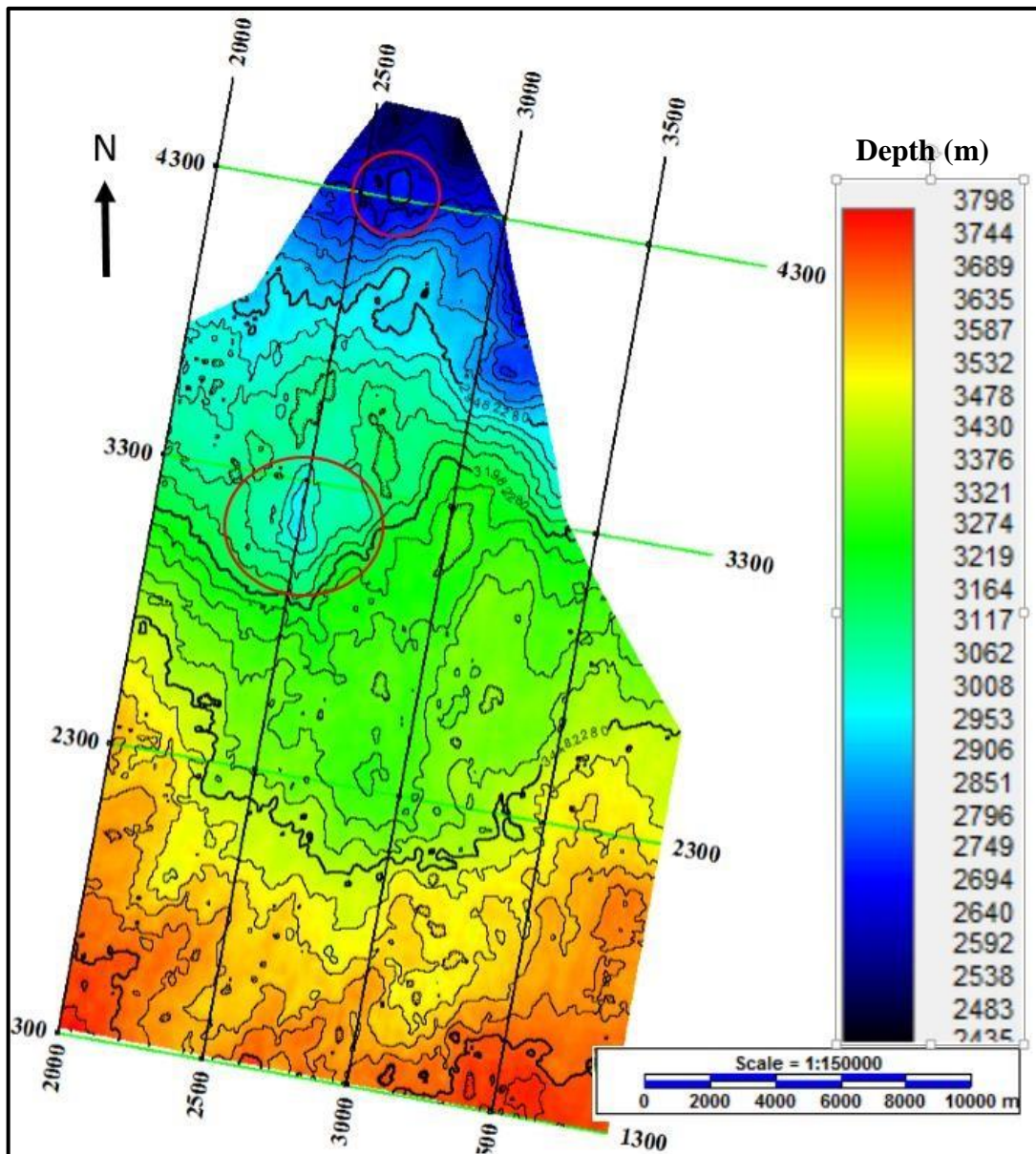


Figure 6.25a: Depth Structural Map of Top Santonian

The surface of the base Santonian from seismic reference datum ranges between 2585 m at the north to 4004 m and dipping towards the south as indicated on figure 6.25b. The four way closures (anticlinal features) are indicated in the red circles labelled on both Figure 6.25a and Figure 6.25b. Deposition of sediments may follow the sloping subsurface topography.

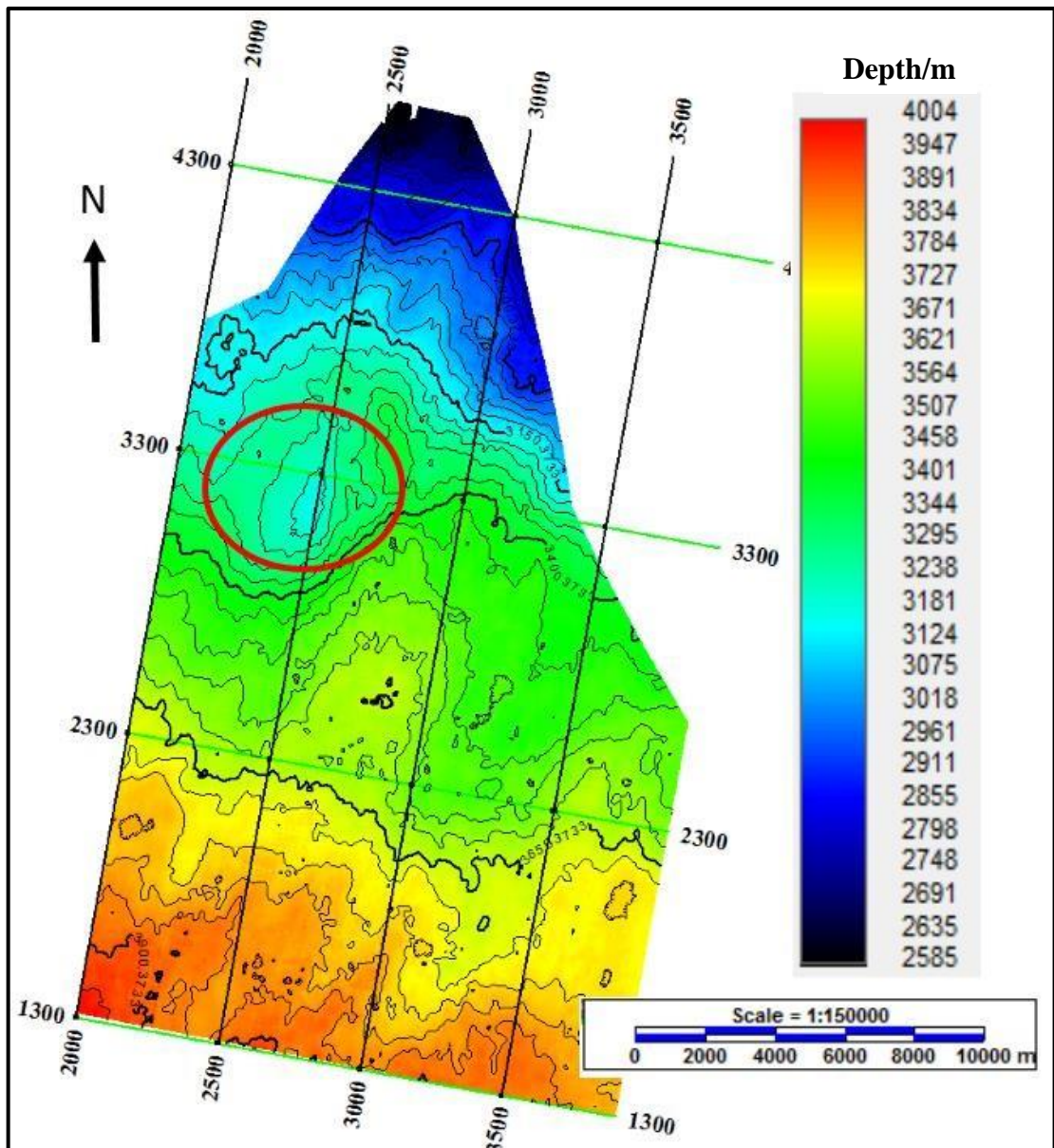


Figure 6.25b: Depth Structural Map of Base Santonian

### 6.8.2 Isopach Map

Figure 6.26 is the Isopach map of the Santonian formation. It shows a thickening of the reservoir sediments at the centre. The Santonian gets thinner away from the centre and towards the eastern and western flanks respectively. This can be inferred as a basin or fan.

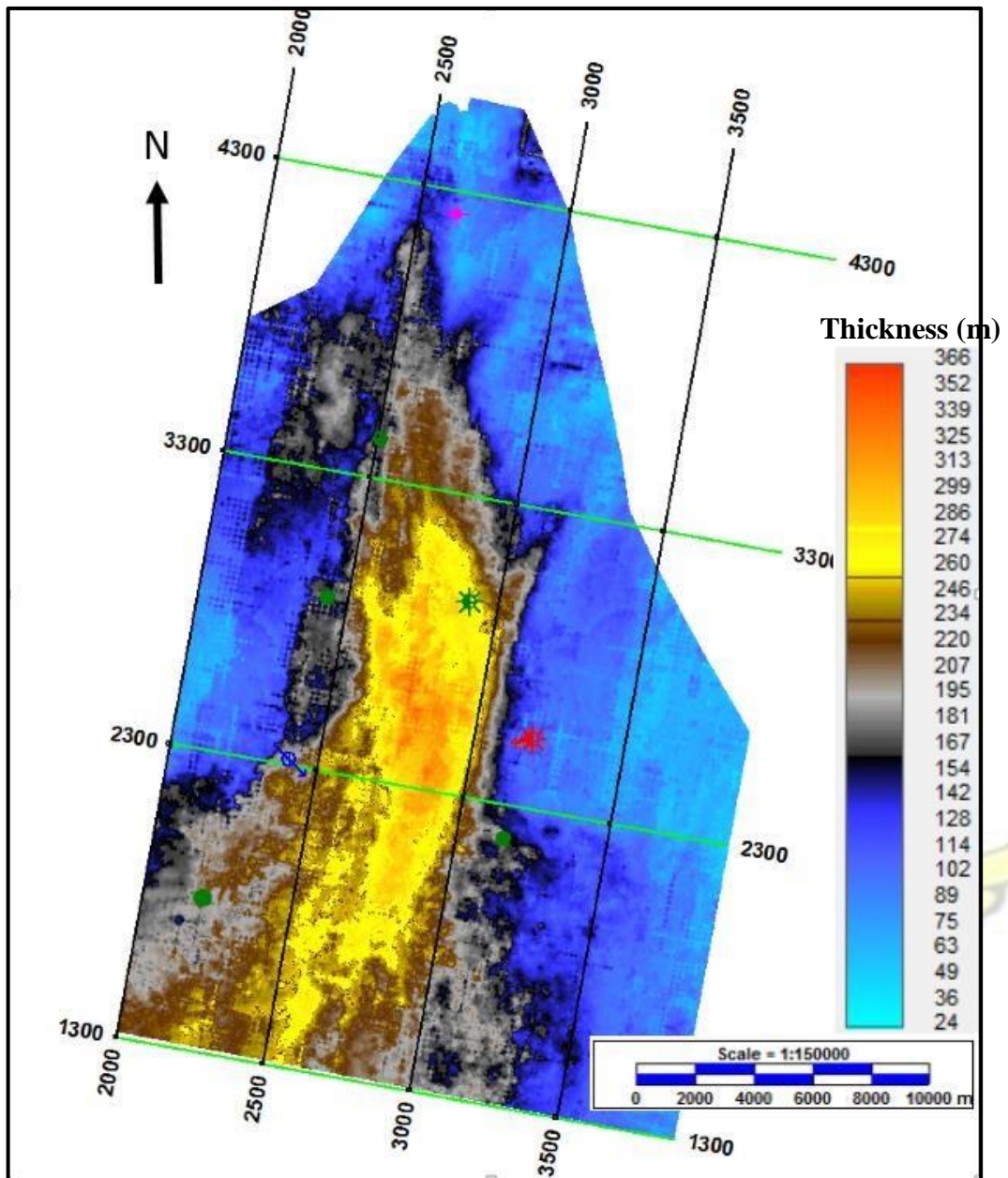


Figure 6.26: Santonian Isopach map

### 6.9 Volume Attribute Maps Interpretation of the Santonian

Figure 6.27a shows the Santonian sand deposition fairway indicated in the red polygon delineated by extracting amplitude on the reflectivity data (Tano Depth IT7). The trend showed a complex amalgamated straight to slightly sinuous channels forming the Santonian fan system.

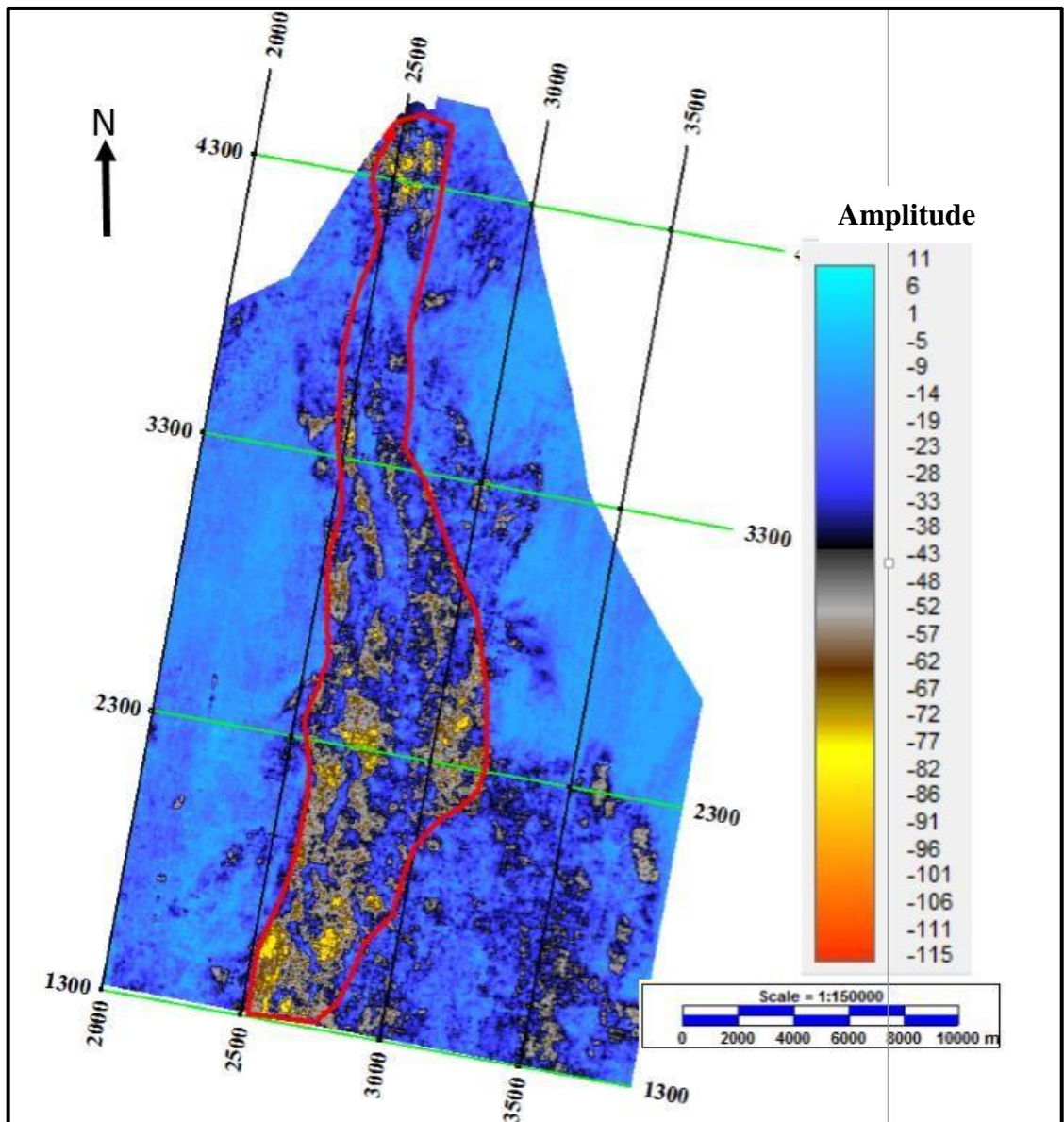


Figure 6.27a: Reflectivity Amplitude Map for the Santonian Interval

Figure 6.27b below is the VATMIN extraction on the Santonian interval. The sand deposits are highlighted in the black polygon. It reveals amalgamated straight channel features which were also inferred from Figure 6.26.

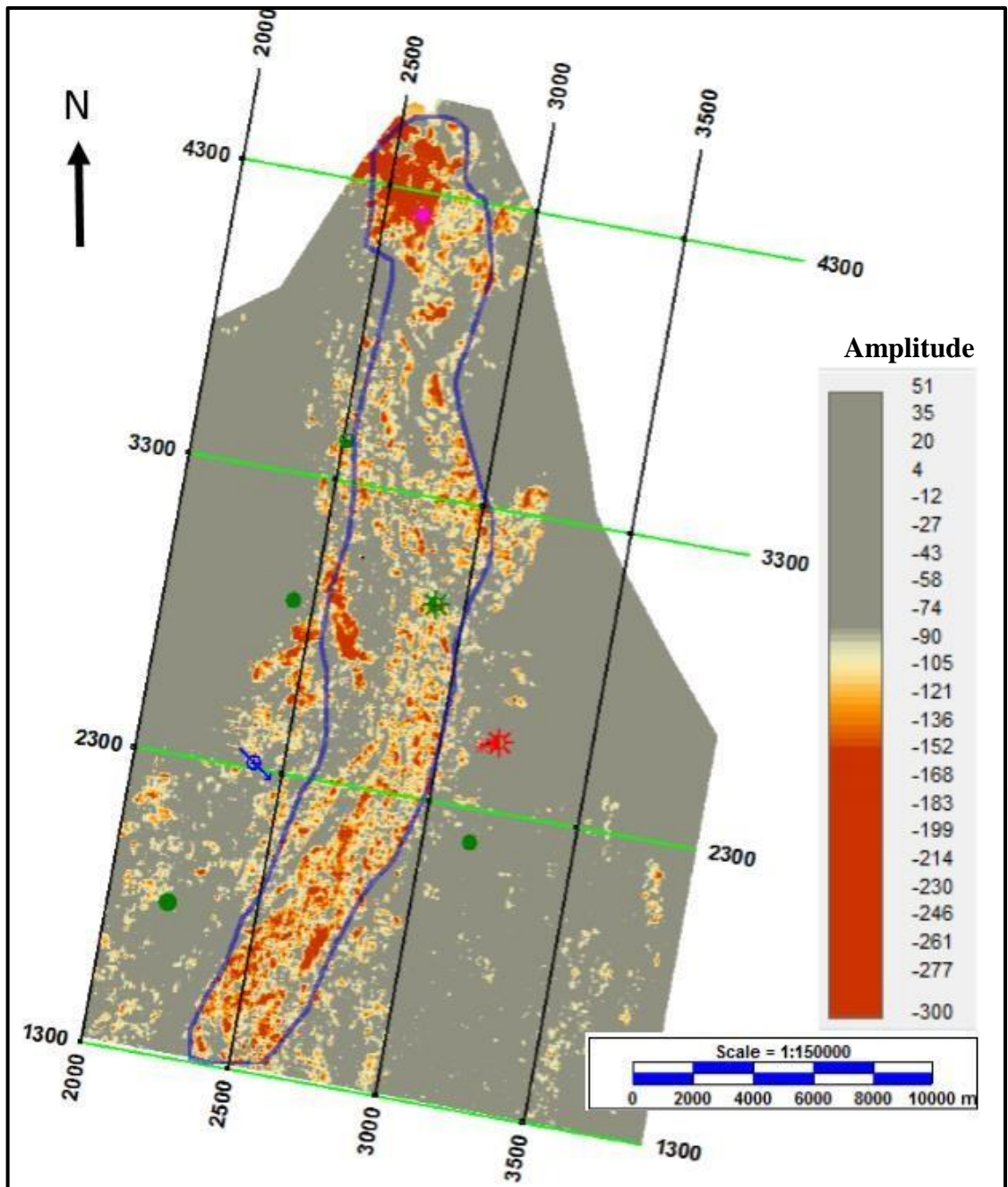
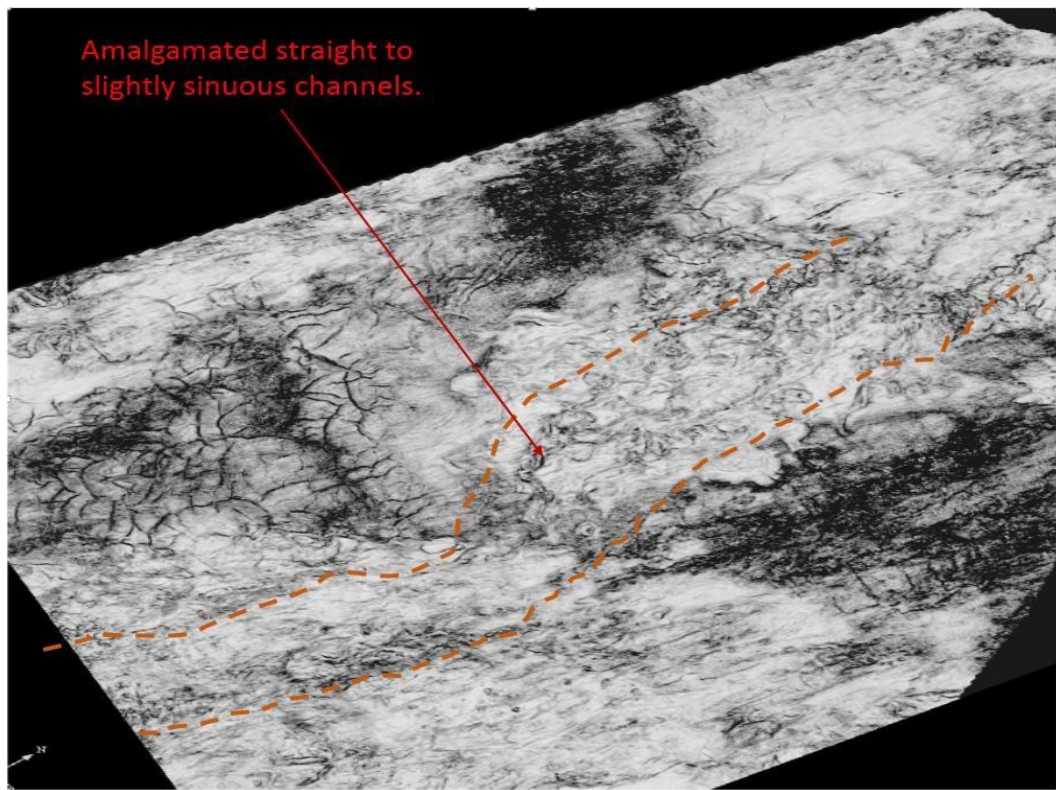


Figure 6.27b: VATMIN Amplitude Extraction on the EEI data (EEI Chi80)

### 6.10 Interpretation of Coherency Slices

The coherency slice were computed to study the depositional environment within the Santonian formation. Figure 6.28a and 6.28b show the coherency slice for the near base and near top of the Santonian formation.



Amalgamated straight to slightly sinuous channels

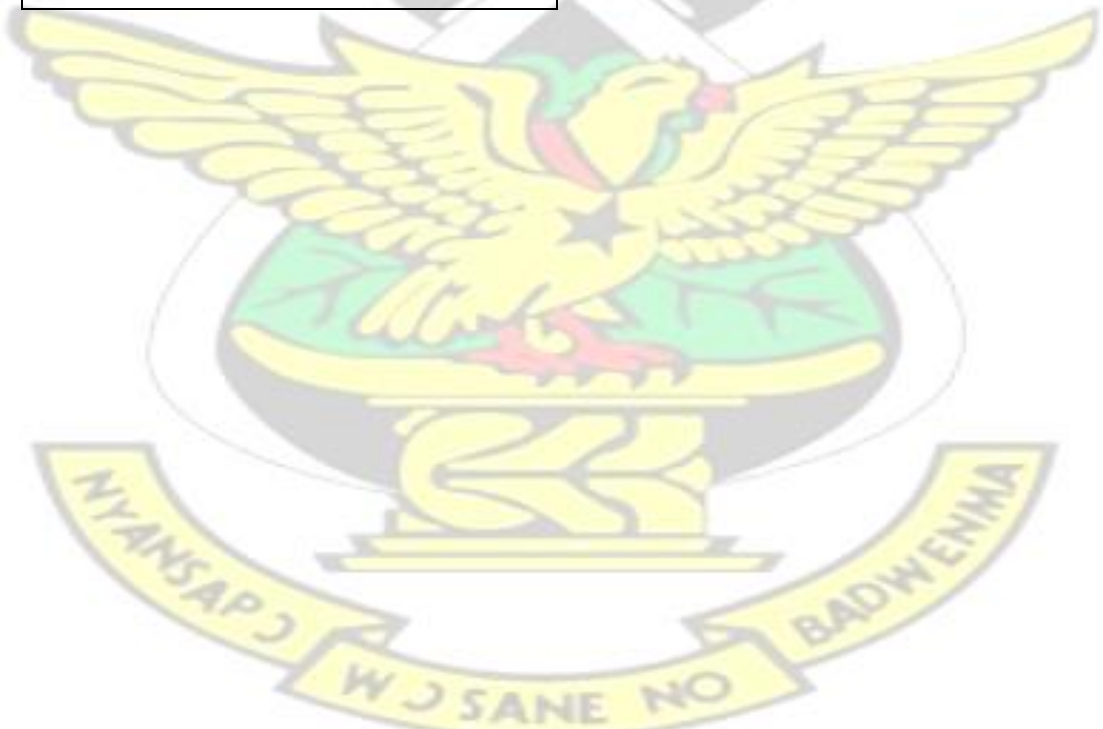


Figure 6.28a: Coherency slice near top of Santonian.

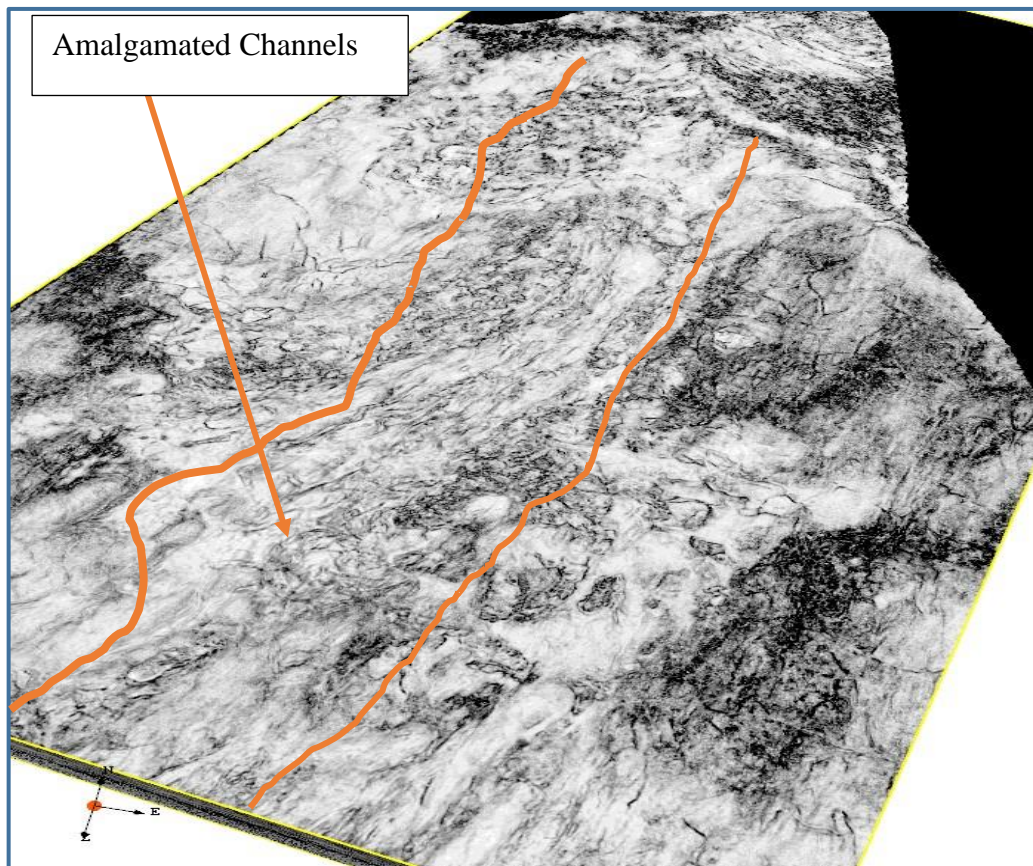


Figure 6.28b: Coherency Slice near the base of Santonian  
 The Santonian coherency image revealed river channel at the middle, as seen on Figure 6.28a and Figure 6.28b. This confirmed the straight to sinuous channel inferred from the amplitude extraction maps, and gives a good validation of the depositional environments. From the coherency slices no clear channel axes can be seen.

### 6.11 Interpretation of Architecture Element Maps

The Santonian package consists of amalgamated channel systems of varying depositional environment observed on architecture element maps. Although the amplitude extraction from Figure 6.27a and Figure 6.27b revealed a single confined straight to slightly sinuous channel hosting the good sands, the architecture elements give details of the internal depositional features of the Santonian sand fairway.

Figure 6.29 revealed a braided channel system. The channel is clearly formed as shown in Figure 6.30. It meandered at the middle of the channel and became less sinuous further basinwards. This may be regarded as complex reservoir geometry and variable distribution of sandstones.

Figure 6.31 and Figure 6.32 show deposition of sediments with no clear channel axis. No clear formation of channels on interval S5 and S6 as seen on Figure 6.33 and Figure 6.34. Figure 6.35 is a schematic hydrocarbon sand deposition obtained from the combination of all the architecture elements. Below are the architecture elements maps of the Santonian Interval.

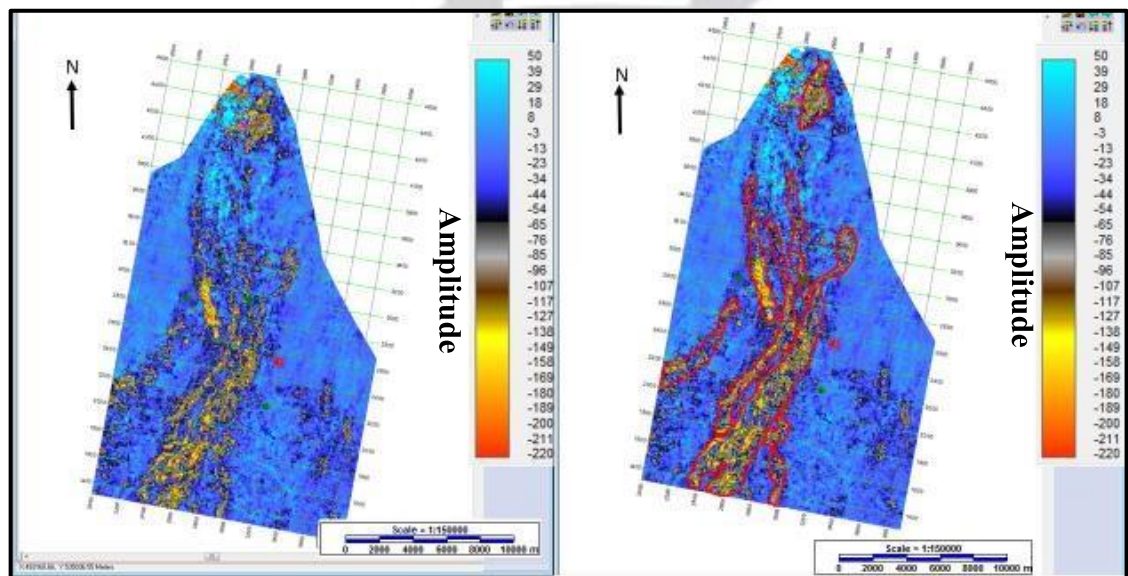


Figure 6.29: Architecture Element Map (Interval S1)

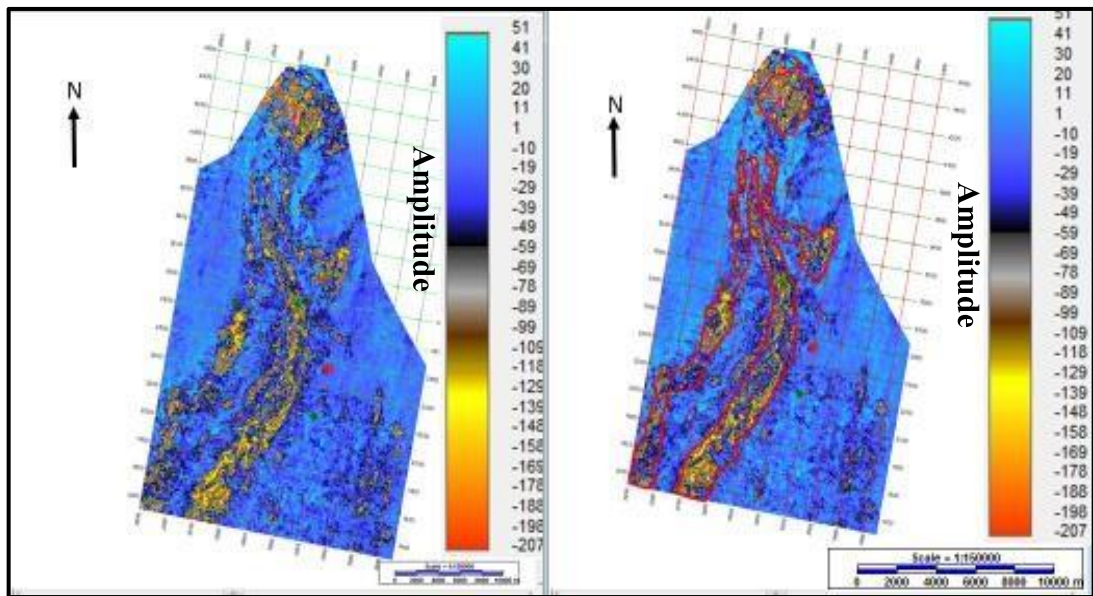


Figure 6.30: Architecture Element Map (Interval S2)

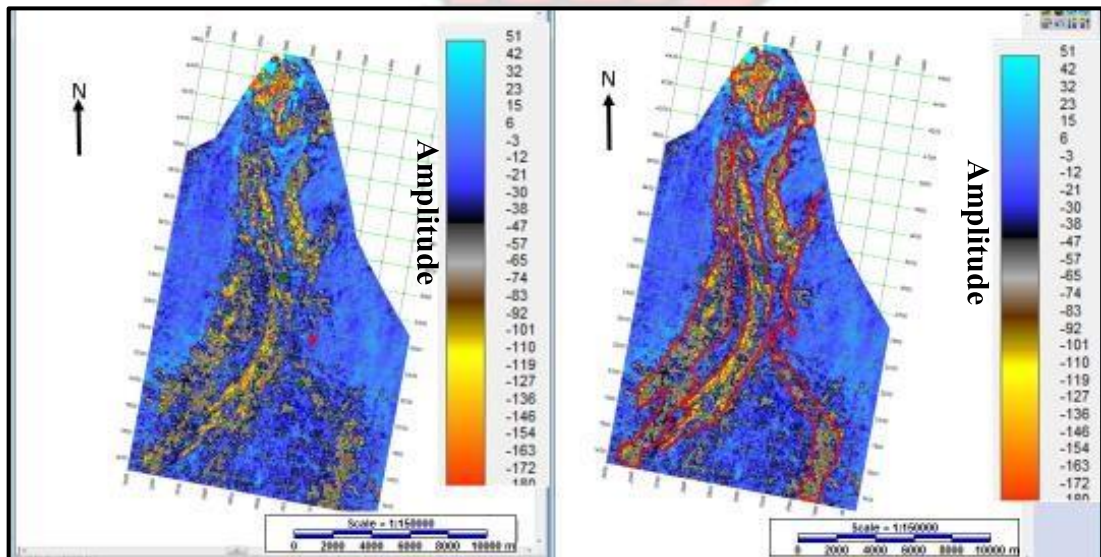


Figure 6.31: Architecture Element Map (Interval S3)

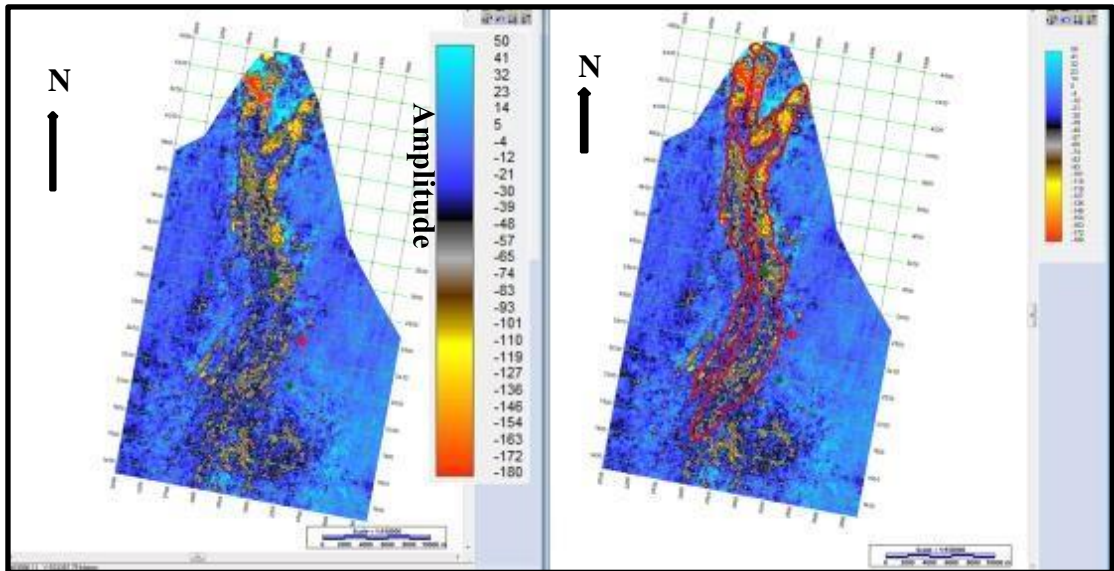


Figure 6.32: Architecture Element Map (Interval S4)

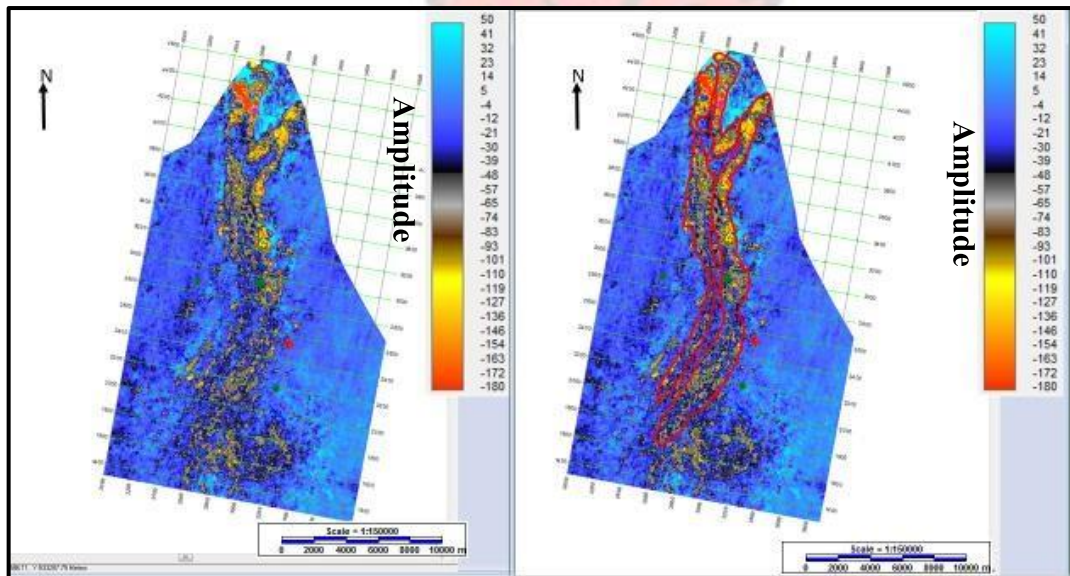


Figure 6.33: Architecture Element Map (Interval S5)

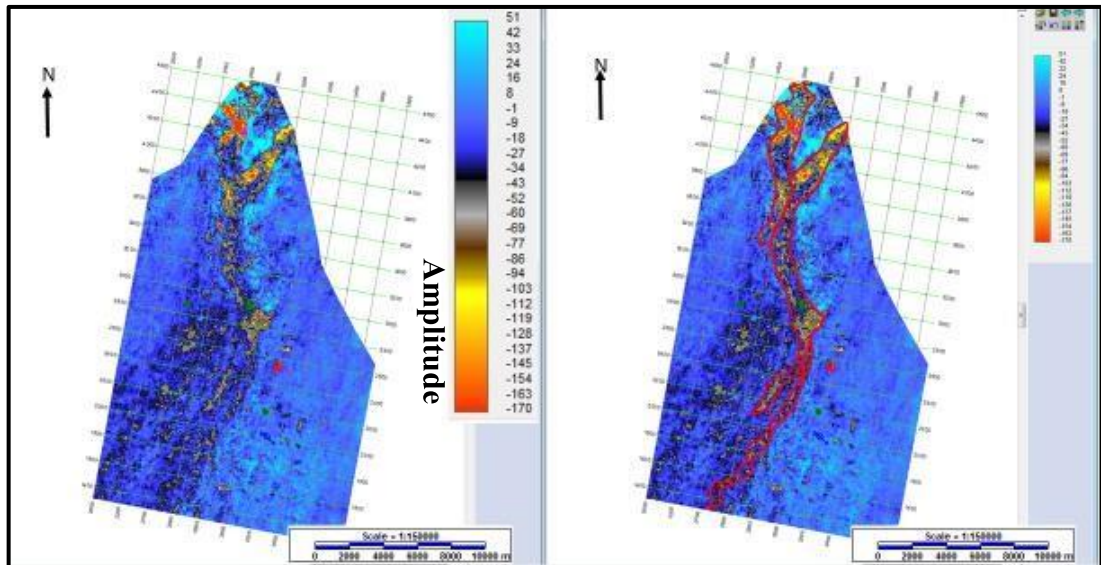


Figure 6.34: Architecture Element Map (Interval S6)

The combined architectural elements as shown on Figure 6.35 below gives the schematic sand deposition maps of the Santonian. Due to the fact that the exploration wells drilled in the TEN fields did not target the Santonian formation, no petrophysical analysis was undertaken. Thus most wells drilled in the TEN fields can be seen to be outside the bright negative amplitude regions within the Santonian which did not give sufficient well log data. Therefore future exploration wells should target the Santonian in order to ascertain the economic viability.

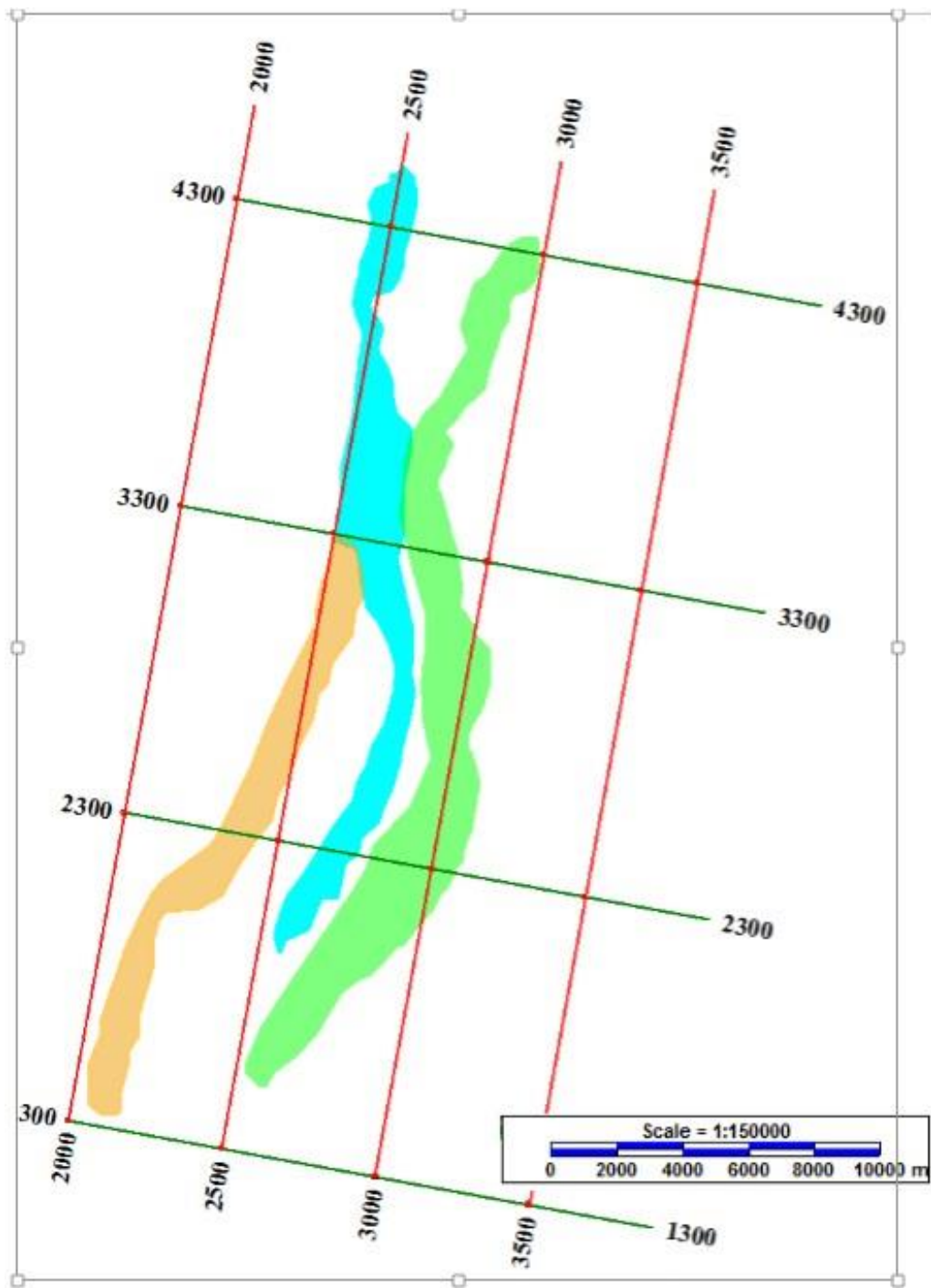


Figure 6.35: Schematic hydrocarbon sand deposition map of the Santonian.

## CHAPTER SEVEN

### CONCLUSION AND RECOMMENDATIONS

## 7.1 Conclusion

Seismic reflectivity (PSDM) data and EEI Data with well logs data were employed in characterizing the reservoirs within the Turonian and the Santonian formations of the TEN field within the Deepwater Tano Block.

Structural interpretation revealed few anticlinal features (four way closures) which may be capable of hosting hydrocarbons. The depth structural maps revealed a sloping subsurface topography for both Turonian and Santonian formations, dipping from the northeast towards the southwest. The thicknesses were estimated to be in the ranges 10401 m and 24-366 m for Turonian and Santonian respectively from Isopach maps. Coherency attribute and the architecture element maps extractions (for Turonian and Santonian intervals as well as ISO-proportional intervals) were effective in delineating hydrocarbon sand areas and the morphology of the depositional environment.

The seismic attribute analyses were successful in delineating two main sand prone depositional fairways in the Turonian formation labelled as Sovereign-1 and Sovereign2 respectively. Sovereign-1 is a complex sinuous channels system with its sand depositions in a well confined to relatively narrow channels and associated spillovers or levees. The mid slope channelized lobe constituted the Sovereign-2 sand fairway located at the eastern flank of the study area. Sovereign-2 is less confined than the Sovereign-1 and with good hydrocarbon sand depositions.

A straight to slightly sinuous channel system comprising braided river system, crevasse splay was also delineated as the host of sands deposition within the Santonian.

Three main reservoir units denoted as R01, R02 and R03 were identified and correlated in Sovereign-1. R01 has average porosity of 17.33 percent, permeability 183.75 mD, 21 percent water saturation, 79 percent hydrocarbon saturation and average net thickness of 34 m. Average porosity value 17.13 percent, 144.45 mD permeability, 35 percent water saturation and 9.4 m net thickness were recorded for R02. R03 has average values of 15.6 percent, 120 mD, 24.5 percent, 75.5 percent and 8.5 m were obtained for the porosity, permeability, water saturation, hydrocarbon saturation and net thickness respectively.

For Sovereign-2 reserve, two main reservoir units namely N01 and N02 identified have the following average reservoir properties. 17.7 percent porosity, 151.85 mD permeability, 26.35 percent water saturation, 73.65 percent hydrocarbon saturation and 37.3 m net pay thickness for N01. N02 oil pool has 17.9 percent porosity, 81.2 water saturation, hydrocarbon saturation of 18.8 percent and permeability of 31.45 mD.

No petrophysical studies have been done for the Santonian interval. This is because the Santonian was not the target of drilled wells in the TEN field. There is therefore the need for detailed petrophysical interpretation of the Santonian due to the fact that amplitude extracts in this study have shown the existence of good sand deposition.

The volume of in-place hydrocarbons was estimated to be 456 MMbbl for Sovereign-1 reserve and 388 MMbbl for Sovereign-2 reserve respectively. This gave a total of 844 MMbbl of in-place hydrocarbon in the Turonian formation of the study area. The estimated volume (844 MMbbl) if put to production at the current production rate of 100, 000 barrel per day as the case in the Jubilee Field in the Tano Basin will last for approximately twenty five (25) years. Sovereign-1 and 2 in the Turonian are therefore of

good reservoir qualities and with high in place volume of hydrocarbon for future development while appraisal well should target the Santonian sand prone areas for detailed analysis and characterization.

The objectives outlined in this thesis have been achieved to a large extent having delineated structural and depositional features, delineated the sand occurrence zones, computed petrophysical properties of the reservoir and having estimated volume of hydrocarbon in place which can be used as the basis for future development of the field.

## **7.2 Recommendations**

Further analysis on the depositional environment can be done to check the control of the depositional morphology on recoverability by convolving the coherence slices, shape of the gamma ray logs and side core images.

Future TEN development wells can target channels axis of the Santonian taking into consideration the bright amplitude extractions within the Santonian.

Furthermore, deterministic volumetric computation should also be undertaken and compared with the probabilistic approach used in this thesis in order to enhance the economic viability of the reserve.

## **REFERENCES**

1. Adda G.W., (2013). The Petroleum Geology and Prospectivity of the NeoProterozoic, Paleozoic and Cretaceous Sedimentary Basins in Ghana: AAPG publication No. 10544 (2013).
2. Aigbedion, I., Aigbedion, H. O. (2011). Hydrocarbon Volumetric Analysis using Seismic and Borehole Data over Umoru Field, Niger Delta-Nigeria, *Int. J. Geosci.*2: p. 179-183.
3. Ajisafe, Y. C., & Ako, B. D. (2013). 3D Seismic Attribute for Reservoir Characterization of Y Field Niger Delta, Nigeria. *IOSR Journal of Applied Geology and Geophysics (IOSR-JAGG)*. v. 1, Issue 2 (Jul.-Aug. 2013), p 23-31.
4. Anadarko. (2011). Exploration of the Transform Margin of West Africa. Houston: Anadarko Petroleum Cooperation, AAPG.
5. Archie, G. E. (1942). The Electrical Resistivity log as an Aid in Determining Some Reservoir Characteristics: *Petroleum Technology*, V.S, p. 54-62.
6. Atta-Peters, P., Garrey (2014). Source Rock Evaluation and Hydrocarbon Potential in the Tano Basin, South Western Ghana, West Africa: *International Journal of Oil, Gas and Coal Engineering*. Vol. 2, No. 5, pp. 66-77. doi: 10.11648/j.ogce.20140205.11
7. Bahorich, M., & Farmer, S. (1995). 3D Seismic Discontinuity for Faults and Stratigraphic Features: Coherence cube. *The Leading Edge*, v. 14, p. 1053-1058.
8. Baker Hughes. (1999). *Petroleum Geology*. Houston USA: Baker Hughes. p. 25-45
9. Beaupretre, S. (2015). Seismic Interpretation Workshop: IFP Training, October 12-23.
10. Boggs Jr, S. (1995). *Principles of Sedimentary and Stratigraphy*, Prentice Hall, p. 774.

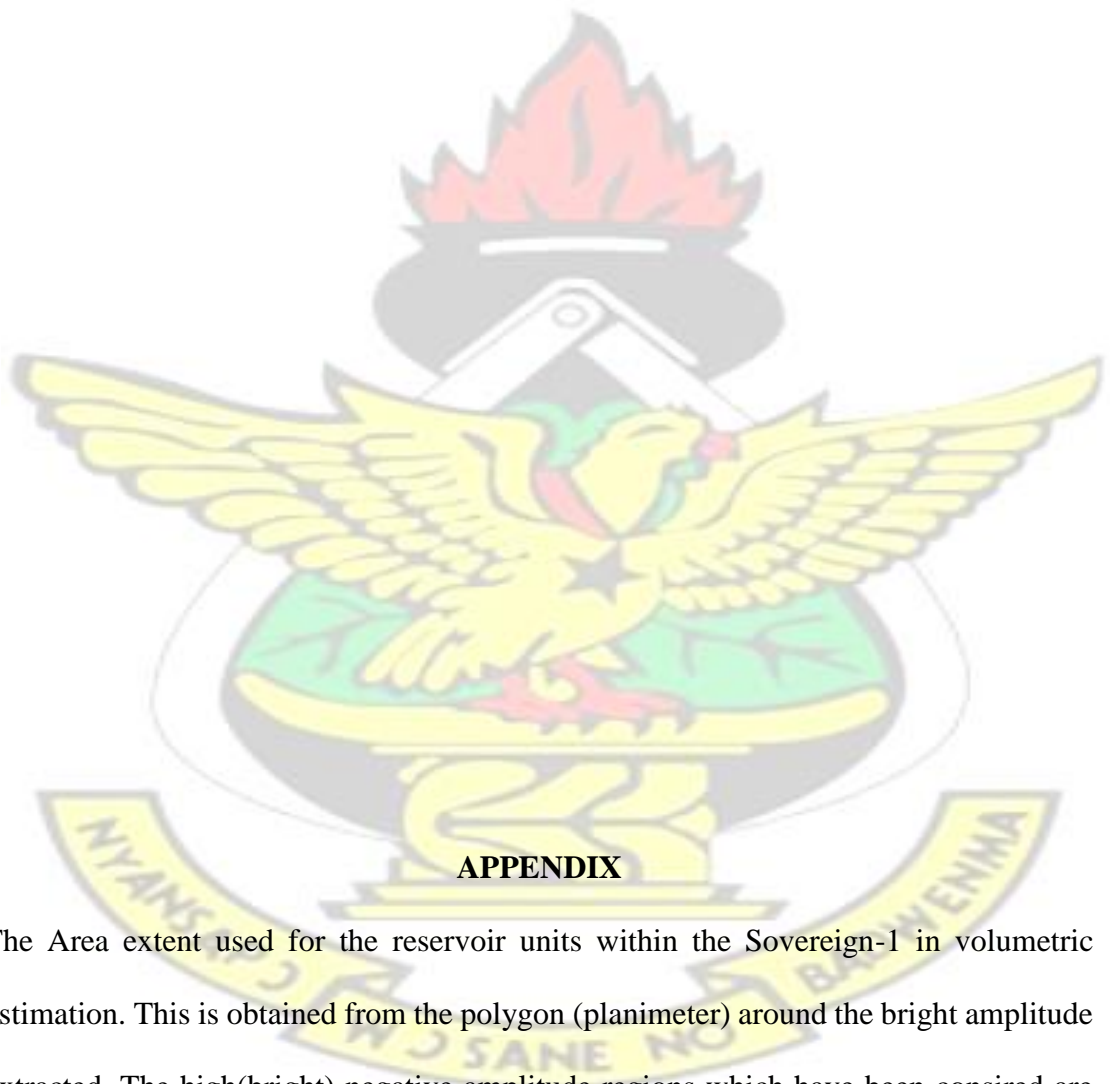
11. Brown A. R. (1996). Seismic Attributes and their Classification: The Leading Edge, v.15, p. 1090.
12. Brownfield, M. E., & Charpentier, R. R. (2006). Geology and Total Petroleum Systems of the Gulf of Guinea Province of West Africa: U.S Geological Survey Bulletin 2207-c, p. 32.
13. Chopra, S., & Michelena, R. J. (2011). Special Section: Reservoir Characterization. The Leading Edge, January 2011. p. 35-37.
14. Chopra, S., and Marfurt, K. J., (2007). Seismic attributes for prospect identification and reservoir characterization.
15. Chopra, S., Lines, L. R., Schmitt, D. R., & Batzle, M. L. (2010). Heavy Oils: Reservoir Characterization and Production Monitoring: SEG Geophysical Development Series No. 13, p. 1-2.
16. Davies, D. W. (1986). The Geology and Tectonic Framework of the Republic of Ghana and the Petroleum Geology of the Tano Basin, Southwestern Ghana. Internal Report, Ghana National Petroleum Cooperation.
17. Dean, L., & Mireault, R. (2008). Reservoir Engineering for Geologists: Part 3: Production Decline Analysis. Canadian Society of Petroleum Geologists Reservoir, Vol. 35, Issue 1. p. 12-18.
18. Doligez, B., Bessis, F., Burrus, J., Ungerer, P., & Chenet, P. Y. (1986). Integrated Numerical Simulation of Sedimentation, Heat Transfer, Hydrocarbon Formation and Fluid Migration in A Sedimentary Basin: The Themis Model. Thermal Modelling In Sedimentary Basins. Proceedings of The 1st IFP Research, Conference On Exploration, Carcans, June 3-7, 1986, p. 173-195.
19. Fowler, M. L., Young, M. A., Madden, M. P., & Cole, E. L. (1999). The Role of Reservoir Characterization in the Reservoir Management Process, Reservoir Characterization – Recent Advances, AAPG Memoir 71, p. 3-31.

20. Francis, A., & Hicks, G. J. (2006). Porosity and Shale Volume Estimation for the Ardmore Field using Extended Elastic Impedance. EAGE. Vienna: EAGE.
21. Ghana National Petroleum Cooperation, (1998). Southern Ghana Regional Biostratigraphic and Geochemical Review. Vol. 1. Report Number 5322/1b.
22. Ghana National Petroleum Cooperation (GNPC). (2015). History of explorationGhana. [www.gnpcghana.com/sitepages/contentpage.aspx?itemIp=itemtitle=history of exploration in Ghana](http://www.gnpcghana.com/sitepages/contentpage.aspx?itemIp=itemtitle=history%20of%20exploration%20in%20Ghana), date accessed 3 Nov, 2015.
23. Haldorsen, H. H., Damsleth, E. (1993). Challenges in reservoir characterization. *Geohorizons*, Vol. 77, no. 4
24. Herron Donald, A. (2011). First Steps in Seismic Interpretation. Geophysical Monograph Series No 16, p. 21-35.
25. Hicks, G. J., Francis, A. (2006). Extended Elastic Impedance and its Relation to AVO Crossplotting and Vp/Vs. EAGE Vienna. Vienna: EAGE.
26. Kearey, P., Michael, B., & Ian, H. (2002). An Introduction to Geophysical Exploration, 3rd Ed., Blackwell Science Ltd. p. 34-38.
27. Kramers, J. W. (1994). Integrated Reservoir Characterization from the Well to the Numerical Model, Proceedings, 14<sup>th</sup> World Petroleum Congress, John Wiley & Sons.
28. Lee M., Cox P., Cheshire O., Plum S., Nyamaah L. A. B. (2014). Reservoir Characterization of the Paradise and Hickory Discoveries offshore Ghana: Integration of Depositional and Diagenetic Concepts: Search and Discovery Article No 50985.
29. Miall, A. D. (1996). The Geology of Fluvial Deposits – Sedimentary Facies, Basin Analysis and Petroleum Geology. Springer Verlag, Berlin Heidelberg, p. 616.

30. Naves, F. A., Mustafa, H. M., & Ruddy, P. M. (2004). Pseudo-Gamma Ray Volume from Extended Elastic Impedance Inversion for Gas Exploration. *The Leading Edge* 23(6), p.5 36-540.
31. Normark, W. R., Piper, D. J. W. & Hess, G. R. (1979). Distributary Channels, Sand Lobes, Mesotopography of Navy Submarine Fan, California Borderland, with Applications to ancient Fan Sediments: *Sedimentology*, v.26, p. 749-774.
32. Oyedele, K. F., Ogagarue, D. O. & Mohammed, D. U. (2013). Integration of 3D Seismic and Well log Data in the Optimal Reservoir Characterisation of EMI Field, Offshore Niger Delta Oil Province, Nigeria. *American Journal of Scientific and Industrial Research*, 4(1). p. 11-21.
33. Posamentier, H. W., & Walker, R. G. (2006). Facies Model Revisited: Deepwater Turbidite and Submarine Fans: *SEPM Special Publication no. 84*. p. 397-520
34. Posamentier, H. W., Kolla V. (2003). Seismic Geomorphology and stratigraphy of depositional elements in Deep Water Settings, *Journal Sedimentary Research*, Vol.73, No.3, P. 367-388
35. Pyles, D. R. (2007). Architectural Elements in a ponded Submarine Fan, Carboniferous Ross Sandstone, Western Ireland: *AAPG Studies in Geology*, v. 56.
36. Reading, H.G., Richards, M. (1994). Turbidite systems in deep-water basin margins classified by grain size and feeder system. *AAPG bulletin* 78(5), 792-822
37. Russell, B. (1988). Introduction to Seismic Inversion Methods. SEG Course Notes.
38. Russell, B., Hampson, D. (2006). The old and the new in seismic inversion. *CSEG Recorder*, 31(1), 5-11.
39. Ryder, M. (2002). Geological Interpretation of Well Logs. 2nd Ed, Ryder-

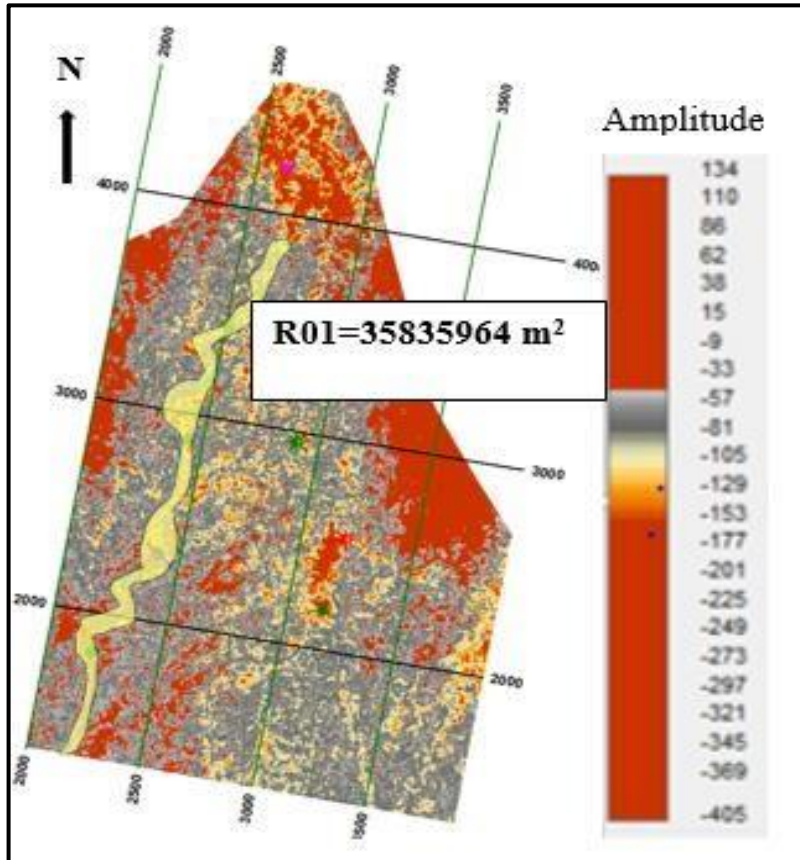
- French Consult Ltd., p. 1, 32.
40. Schlumberger. (1991). Principles of Log Interpretation. Training Manual. p. 1-2, 45-60.
41. Shahri, S. A. G. (2013). Application of Extended Elastic Impedance (EEI) to Improve Reservoir Characterization. Unpublished Thesis.
42. Sheriff, R. E. (1992). Basic Petrophysics and Geophysics, in Reservoir Geophysics, R. E. Sheriff, ed., Investigations in Geophysics No. 7, Society of Exploration Geophysicist, Tulsa, OK. P. 37-49.
43. Sheriff, R. E. (2002). Encyclopedic Dictionary of Exploration Geophysics, 4th Edition: SEG Geophysical Reference Series No. 1.
44. Slatt R. M. (2006). Stratigraphic Reservoir Characterization for Petroleum Geologists, Geophysicists, and Engineers: Handbook of Petroleum Exploration and Production. v. 6 p. 200-311.
45. Subrahmanyam D., Rao P. H. (2008). Seismic Attributes- A Review: 7<sup>th</sup> International Conference and Exposition on Petroleum Geophysics. p.398
46. Sutherland, R. (2008). Explorational history and regional geology. Tullow Ghana.
47. Telford, W. M., Geldart, L. P., & Sheriff, R. E. (1990). Applied Geophysics. 2nd Edition, Cambridge University Press, P137, p. 644-646.
48. Whitcombe, D. N. (2002). Elastic Impedance Normalization. Geophysics, 67 (1), p. 60-62.
49. Whitcombe, D. N., Connolly, P. A., Reagan, R. L., & Redshaw, T. C. (2002). Extended Elastic Impedance for Fluid and Lithology Prediction. Geophysics, 67 (1), 63-67.

# KNUST

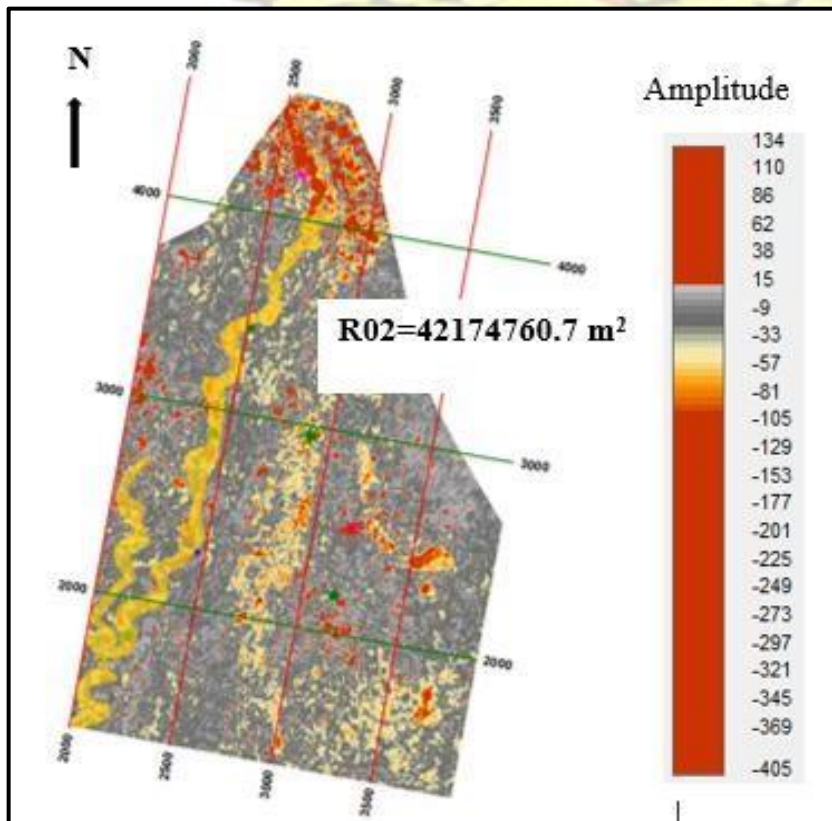


## APPENDIX

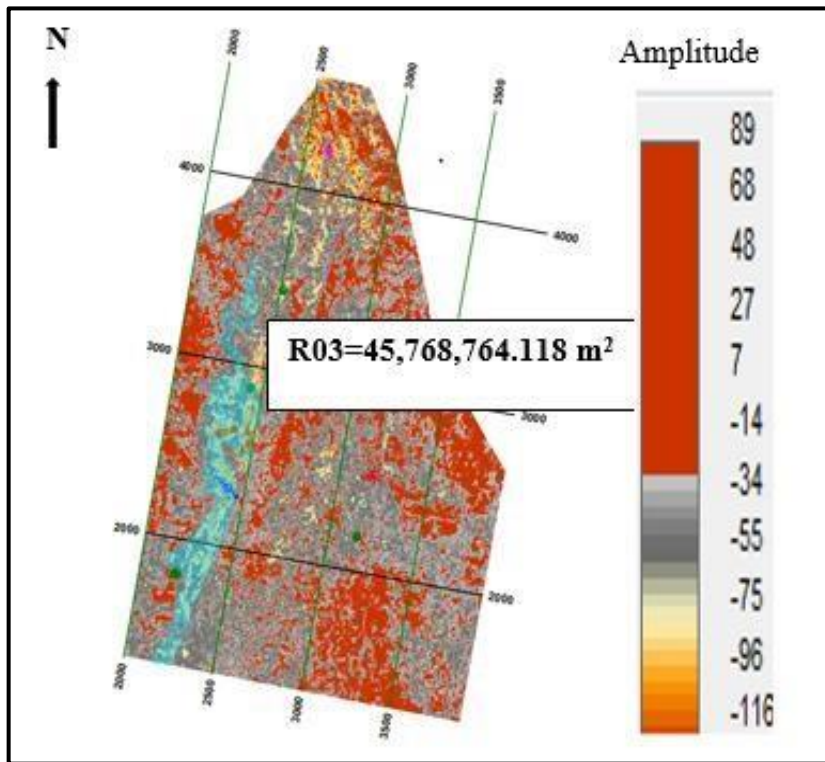
The Area extent used for the reservoir units within the Sovereign-1 in volumetric estimation. This is obtained from the polygon (planimeter) around the bright amplitude extracted. The high(bright) negative amplitude regions which have been consired are highlighted with the different colours and their respective areas. The reservoir units (R01,R02 and R03) are shown below.



(a) Area extent of R01 Reservoir Unit.

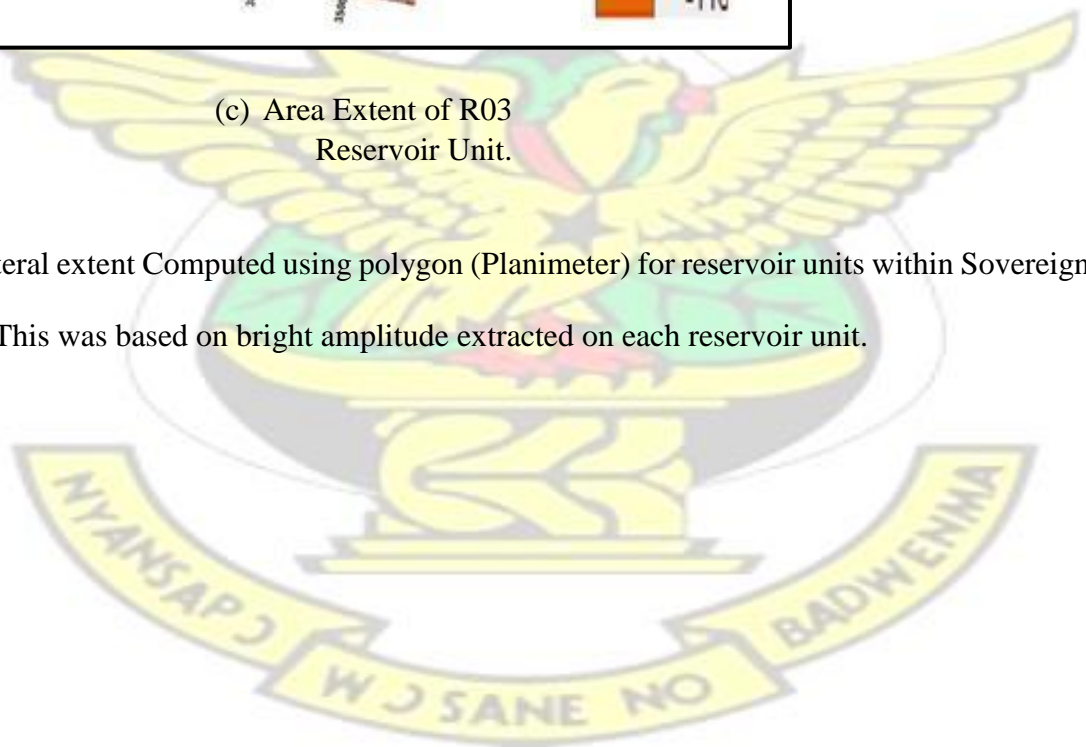


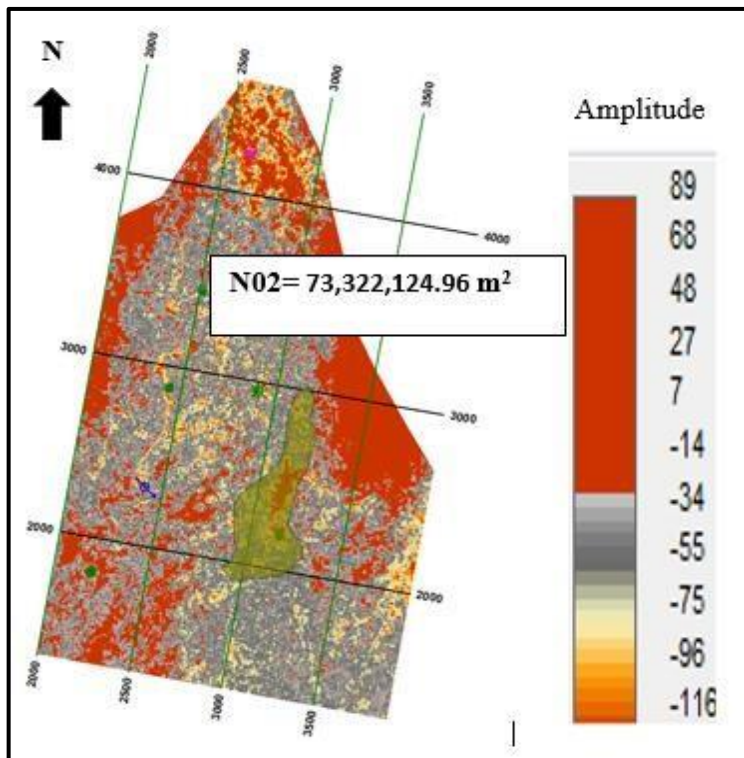
(b) Area Extent of R02  
Reservoir Unit.



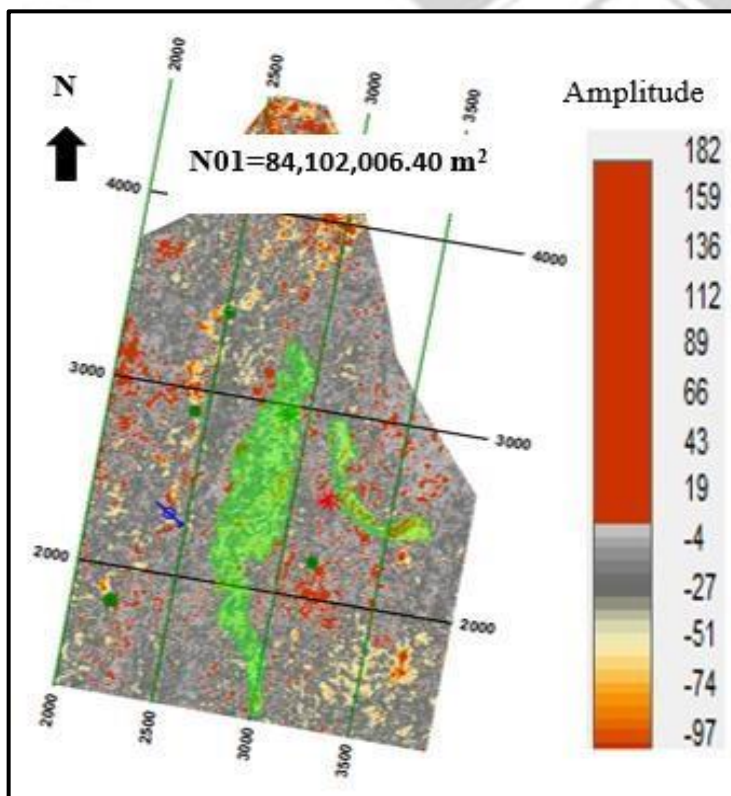
(c) Area Extent of R03  
Reservoir Unit.

Lateral extent Computed using polygon (Planimeter) for reservoir units within Sovereign-  
2. This was based on bright amplitude extracted on each reservoir unit.





(d) Area extent of N02 Reservoir unit.



(e) Area Extent of N01 Reservoir Unit.

# KNUST

